PLASMA OSCILLATIONS IN LOW PRESSURE GASEOUS DISCHARGES

ROBERT J. KETCHEL
and
WILLIAM M. ZOBEL

PLASMA OSCILLATIONS

IN

LOW PRESSURE GASEOUS DISCHARGES

* * * * *

Robert J. Ketchel

and

William M. Zobel

PLASMA OSCILLATIONS

IN

LOW PRESSURE GASEOUS DISCHARGES

by

Robert J. Ketchel

Lieutenant, United States Coast Guard

and

William M. Zobel

Lieutenant Commander, Civil Engineer Corps

United States Navy

Submitted in partial fulfillment of
the requirements for the degree of

MASTER OF SCIENCE
IN
PHYSICS

United States Naval Postgraduate School
Monterey, California

1 9 6 3

PLASMA OSCILLATIONS

IN

LOW PRESSURE GASEOUS DISCHARGES

by

Robert J. Ketchel

and

William M. Zobel

This work is accepted as fulfilling

the thesis requirements for the degree of

MASTER OF SCIENCE

IN

PHYSICS

from the

United States Naval Postgraduate School

ABSTRACT

This is a continuation of work at the U. S. Naval Postgraduate School under Professor N. L. Oleson, investigating oscillations in low pressure ionized gases. Druyvesteyn analysis (using electronic methods for obtaining first and second derivatives of probe current versus probe potential) and Langmuir probe techniques, are utilized for the investigation of discharges in Neon, Argon, and Krypton at ten microns pressure. Plasma densities as determined from the positive ion section of the probe current curves, from Druyvesteyn analysis, and from observed electron oscillation frequencies, are compared with oscillation amplitudes. Electron oscillations were not detected throughout the discharge; however, at some positions multiple frequencies were detected. Ion oscillations, detected throughout the discharge, corresponded in magnitude to Langmuir electrostatic sound waves, and peaked in amplitude with the electron oscillations.

ACKNOWLEDGMENTS

Particular appreciation is expressed to Professor Norman L. Oleson for his guidance, support, and cheerful encouragement throughout the course of our work. To Professor A. W. M. Cooper we extend our thanks for the loan of several pieces of equipment that saved us valuable time in the construction of our vacuum system. Our appreciation is expressed to Professor Gilbert F. Kinney, Chairman of the Department of Chemistry and Metallurgy, for the loan of the electronic equipment that made possible the recording and reduction of our data. To our predecessors, Lieutenant D. M. Alderson, Jr., USN, and Lieutenant J. D. Leonard, Jr., USN, go our thanks for their time and assistance in familiarizing us with the operation of the equipment and the problems involved in this type of investigation. In addition, the time and work that they expended in perfecting the design of the cathode heater was particularly helpful in that it provided us with an electrode that performed without breakdown for the duration of our experimentation. To Mr. Robert Smith our thanks are expressed for his help with our electronics maintenance problems. To Mr. Micheal O'Dea we extend our appreciation for his work in fabricating our Hook Gauge Manometer. To Messrs. Kenneth C. Smith, Robert C. Moeller, Milton K. Andrews, Allen N. Goodall, and Raymond Garcia, our thanks are given for their continuous advice and valuable assistance in technical matters. Last but not least, particular appreciation is reserved for Mr. John M. Calder whose craftsmanship in glass blowing provided us with a vacuum system that was problem-free during our entire nine months of operation.

TABLE OF CONTENTS

LIST OF ILLUSTRATIONS

List of Illustrations (Continued)

LIST OF SYMBOLS

A	-	Surface area of the probe
γ	-	Adiabatic compression coefficient
e	-	Electronic charge
f_e	-	Frequency of electron oscillation
f_i	-	Frequency of ion oscillation
I_d	-	Discharge current
I_e	-	Electron current
I_i	-	Ion current
I_p	-	Probe current
i_{re}	-	Random electron current at space potential
k	-	Boltzman's constant (or, in one case, a constant for ion density correction)
λ	-	Wave length
m_e	-	Mass of the electron
m_i	-	Mass of the ion
n_e	-	Electron density
n_i	-	Ion density
T_e	-	Electron temperature
T_i	-	Ion temperature
V_d	-	Discharge voltage
V_i	-	Amplitude of ionic oscillation
V_p	-	Probe potential
V_{sp}	-	Space potential

1. Introduction.

In recent years, man's desire for greater knowledge in the field of plasma physics has been intensified. Major scientific programs in space exploration, thermo-nuclear research, and electronics, to name only a few, have required and will continue to require, an ever-better understanding of the basic physical processes occurring in highly-ionized, gaseous, conducting mediums.

The state in which matter exists is basically determined by the average kinetic energy of its particles. On earth, a relatively cold, dense fragment of our universe, we have become accustomed to dealing with three states of matter: the solid, the liquid, and the gaseous. The plasma, on the other hand, which may be regarded as a fourth state of matter, actually makes up nearly 99.9% of all space, and may exist whenever the kinetic energy of its particles exceeds the ionization potential of its atoms, which is usually a few electron volts /1/.

On earth, the medium most closely resembling an ideal plasma is a partially ionized gas, such as may be found in the positive columns of glow and arc discharges. In fact, Langmuir and Tonks /2/ originally defined the word "plasma" in these terms when they stated:

> The word "plasma" will be used to designate that portion of an arc type discharge in which the densities of ions and electrons are high but substantially equal. It embraces the whole space not occupied by the sheath.

It is in just this sort of laboratory-created plasma that our research

has been carried out; specifically, in vacuum tube glow discharges in Neon, Argon, and Krypton.

Under the guidance of Professor N. L. Oleson, this project is a continuation of work carried out in the past few years in the investigation of electron ion oscillation phenomena occurring in low pressure rare gas discharges.

2. Previous Work.

In 1924, Langmuir and Mott-Smith /3/ developed the first sound theoretical technique for the study of electrical discharges in low pressure gases with an auxiliary electrode, known as a "probe". Prior work with probes had been limited in value by a failure to recognize the importance of sheath formations in the determination of the true space potential of the discharges investigated. With the advent of the new theory, the study of discharges in an ionized gaseous plasma was revitalized.

In 1925, Langmuir /4/ reported that there were apparently three energy groups of electrons present in a diode-type discharge. These he classified as (1) "primary", (2) "secondary", and (3) "ultimate" electrons. The "primary" electrons were defined as those keeping nearly all of the momentum gained in traversing the ion sheath; the "secondary" electrons as those having a Maxwellian distribution of energies proportional to the energy of the primaries; and the "ultimate" electrons as those having a Maxwellian distribution of energies independent of the primaries' and much lower than the secondaries'. On the basis of these observations, Langmuir proposed that a phenomenon he called "scattering" involved the transfer of energy between electrons in the discharge.

Experiments by Dittmer /5/ showed that the scattering phenomenon was occurring in a region that could be defined between the cathode and some point a constant distance from it. He also noted that the scattering region approached the cathode with an increase in tube current, and predicted that the phenomenon may be due to oscillatory motion of plasma particles. He could, however, detect no oscillations with his equipment.

In 1929, Tonks and Langmuir /6/ developed a simple theory for electron and ion oscillations by viewing the electrons as oscillators embedded in a jelly-like substance made up of the ions of the plasma. This theory predicted electron oscillations of a natural frequency given by,

$$f_e = \left(\frac{ne^2}{\pi m_e}\right)^{1/2} \text{ cps.}$$

and ion oscillations with an upper frequency limit given by,

$$f_i = \left(\frac{m_e}{m_i}\right)^{1/2} f_e$$

Tentative verification of this theory was made by detecting oscillations in the 300 to 1000 megacycle range, which corresponded reasonably well with the predicted frequencies.

In 1939, Merrill and Webb /7/ reported on investigations in a low pressure mercury arc discharge using the probe technique to determine a possible relation between plasma oscillations and scattering as suggested by Tonks and Langmuir. They found that scattering occurred in several narrow regions and was associated with oscillations which agreed with the Langmuir frequency within ten percent. They concluded that the [illegible] oscillations receiving energy from the fast electrons [illegible] energy to some of the electrons.

From 1939 through 1947 [illegible] vided important observations [illegible]

a. [illegible]
   the external circuit [illegible]
   tion of the oscillations [illegible]
   tube.

b. [illegible]

c. The frequency of oscillations varies directly with gas pressure.

d. The amplitude of the detected oscillation signal depends on the electrode geometry and upon which electrodes are used for detection of oscillations.

Emeleus /9/ has pointed out the value of visual observations in low voltage electrical discharge studies using oxide-coated cathodes in Argon at a few microns pressure. A sketch showing the major sectors of a gaseous discharge in which high frequency oscillations are present, follows:

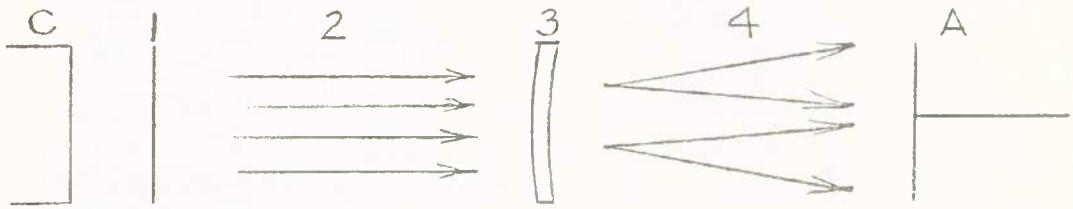

C, cathode; 1, cathode sheath; 2, primary beam;
3, meniscus;4,scattered beams; A, anode.

The principal static potential drop occurs in region 1, while the remainder of the discharge is essentially at the anode potential.

Easley /10/ in probe technique investigations of a mercury discharge demonstrated the importance of probe cleanliness for accurate measurements.

Oleson and Found /11/ have shown that non-linear logarithmic plots of probe data were obtained in discharges in which moving striations were present. The logarithmic plots obtained looked as though two Maxwellian distributions were present in the discharge. It had become fairly evident that in many discharges at low pressure, a Maxwellian distribution did not exist. Greater effort was therefore aimed at determining new techniques for calculating the actual electron energy distribution function rather

than assuming it to be Maxwellian.

As early as 1939, Druyvesteyn /12/ had shown that the electron energy distribution could be found from the expression:

$$N_{f(energy)} = \frac{2}{Ae}\left(\frac{2m_e V_p}{e}\right)^{1/2}\frac{d^2 I_p}{dV_p^2}$$

where $N_{f(energy)}$ is the number of particles per unit of energy per unit volume. (Normally units of reciprocal electron volts and reciprocal cubic centimeters are used).

But, in spite of Druyvesteyn's development of this relation, no significant work was conducted to obtain energy distributions because of the inherent inaccuracies involved in the tedious graphical method of obtaining the second derivative of probe current with respect to probe voltage.

Medicus /13/, in 1956, developed a technique for determining the energy distribution function from probe characteristic curves that were plotted with an X-Y recorder. This method is one in which tangents are drawn to the probe characteristic curve and the difference between the tangents represent the second derivatives. The actual probe curves may be used as recorded only if the ion current is small relative to the electron current, or if the ion current aries linearly with the voltage. If not, the net electron current must be used.

Takayama, Ikegumi, and Miyozaki /14/ developed a radio frequency technique of determining the plasma resonant frequency in a gaseous discharge. They found that if a radio frequency signal is superimposed on a probe maintained negative to space potential, a resonant current increase will appear in the circuit at the Langmuir frequency.

Allis /15/ has suggested that plasma oscillation growth may be correlated with decreasing plasma density gradients. He indicated that the average beam velocity of a monoenergetic beam of electrons passing through a

plasma is reduced by the growing amplitude of the oscillations. This would indicate that the beam energy is being transferred into field energy in the wave and increased kinetic energy of the random plasma electron group. Recent work by Mahaffey, McCullagh, Garscadden, and Emeleus /16/ is pertinent in correlating growth or decay of oscillations with plasma density gradients. They conclude that some correlation exists between the growth or decay of oscillations and the motion of the electron beam down and up a plasma concentration gradient which is in general agreement with the plasma dispersion theory.

Garscadden /17/ and Emeleus /18/ have pointed out subsequently that measurements taken with Langmuir probes in oscillating discharges must be carefully interpreted. This is especially true in the case of electron concentration and space potential determination. They point out that some of the detail in the results previously published regarding electron concentration versus oscillation intensity may not be real.

Allen /19/ studied Argon using a spectroscopic technique that detected scattered electrons by their excitation of high energy lines. Allen found good correlation between the measurements made by spectroscopic and probe techniques. In studying oscillation amplitudes and electron energy distributions, he found a sudden increase in oscillation amplitude to a maximum close to the anode side of the meniscus, and a decrease coupled with secondary maxima towards the anode.

Kojima, Kato, and Hagiwara /20/ studied plasma oscillations by using a super-regenerative detector. Many plasma oscillations were observed without auxiliary electron beams; however introducing small beams into the main plasma increased the amplitude of the oscillations, yet did not change their frequencies. Plasma oscillations were also detected from outside the tube

by use of a small antenna. Since no probe was necessary in this technique, it was shown that thick ion sheaths were not necessary for the excitation of plasma oscillations. Many plasma oscillations were detected having slightly different frequencies, and in a later work /21/ they describe more fully this result. They find three discrete plasma frequencies that correspond to (1) the central region of the beam, (2) the region near the edge of the beam, and (3) the outer plasma region near the walls of the tube.

Alexeff and Neidigh /22/ have conducted a study of ionic sound waves in plasmas. They have observed self-excited ionic sound wave oscillations both in magnetically supported plasma columns and in spherical discharge tubes. The oscillations show the expected overtones, and a dependence on wavelength, ion mass, and electron temperature as expected.

3. Equipment.

Figures 1 through 3 are photographs of the laboratory equipment and its general arrangement. The equipment used can be divided into five main component groupings as follows:

(1) Gaseous discharge tube.

(2) Vacuum system for evacuating the tube and the pressure calibration system.

(3) Pressure measurement devices.

(4) Frequency detection and measuring equipment.

(5) D. C. electrical circuitry.

A brief description of each of these five groupings, their construction and/or history, and general comments concerning them is as follows:

(1) Gaseous discharge tube. Figures 4 and 5 are a photograph and a detailed drawing of the tube (diode.) This is the same tube used by Leonard and Alderson in their work during 1961-1962 /23/. No changes were made to the tube other than repairing one of the double-probe tungsten wires. The electrodes were mounted on cylindrical iron cores sealed in pyrex to enable them to be moved within the tube by application of an external magnetic field. Electrical leads to the electrodes were coiled multi-strand oxygen-free copper, insulated where necessary with ceramic beads. Attachment to the tungsten seals at both ends of the tube and at the electrodes was by spot-welded nickel straps. The cathode was an indirectly heated dispenser type cathode supplied by Semicon of California, Incorporated. This cathode has an evaporation rate of one microgram per

centimeter per hour and negligible sputtering. The cathode was 28.5 mm. long, 22.1 mm. in diameter, and had a concave face with a radius of curvature of 36.7 mm. The cathode heaters were made from 20 mil malleable tungsten wire wound into a coil 14.2 mm. in diameter and consisting of 15 turns. Operating temperature (face of cathode) of 1100°C required approximately 13.7 amperes. Approximately 20 minutes was required to reach this temperature equilibrium, which was maintained to within $\pm$ 5°C during each data run.

The anode was a 26 mm. diameter, 20 mil thick, nickel disk. The probes were constructed of 5 mil tungsten wire sheathed in pyrex to within 3.9 millimeters of the end. To prevent conduction on the surface of the glass due to contamination, the probe had a 5 mil stand-off from the glass sheath.

(2) Vacuum System. The vacuum system was capable of a vacuum of the order of 10^{-8} millimeters of Hg and was tested leak-free with the Veeco MS-9 Helium Leak detector which is capable of detecting leaks as small as 1×10^{-18} cubic centimeters per second. Pumping was done with a three-stage air-cooled oil diffusion pump, using Octoil-S, and a mechanical fore pump. The vacuum system was divided into two sections: an "internal" section consisting of the discharge tube and vacuum gauges; and an "external" section consisting of connecting tubing to bottles of argon, neon, and krypton gas, and of an oil manometer for pressure measurement and vacuum gauge calibration. The internal section was separated from the external system by a liquid air trap, and could be isolated completely by a

Granville-Phillips bakeable bellows type valve. There were no stopcocks in the internal system, and all stopcocks in the external system were vacuum type, lubricated by Type N Apiezon grease. The internal system was baked out by an overhead removable oven. The external system, separated from the pumps by a second liquid air trap, was baked out with heating tapes. The anode and all other metal parts within the discharge tube were out-gassed with an induction heater.

(3) Pressure Measurement Devices. Vacuum measurement in the high vacuum region (10^{-4} to 10^{-8} mm of Hg) was by a Veeco RG-75, Baird -Alpert type ionization gauge and Veeco Vacuum Gauge control RG31A.

Vacuum pressures in the micron range were measured primarily by a manometer, using the following method: A relatively small volume (V_1) of the external system, connected to the manometer, was filled with sufficient gas to give a manometer reading of over 200 mm. The manometer could be read to within $\pm$ 0.1 mm. by a telescope with hairline. The gas within volume V_1 was then allowed to expand into the combined volumes of the external system and the internal system (V_2). The new manometer reading, still over 15 mm., was again recorded and the volume ratio V_1/V_2 calculated. After repeating this procedure numerous times, using each of the three gases, the ratio V_1/V_2 was determined to be 26.2 $\pm$ 0.5. Subsequently, by filling volume V_1 to a pressure 26.2 times as great as the pressure desired in the discharge tube (even the smallest pressures required could be read with an error of less than

2%), and allowing the gas to expand into the greater Volume V_2, pressures in the micron range were obtained in the discharge tube, accurate to $\pm$ 5% ($\pm$ 0.5 microns in 10 microns, $\pm$ 2.5 microns in 50 microns). In order to obviate the time-consuming use of the manometer-expansion process on every experimental run, we spent considerable time during the earlier portion of our work attempting to calibrate the Veeco RG-75 ionization gauge and the resistor-modified RG31A control (as used by Alderson and Leonard in 1961-1962) in the micron range.

The first attempt at calibration was in Neon with the McLeod gauge used by Alderson and Leonard (See Appendix of their work /23/). After several attempts, it was obvious that the modified Veeco control gauge reacted strangely in the 30-60 micron range. As the pressure increased in the micron range, the meter reading would steadily increase until an off-scale reading was obtained (later it was determined that for our particular RG-75 gauge this was reproducibly at 30 microns). With further increase in pressure (as measured by the McLeod gauge) the meter reading would return to an on-scale value, giving a spurious reading. Thinking that our calibration vacuum system may have become contaminated with air, water vapor, or other gases, we ceased this calibration attempt.

Our second attempt at calibration was on the vacuum system as connected to our experimental discharge tube. Not being able to subject the system to mercury vapor contamination from a standard McLeod gauge, we connected a modified hook gauge,

using octoil, to the system. The basic hook gauge assembly, manufactured by the Dwyer Manufacturing Co., for reading vacuum pressures in the millimeters of Hg range, was modified to read pressures in the micron range in accordance with information obtained from Mr. Louis Biagi of the Lawrence Radiation Laboratory, at the University of California at Berkeley. A photograph of the modified assembly is shown in Figure 6.

Due to difficulties encountered in its modification, the hook gauge assembly was not made leak-free in time to permit its use in our work; however, we believe that with relatively minor modifications it can become a valuable tool for making continuous readings of tube pressure in the micron range (to $\pm$ 0.2 micron). On our third attempt at calibration of the RG-75, using the manometer-expansion method previously outlined, we were successful in calibrating our specific gauge (with its modified control) for Neon gas so that reproducible pressures could be determined from it. On attempting to calibrate the Veeco gauge for Argon and Krypton, we experienced considerable difficulty in obtaining satisfactorily reproducible pressures. We are therefore reporting pressures in the micron range as established by the manometer-expansion method, corrected for pressure change due to the increased temperature of the gas during operation. These pressures are considered accurate to $\pm$ 5%. A Westinghouse type 7903 high pressure ionization gauge was also installed in the system; however, continuing control circuit difficulties precluded its use. This instrument is designed to operate in the 1×10^{-5} to 5×10^{-1} mm. of Hg range and is potentially valuable in future work.

(4) Frequency detection and measuring devices. A cavity wave meter test set, Model AN/UPM 2 with a frequency range of 80-1220 megacycles, was used to detect electron oscillation frequencies by capacitive coupling with a wire probe. The DC signal from the detector crystal of the cavity wave meter was fed to a Hewlett-Packard Model 425 A DC micro-volt-ammeter. Currents as small as 10^{-12} amperes could be detected with this instrument. Ion oscillations were detected and measured by directly coupling a Tektronix Type 543 oscilloscope to the probe.

The circuits for obtaining frequency data were coaxial lines from the probe to the wave meter in the case of electron oscillations, and to the oscilloscope through a 1000 cycle high-pass filter for ion oscillations. The high pass filter was included to eliminate low-frequency electrical noise in the laboratory.

(5) DC Electrical Circuitry. A diagram of the DC electrical circuitry is shown in Figure 7. The cathode heaters were fed by a DC power supply from a battery charger, in parallel with a battery bank of 10 nickel-iron 6-volt batteries (5 parallel with 5) to minimize voltage fluctuations (shown only as a battery supply on the diagram).

Cathode to Anode tube voltage (Vd) was supplied by a Kepco Labs model 1250 B voltage-regulated DC power supply, capable of supplying from 0-1000 volts at 0-500 milliamperes.

Probe to Anode voltage was controlled as follows:

(a) A triangular wave voltage signal, 15 volts peak to

peak, and varying linearly with time, was obtained from a Hewlett-Packard Low Frequency Function Generator, Model 202A.

(b) This voltage was supplied to a nominal gain-ten amplifier in a Donner Analog Computer, Model 30[1], with problem board Model 30-6.

(c) The amplified voltage signal was then biased by one of the initial condition power supplies of the computer.

(d) The biased signal was then supplied to the anode to obtain the desired positive and negative voltage excursions between probe and anode.

In order to outgas the probe by ohmic heating prior to taking each probe characteristic, a constant DC voltage was supplied to the probe from two of the initial condition power supplies of the computer.

Current drawn by the probe as a result of the imposed varying probe-anode potential was passed through a 500 ohm resistor to obtain a voltage proportional to probe current (the effect of the voltage drop in this resistor on probe potential was less than one per cent and was considered negligible). This proportional voltage was then fed through two gain-ten amplifiers on the computer. The amplified signal was

[1]The Donner Analog Computer, Model 30, has 10 operational amplifiers which operate in the range of -100 to +100 volts with a long time stability better than 0.5% of full scale value, maximum drift characteristic of 4 millivolts per hour with a short term random drift less than $\pm$ 2 millivolts. Five initial condition, regulated, DC power supplies, 0-100 volts are available on the computer.

then supplied to an F. W. Mosely Autograph X-Y recorder, Model 2-S[1] either directly as I_p, or through a combination of one or two cascade RC differentiator circuits (time constant .025 seconds) as $\frac{dI_p}{dV_p}$ or $\frac{d^2I_p}{dV_p^2}$.

[1]The F. W. Mosely Autograph X-Y Recorder, Model 2-S, has a full scale range on the horizontal axis of from 0-7.5 millivolts to 0-150 volts. The vertical axis has a full scale range of from 0-5 millivolts to 0-100 volts. Input impedances on both scales are of the order of 2 megohms. The recorder is accurate to 0.25% of full scale on all ranges, when calibrated. Calibration drift is negligible.

4. Procedures.

Preparation of the System.

To insure the purity of the gas under investigation, the system was pumped out to as high a vacuum as possible. This was a vacuum of the order of 1×10^{-7} millimeters of Hg. To obtain this high vacuum, the entire system was first pumped to a vacuum of approximately 1×10^{-5} mm of Hg, and then pumped on while the system was baked out. The internal section of the system was baked with a portable oven at approximately 350°C while the external system was baked with heating tapes at approximately 250°C. This baking process was continued for approximately twelve hours until a vacuum of the order of 1×10^{-6} mm of Hg was obtained.

The anode was then heated by means of an induction heater to drive out absorbed gas. The cathode was brought to a temperature of 1100°C and maintained at this temperature for approximately one hour. By pumping on the system during the induction heating of the anode and the operation of the cathode, a vacuum of the order of 1×10^{-7} mm of Hg was obtained.

A large amount of gas was found to be absorbed in the cathode, so with the introduction of each new gas, the system was flushed and filled three times. This was done by admitting a charge of gas at about 20 microns pressure, to the tube in a cold condition, bringing the cathode to a temperature of 1100°C, and obtaining and holding a discharge for thirty minutes. The cathode was then allowed to cool while the system was pumped to about 1×10^{-7} mm of Hg. After the cathode had cooled the procedure was twice repeated.

At the time of making a data run, the system was filled with gas from an initial vacuum of about 1×10^{-7} millimeters of Hg. The pressure of gas admitted to the tube was measured by means of the manometer method outlined

in the equipment section. After filling, the cathode was brought to a temperature of 1100°C and allowed to reach equilibrium. This required approximately 30 minutes. A cathode heater current of 13.7 amperes was necessary to maintain this temperature.

All electronic equipment was turned on during the initial stages of preparation for the data run so that the equipment would be stabilized by the time the actual data run was made.

While the cathode temperature was reaching equilibrium, the desired initial probe position and cathode to anode spacing were set. This was done by setting the cathetometer to a desired reference position for the cathode and then moving the cathode by means of a solenoid until its front face was lined up with the reference mark. The cathetometer was then traversed to the probe and a measurement made of its position. Finally, the cathetometer was traversed to the desired anode position and the anode moved to coincide with it. In making settings and measurements the cathetometer was always traversed in one direction only, so that backlash error would be reduced. This procedure was followed for making all cathode, anode, and probe settings.

A discharge was obtained when the cathode reached operating temperature, and the desired tube discharge current was set by properly varying the tube power supply voltage and the tube circuit resistance. The discharge was then allowed to stabilize and the cathode temperature allowed to reach equilibrium.

Data Taking Procedures.

The discharge circuit was operated in a floating condition with no point being grounded. The probe circuitry was directly coupled to the anode, thus supplying a signal between the probe and the anode of the desired positive and negative voltage excursion. The current drawn by the probe on passing through a resistance (Rp), provided a voltage signal proportional to probe

current. After amplification by two gain-ten amplifiers, signal was plotted on the Y axis of the X-Y recorder as a function of the probe to anode potential. Voltages proportional to $\frac{dI_p}{dV_p}$ and $\frac{d^2I_p}{dV_p^2}$, obtained by feeding the voltage proportional to probe current to one or two differentiating R-C circuits, were also plotted as functions of probe to anode potential on the X-Y recorder (See Figure 7). The three plots made were of greatly different amplitude, so different calibrated scales of the X-Y recorder were used.

Immediately prior to each plot the probe was outgassed with 50 to 125 volts from a constant voltage power supply.

The data curves were calibrated by measuring the actual probe current with a milliameter at the extreme probe to anode potentials for the initial probe position. The $\frac{dI_p}{dV_p}$ curve was calibrated by measuring the slope of the I_p vs. V_p curve at the point of the maximum of the derivative. The $\frac{d^2I_p}{dV_p^2}$ curve was calibrated by measuring the slope of the $\frac{dI_p}{dV_p}$ vs. V_p curve at the point of the maximum of the second derivative curve. These calibrations were then checked at various other points on the same curve and against curves of other sub-runs to insure accurate calibrations. The X input of the X-Y recorder was a varying probe to anode potential. This potential was obtained from a low frequency function generator with a triangular wave output, amplified by a gain-ten amplifier, and then biased to the desired voltage excursion. Calibration of the X-Y recorder was then obtained by measuring the probe to anode voltage (to $\pm$ 2 volts) with a vacuum tube volt meter at the extreme points of excursion.

The next step was the observation of ion oscillations. The probe circuitry was disconnected and the oscilloscope lead was directly coupled to the probe through a 1000 cycle high pass filter. The anode was grounded for this observation and the shield of the oscilloscope lead was grounded common

to it. The oscilloscope display was photographed and then later analyzed for amplitude and frequency of the observed signal.

A determination of electron oscillation frequency and relative amplitude was then made. This was done by capacitively coupling a cavity wave meter to the probe, with the probe circuitry dis-connected and the anode grounded. The output current of the cavity wave meter was measured by a micro-micro ammeter, with a deflection of this meter (at resonance) from its ambient value being an indication of the presence of an electron oscillation. The amount of the deflection indicated the relative amplitude of the electron oscillations and the scale reading of the wave meter indicated its frequency. The cavity wave meter tuning was a very slow and careful operation to ensure that resonant deflections were not missed or hidden by random deflections of the meter.

At this point the probe, cathode, and anode were repositioned for the next data point and the amplifiers were checked for proper balance. This procedure was then repeated for all desired probe positions.

5. Results.

General.

During 1961-62 Alderson and Leonard /23/ reported considerable information on the behavior of Neon at a pressure of 58 microns. Their pressure determination was based on readings from a Veeco RG-75 ionization gauge modified to read in the micron range and calibrated against a McLeod gauge. At the beginning of our work in 1962-63, we attempted to continue the calibration of the Veeco gauge (which we had commenced calibrating with Alderson and Leonard) so as to use it in working with Argon and Krypton as well as Neon. Our initial attempt was to calibrate a new RG-75 gauge in Neon to confirm the earlier calibration. At that time we found that the new gauge was erratic in the micron range[1], and decided to shift to our manometer-expansion method. (See section on equipment.) Subsequent investigation of Neon using our manometer pressures (and comparing Id-Vd characteristic curves, electron oscillation frequencies, and discharge appearance with Alderson and Leonard's work) indicated that their work was done at 30 to 35 microns pressure, rather than 58 microns. We were able to match their data satisfactorily in this pressure range.

It was our original intent to study discharges in Neon, Argon, and Krypton under identical conditions of pressure, electrode spacing, and discharge current; however, as our work progressed we found it necessary to modify our original plans in order to work at those conditions which appeared to be most worthy of investigation.

[1]The Veeco RG-75 ionization gauge and its associated control are designed by the manufacturer to function at pressures of 1×10^{-3} mm. of Hg to 1×10^{-9} mm. of Hg.

Since Alderson and Leonard had covered the 30-35 micron pressure range in Neon we decided to investigate Neon at 10 microns and to continue at that pressure in Argon and Krypton. In Neon at 10 microns we discovered that the maximum current for which a discharge could be consistently maintained was 30 ma. At currents below 30 ma the discharge was diffuse, exhibiting no "beam" between cathode and anode. As we increased the current above 30 ma (by increasing the supply voltage across the tube) the discharge would shift radically into a focused beam, the voltage between anode and cathode would rise (at first slowly and then with increasing speed as the discharge changed), and the discharge would then suddenly collapse. After a collapse, we were immediately able to re-initiate a discharge by dropping the supply voltage and then slowly increasing it; however, upon re-initiation, the discharge voltage-current characteristics were always altered from those observed prior to collapse. For corresponding currents, values of voltage between anode and cathode were from two to three volts higher, but the shape of the Id-Vd characteristic curve remained substantially the same. After a period of the order of 30 minutes, the values of voltage and current would return to their pre-collapse values. Similar collapse behavior was detected in Neon for pressures up to 40 microns (we made no investigation of pressures higher than this); however, the current at which collapse occurred increased as we increased pressure, so that at pressures of 30-40 microns a discharge could be maintained with currents of up to 75 ma.[1]

In view of the above, we selected a current of 30 ma for our investigations

[1] The collapse phenomena at certain higher currents in 10-40 micron pressure Neon discharges (not seen in Argon or Krypton) was observed by Alderson and Leonard during the previous year's work [illegible] and has been observed by C. F. Hoegquist in his current work at [illegible] using a discharge tube in which electrode spacing greatly [illegible] hours.

Since Alderson and Leonard had covered the 30-35 micron pressure range in Neon we decided to investigate Neon at 10 microns and to continue at that pressure in Argon and Krypton. In Neon at 10 microns we discovered that the maximum current for which a discharge could be consistently maintained was 30 ma. At currents below 30 ma the discharge was diffuse, exhibiting no "beam" between cathode and anode. As we increased the current above 30 ma (by increasing the supply voltage across the tube) the discharge would shift radically into a focused beam, the voltage between anode and cathode would rise (at first slowly and then with increasing speed as the discharge changed), and the discharge would then suddenly collapse. After a collapse, we were immediately able to re-initiate a discharge by dropping the supply voltage and then slowly increasing it; however, upon re-initiation, the discharge voltage-current characteristics were always altered from those observed prior to collapse. For corresponding currents, values of voltage between anode and cathode were from two to three volts higher, but the shape of the Id-Vd characteristic curve remained substantially the same. After a period of the order of 30 minutes, the values of voltage and current would return to their pre-collapse values. Similar collapse behavior was detected in Neon for pressures up to 40 microns (we made no investigation of pressures higher than this); however, the current at which collapse occurred increased as we increased pressure, so that at pressures of 30-40 microns a discharge could be maintained with currents of up to 75 ma.[1]

In view of the above, we selected a current [illegible] for our investigations

[1] The collapse phenomena at certain higher currents in a 10-40 micron pressure Neon discharge (not seen in Argon or Krypton) was observed by Alderson and Leonard during the previous year's work [illegible] and has been observed by C. F. Bergquist in his current work at the [illegible] using a discharge tube and electrode spacing greatly [illegible] ours.

of Neon. Later in the work, while investigating Argon and Krypton we found that a current of 30 ma (pressure 10 microns) produced fewer and weaker electron oscillations than currents of 100-120 ma, which could be maintained in those gases without difficulty. On the other hand, at pressures of 30-35 microns in Argon and Krypton no electron oscillations could be detected with our instruments. We therefore maintained our pressure at 10 microns, but changed our discharge current from 30 ma in Neon to 100 ma in Argon and 115 ma in Krypton (A slight flicker occurring at 100 ma in Krypton was not visible at 115ma). All other discharge parameters were identical for all data runs.

Two main data runs were conducted in Neon (numbered 19 and 21) and one each in Argon (number 39) and Krypton (number 40). Figures 8 through 11 are "master" data recapitulations for each run in the various gases. Figures 12 through 36 are the actual X-Y recorder plots of Ip, $\frac{dI_p}{dV_p}$, $\frac{d^2I_p}{dV_p^2}$ versus Vp for representative probe positions in the various gases. In the interest of brevity, plots for some probe positions have been omitted where the information contained on them was very similar to plots for adjacent probe positions; however, values of space potential, electron temperature, density, etc. as obtained from the omitted plots are shown both on the "master" data sheets and in other figures throughout the report. Tube current-voltage characteristic curves for each run are shown in figures 37 through 39. In addition to the main data runs, several supplementary data runs were made in which pressures and discharge currents were varied to observe changes in discharge appearance and in electron and ion oscillations with these variations. No plots of probe current or its derivatives were made on these runs.

The appearance of the discharge for all main runs was essentially the same (except, of course, for color). It was diffuse, exhibiting no "beam"

appearance between anode and cathode (See Figure 40). No "meniscus" was observed. On some of our supplementary runs we observed different discharge forms as shown in figure 41.

Space Potential.

Plots of space potential versus probe position for each main data run are shown in figures 42 through 45. First, for each probe position a value of space potential was determined from the maximum value of $\frac{dI_p}{dV_p}$ and the zero of $\frac{d^2I_p}{dV_p^2}$ versus Vp. The two curves gave what we considered to be essentially the same value of space potential except for a maximum one-volt lag that was apparently inherent in the recorder between Ip and $\frac{dI_p}{dV_p}$ and $\frac{dI_p}{dV_p}$ and $\frac{d^2I_p}{dV_p^2}$. Second, for each probe position a value of space potential was determined from the first break from linearity of the ln Ie vs. Vp curve. (See Figure 46 for a sample plot). Third, for comparison purposes, a value of space potential was determined by the method of intersection of two tangents to the ln Ie versus Vp curve. (See Figure 46). As can be seen from figures 42 through 45, the values of space potential obtained from the first and second methods are in fairly close agreement, particularly on the anode side of the region of maximum interaction. From the resulting plots of space potential vs. probe position, using the first and second methods, a "best" value of space potential was determined graphically and used in all succeeding calculations.

While the shapes of space potential versus probe position curves were consistent between runs, and were as expected, the negative values for runs 19 and 39 were not expected. We believe these negative values are spurious (although relative values between probe positions are correct) due to slight inaccuracies in our method of determining maximum and minimum values of imposed probe to anode potential. These values, as determined by a vacuum tube

voltmeter placed across the probe and the anode (See Figure 7 and the procedure section), were determined to within $\pm$ 2 volts by recording the maximum and minimum excursions of a moving meter needle. Based on this determination, the probe to anode voltage (Vp) scale on our X-Y recorder plots was calibrated. Since values of space potential are in most cases only one to two volts negative, a two volt inaccuracy in the VTVM reading could account for negative values which should actually be positive. In our opinion, this inaccuracy in our Vp scale calibration affects only the absolute value of space potential and none of our other data.

Electron and Ion Densities.

Plots of electron and ion density versus probe position are shown in figures 47 through 50 for all data runs.

The electron density was determined from the random electron current at space potential, by Druyvesteyn analysis, and also from the frequency of electron oscillations.

In using the method of random electron current at space potential, the value of space potential was the estimated best value obtained from plotting the results of the several methods of determination. The value of the electron temperature used was also the estimated best value (see Electron Temperature Section, which follows). The relationship for electron density by this method is:

$$n_e = \frac{i_{re}}{Ae}\sqrt{\frac{2\pi m_e}{k T_e}}$$

where kT_e is in ergs, m_e in grams, i_{re} in statamps, A in cm^2, and e in statcoulombs.

In the Druyvesteyn analysis /12/, the product of $Vp^{1/2}\,\frac{d^2 I_e}{d V_p^2}$ plotted against Vp gives the shape of the electron energy distribution function. The area under this curve obtained by numerical integration is the

electron density. Thus:

$$n_e = \int \frac{2}{Ae}\left(\frac{2m_e}{e}\right)^{\frac{1}{2}} V_p^{\frac{1}{2}} \frac{d^2I_p}{dV_p^2}\, dV_p$$

using the MKS system of units. The probe used had a surface area of 1.557 x 10^{-6} m^2, resulting in a final expression:

$$n_e = \int 2.72 \times 10^{13} V_p^{\frac{1}{2}} \frac{d^2I_p}{dV_p^2}\, dV_p$$

where Vp is in volts and $\frac{d^2I_p}{dV_p^2}$ is in amps/volt^2. The integration is carried out over areas where $\frac{d^2I_p}{dV_p^2}$ has a positive value.

Observation of the probe characteristic curves revealed that not all electron energies were being included in the energy distributions for the runs in Neon. It was observed that the $\frac{dI_p}{dV_p}$ curve had noticeable shape for a region of approximately 25 volts before the slope was represented by a $\frac{d^2I_p}{dV_p^2}$ plot (See Figures 12, 13, 14, for examples).[1] Thus a number of electrons were in effect not included in the energy distribution function. An approximate correction for this loss in Neon was made by extending the plot of $\frac{d^2I_p}{dV_p^2}$ from the last readable ordinate out along a straight line until the $\frac{dI_p}{dV_p}$ curve was at zero. This correction factor was determined to be a constant value of 1.55 for both runs in Neon. Such a correction was not necessary for the runs in Argon and Krypton as the first and second derivatives corresponded very well.

Electron density was also determined from the relationship $n_e = \left(\frac{f_c}{8980}\right)^2$

[1]This is due to an insensitive response of the X Y recorder at very small probe currents. It did not occur in Argon and Krypton runs since discharge currents were 3 to 4 times as great and resultant probe currents were 10 times as great.

in the regions where electron oscillations were detected. In this relationship, "f_e" is the detected frequency in cycles per second.

Ion densities were determined from the positive ion region of the probe characteristic curves by the method of Langmuir. The relationship for ion density is:

$$n_i = \sqrt{\frac{\pi^2 m_i}{2e^3 A^2} \frac{d(I_p^2)}{dV_p}}$$

where e is in esu, A in cm^2, m_i in grams, and $\frac{d(I_p^2)}{dV_p}$ in statamps^2/statvolt.

For Neon this expression is:

$$n_i = 4.09 \times 10^{15} \left[\frac{d(I_p^2)}{dV_p}\right]^{\frac{1}{2}}$$

For Argon:

$$n_i = 5.76 \times 10^{15} \left[\frac{d(I_p^2)}{dV_p}\right]^{\frac{1}{2}}$$

For Krypton:

$$n_i = 8.35 \times 10^{15} \left[\frac{d(I_p^2)}{dV_p}\right]^{\frac{1}{2}}$$

where $\frac{d(I_p^2)}{dV_p}$ is in amp^2/volt

(See Figure 51 for a sample plot)

Ion densities computed by this method were found to be greater than the densities obtained from the random electron current and the Druyvesteyn analysis. The ion densities were corrected by a factor $k \sqrt{\frac{T_i}{T_e}}$ similar to that proposed by L. S. Hall /24/, and used by Leonard and Alderson during the previous year's work. In this correction we assumed a constant ion temperature of 1000°K (as did Leonard and Alderson), and for electron temperature used the estimated best value as determined from the two methods described in the electron temperature section of these results. A value of "k"

was then determined for each gas that gave agreement between the ion and electron densities. For Neon "k" was determined to be 0.6, for Argon k = 1.25, and for Krypton k = 1.0. It may be of interest to note that we found $\frac{K_{argon}}{K_{neon}} = 2.08$ while Alderson and Leonard found $\frac{K_{argon}}{K_{neon}} = 2.0$, although the values were determined from experiments performed under different conditions.

With only a few exceptions, excellent agreement was found between the several methods of density determination (Figures 47 through 50). In the maximum interaction region in Krypton (between 28 and 34 volts on Figure 50), the densities as determined by Druyvesteyn analysis and the other methods do not correspond. In Neon (Figures 47 and 48) the densities calculated from observed electron oscillation frequencies do not correlate well with those determined by the other methods, but in this case the oscillations detected were weak and few in number.

Electron Temperature

Plots of electron temperature, expressed as energy, against probe position are shown in Figures 52 through 55. Electron temperatures were determined by the method of Langmuir /3/. In this method the electron temperature is the reciprocal of the slope of the plot of ln Ie vs. Vp. (See Figure 46 for a sample plot).

Average electron temperatures, expressed as energies, were also determined from the energies described by the electron energy distribution functions. These were calculated by numerically integrating the electron energy distribution function as:

$$\overline{eV} = \frac{\int_{V_{p1}}^{V_{p2}} V_p^{3/2} \frac{d^2 I_p}{dV_p^2} \, dV_p}{\int_{V_{p1}}^{V_{p2}} V_p^{1/2} \frac{d^2 I_p}{dV_p^2} \, dV_p}$$

The excellent agreement of the two methods is shown on the plots. The estimated "best value" of electron temperature determined by a visual averaging of the results of the two methods, is also shown.

Electron Energy Distributions.

Electron energy distribution functions for several runs are shown in Figures 56 through 66. These electron energy distribution functions were determined by the method of Druyvestyn /12/ and are obtained from the product $V^{\frac{1}{2}} \frac{d^2 I_p}{dV_p^2}$. This product was plotted against Vp to give the shape of the electron energy distribution function.

Beam electrons were not seen in the runs in Neon as plots appeared to be zero in the region within ten millimeters of the cathode. Beam electrons were not seen in the runs in Argon although very substantial $\frac{d^2 I_p}{dV_p^2}$ plots were obtained in the region near the cathode.

Another form of discharge was observed in Argon by accident in which a definite focused beam type structure was visibly evident. While working with the "normal" diffuse type discharge (at ten microns) the current was increased until the discharge suddenly collapsed. Upon reinitiation, the focused type appeared. (See Figure 41). In this type of discharge the presence of the beam electrons was clearly seen in the $\frac{d^2 I_p}{dV_p^2}$ plot; however, this form of discharge could not be maintained for more than a few minutes, after which time it would gradually change to the more diffuse type that was investigated on our main runs. This effect was produced several times, and during each transition between discharge forms, we observed the disappearance of the beam or high energy electron group (See Figure 67). As a result of the above, we feel that the appearance of the high energy "beam" electrons is a function of the type of discharge investigated.

The beam electrons were observed in Krypton close to the cathode even

though the discharge was of the diffuse appearing type (See Figure 66).

In an attempt to find some plausible explanation for the appearance of the beam in one discharge and not in another, the mean free paths of the electrons were computed for each run by use of Ramsauer's Probability of Collision versus Electron Energy Curves. The mean free path was computed for electrons near the cathode having an energy equal to the cathode-anode potential, and for the random electrons in the positive column having energies as previously determined by computing electron temperature. The results were:

Run	Mean Free Path at Cathode (cm)	Mean Free Path Random Elect. (cm)
19, 21, Neon	8.3	10
39, Argon	1.5	4.5
40, Krypton	1.0	2.7

No obvious conclusions were drawn from the Mean Free Path data except to point out the need for such a mechanism as plasma oscillations to maintain the discharge.

Ion Oscillations

Ion oscillations were detected through out the length of each discharge in all three gases. Photographs of sample oscillations as shown by oscilloscope trace are shown in Figures 68 through 71 for each run. Values of oscillation frequency and amplitude, as calculated from photographs taken at each probe position, are shown on the master data sheets in Figures 8 through 11.

No ion oscillations near the upper frequency limit predicted by Langmuir's relation:

$$f_i = f_e \left(\frac{m_e}{m_i}\right)^{\frac{1}{2}}$$

were detected.

Plots of ion oscillation amplitude, electron oscillation amplitude, and electron density versus probe position, are shown in Figures 72 through 74 for each run.

Electron Oscillations.

Data on the electron oscillations detected is shown on the master data sheets in Figures 8 through 11. Plots of electron density as determined by electron oscillation frequency are shown in Figures 47 through 50. Electron oscillation amplitude, ion oscillation amplitude, and electron density are plotted against probe position for all runs in Figures 72 through 74.

Supplementary runs were made in Argon in which the discharge current was varied while the probe was maintained at one position. The discharge "form" was "diffuse" for these runs. Plots of electron oscillation frequency against discharge current for these runs are shown in Figures 75 and 76. At many discharge currents two, and in some cases three, different frequencies were detected at the same probe position. This appears to be the same result as was reported by Kojima, Kato, and Hagiwara /20/.

The detection of one, two, or three different frequencies at one probe position was also made in Neon at a pressure of 32 microns and discharge current of 50 ma. This discharge had a visible structure with a central region of a convergent beam and a general glow region surrounding it. The probe was moved to the central region, the boundary region between the two different regions, and the outer region, while being kept at the same distance from the cathode. Again different frequencies of oscillation were detected. This is as reported by Kojima, Kato, Hagiwara, and Matsuzaki /21/. A diagram of this discharge form with the frequencies detected is shown in Figure 41.

6. Conclusions.

Based on information obtained from our investigations, our conclusions are as follows:

First, that we have found evidence in Argon of the theory first advanced by Allis /15/ that oscillations are more likely to grow when a beam of electrons is moving down a plasma electron concentration gradient, and that the maximum intensity will occur at the end of such a gradient (See Figure 73). In Krypton (See Figure 74), the evidence is less convincing, since electron energy concentrations as calculated from observed electron oscillation frequencies, random electron current at space potential, and Druyvesteyn analysis, do not coincide in the very region in which we are most interested (the region of maximum interaction). The structure of the electron concentration cruve as determined by Druyvesteyn analysis indicates the effect (See Figure 74), but by other methods it does not. In both Argon and Krypton, however, we find that after the growth of the oscillations to a maximum they decrease in amplitude with an increase in plasma electron concentration.

Dr. K. G. Emeleus has indicated /18/ that structural depressions of the electron concentration versus position curves, occurring near where recorded electron oscillations are strongest, may be due to partial falsification of the probe analyses on account of the oscillating fields in the plasma. He apparently feels that the structural depressions may be due to inaccuracies in the calculation of electron concentrations from space potential determined from the first break from linearity of the ln Ie vs. Vp curves. He feels that space potential so determined may be negative to true space potential. In our work in Argon, however, we find the structural depression

of the concentration curve coinciding with the strongest oscillations, using not only the ln Ie vs. Vp curves for space potential (and therefrom, concentration) calculation, but also using concentrations calculated from observed oscillation frequencies by the relation $fe = 8980\ n^{1/2}$.

Second, that we have shown the existence of multiple (triple) electron oscillation frequencies at various longitudinal probe positions in a diffuse discharge in Argon. Kojima, Kato, and Hagiwara have reported /20/ triple frequencies in a plasma which they theorize correspond to: (1) electron concentration in the center of the beam, (2) electron concentration in the diffuse body of the plasma, and (3) a sheath reasonance effect occuring at the boundary between the two regions. Our observations, though limited in scope, tend to confirm this theory, and indicate the existence of two separate concentrations of electrons even when the beam is not clearly visible, i.e., when we have a "diffuse" type discharge.

Third, that the value of space potential obtained from the point of first break from linearity of the ln Ie-Vp curve is a value closely representing true space potential. While it is true that for both Argon and Krypton this value is slightly (in the majority of cases one volt or less) negative to the value determined by the maximum of the $\frac{dI_p}{dV_p}$ vs. Vp curve, the correlation between the two separately determined values is extremely good. We feel that the two-tangent method for determining space potential gives a relative picture of potential between longitudinal positions in the plasma, but that its absolute values are higher than true space potential in the majority of cases (See Figures 42 through 45). This confirms the conclusions of Nicoll and Basu in their comparison study of micro-wave and Langmuir probe measurements on a gaseous plasma /25/.

Fourth, that ion densities determined by the slope of the Ip^2 vs. Vp curve must be corrected by a factor $k\sqrt{\frac{T_i}{T_e}}$ to yield densities corresponding to electron densities as calculated from observed electron oscillations (and by other methods). The factor "k" differs for each gas, but has no apparent relation to atomic weight.

Fifth, that the ion oscillations detected in the 100 to 150 KC frequency range are the electrostatic sound waves predicted by Langmuir. In a discharge of the form utilized during this work, where the discharge is not confined to the anode-cathode space, the frequency of these oscillations is not a function of the anode to cathode spacing. In a discharge such as ours, where the length of the discharge is not greatly different from the width, no definite conclusion can be made as to whether the transverse, longitudinal, or azimuthal modes have been excited. For example, using the basic Tonks-Langmuir equation.

$$f = \frac{n}{2\ell}\sqrt{\frac{\gamma k T_e}{m_i}}$$

where γ is the adiabatic compression coefficient of the electron gas in the plasma, having values of 3 for the one dimensional case, 1 for the two dimensional case, and 5/3 for the three dimensional case (in our work we used the value 5/3, as the most representative). $\frac{n}{2\ell}$ is $1/\lambda$ where λ is the wavelength of the ion wave.

and (1) assuming that a longitudinal mode has been excited, we can obtain close agreement between observed and calculated ion frequencies from our data by using values of ℓ, n, and γ as follows.

RUN	GAS	ℓ	n	γ	Calc. Freq.	Observed Frequency
19	Neon	10 cm	2	5/3	139KC	135KC
21	Neon	10 cm	2	5/3	133KC	125KC
39	Argon	10 cm	4	5/3	151KC	145KC
40	Krypton	10 cm	4	5/3	156KC	145KC

or (2) assuming that a transverse mode has been excited, we can obtain close agreement between observed and calculated frequencies by using the following values:

RUN	GAS	ℓ	n	γ	Calc. Freq.	Observed Frequency
19	Neon	5.5 cm	1	5/3	126KC	135KC
21	Neon	5.5 cm	1	5/3	121KC	125KC
39	Argon	5.5 cm	2	5/3	137KC	145KC
40	Krypton	5.5 cm	3	5/3	141KC	145KC

Since 10 cm is the approximate length of all our discharges, and 5.5 cm is the approximate discharge diameter, the observed data can be "made" to fit either situation by an auspicious selection of "n". According to Alexeff and Neidigh /22/ the effect of gas damping of ionic sound oscillations can be serious at 10 microns pressure, and at the higher gas densities the fundamental mode may be prevented from appearing while higher overtones may be detected. This could possibly account for the differing values of "n" between gases.

An attempt was also made to correlate frequencies under the assumption that azimuthal modes had been excited, using the relation used by Alexeff and Neidigh /22/:

$$f = \frac{n}{cd}\sqrt{\frac{\gamma k T_e}{m_i}}$$

where: d = discharge diameter
c = dimensionless constant of 1.00 or 1.51, depending on the boundary conditions
n = constant which varies depending on the particular overtone excited

In this case, we found that at a given probe position, using the electron temperature previously calculated, we could select values of n and c to make the computed frequency agree with that observed. We then attempted

to get similar agreement at other probe positions, however, using the values of n and c already selected, the calculated frequency at any other position, since it was dependent on its electron temperature, could not be made to agree with the observed. Several selections of n and c were made in combination for various probe positions, but still no obvious correlation could be obtained.

For this reason, we conclude that the frequencies are due to electrostatic sound waves, but that the mode is not determinable in our case. Our information does tend toward either a longitudinal or transverse mode, however.

7. Recommendations.

Based on results obtained from our investigation, the following recommendations are offered for future work:

(1) Continue investigation of rare gas plasmas, including Xenon, at various other pressures, discharge currents, and anode-cathode spacings.

(2) Investigate in detail the apparent correlation between oscillation amplitude and electron density, calculating density primarily from oscillation frequencies.

(3) Investigate in detail the occurrence of triple oscillation frequencies and their amplitudes, by moving the probe in and out of the discharge.

(4) Investigate ion oscillation frequencies in tubes of differing length to width ratios.

(5) Determine the cause for the existence or non-existence of high energy "beam" electrons in Argon, that apparently depends upon mode of discharge.

(6) Investigate effects of imposed magnetic fields on oscillations and plasma parameters.

Figure 1. Photograph of Equipment Components

Figure 2. Photograph of General Arrangement of Laboratory Equipment

Figure 3. Photograph of General Arrangement of Laboratory Equipment

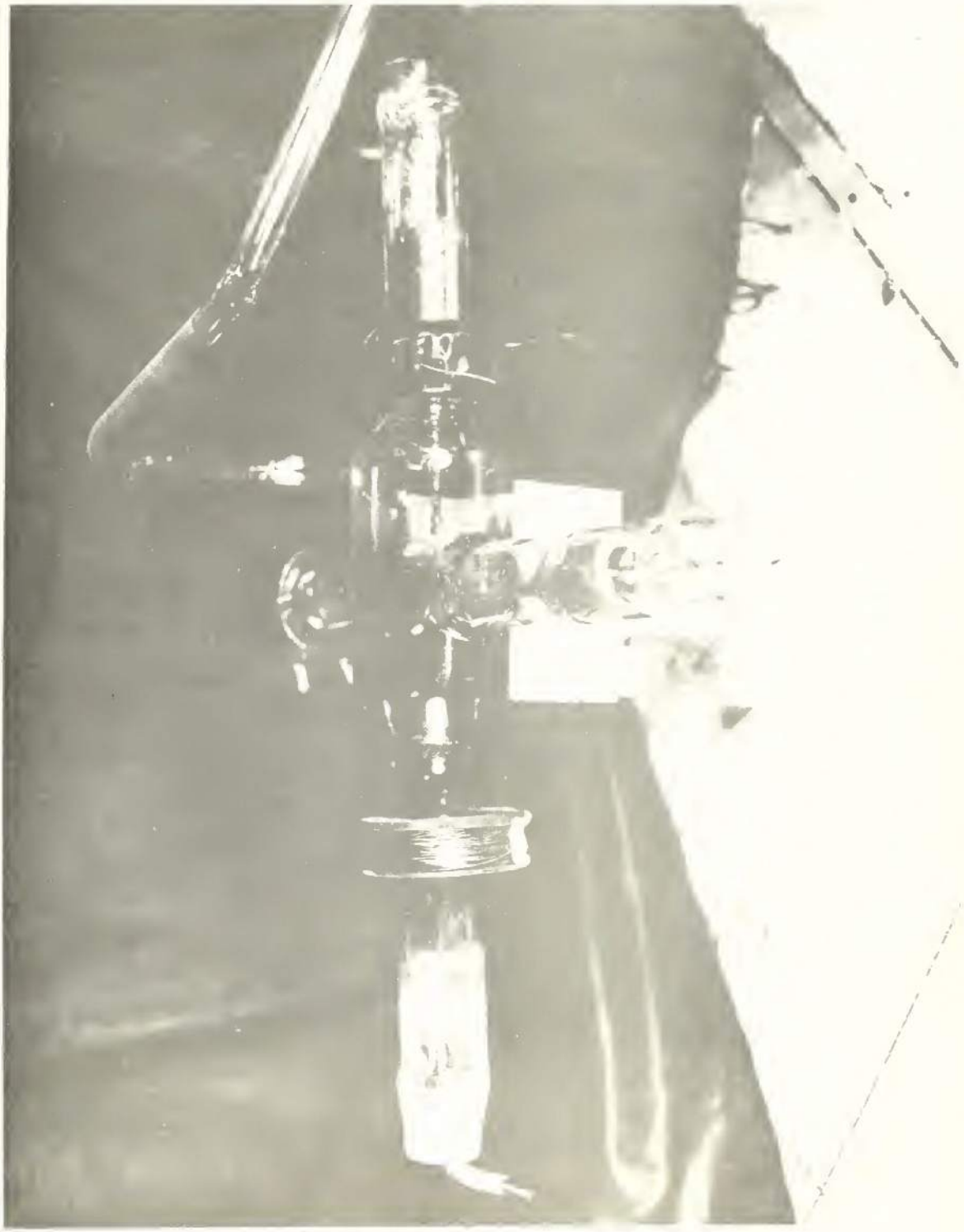

Figure 4. Photograph of Discharge Tube

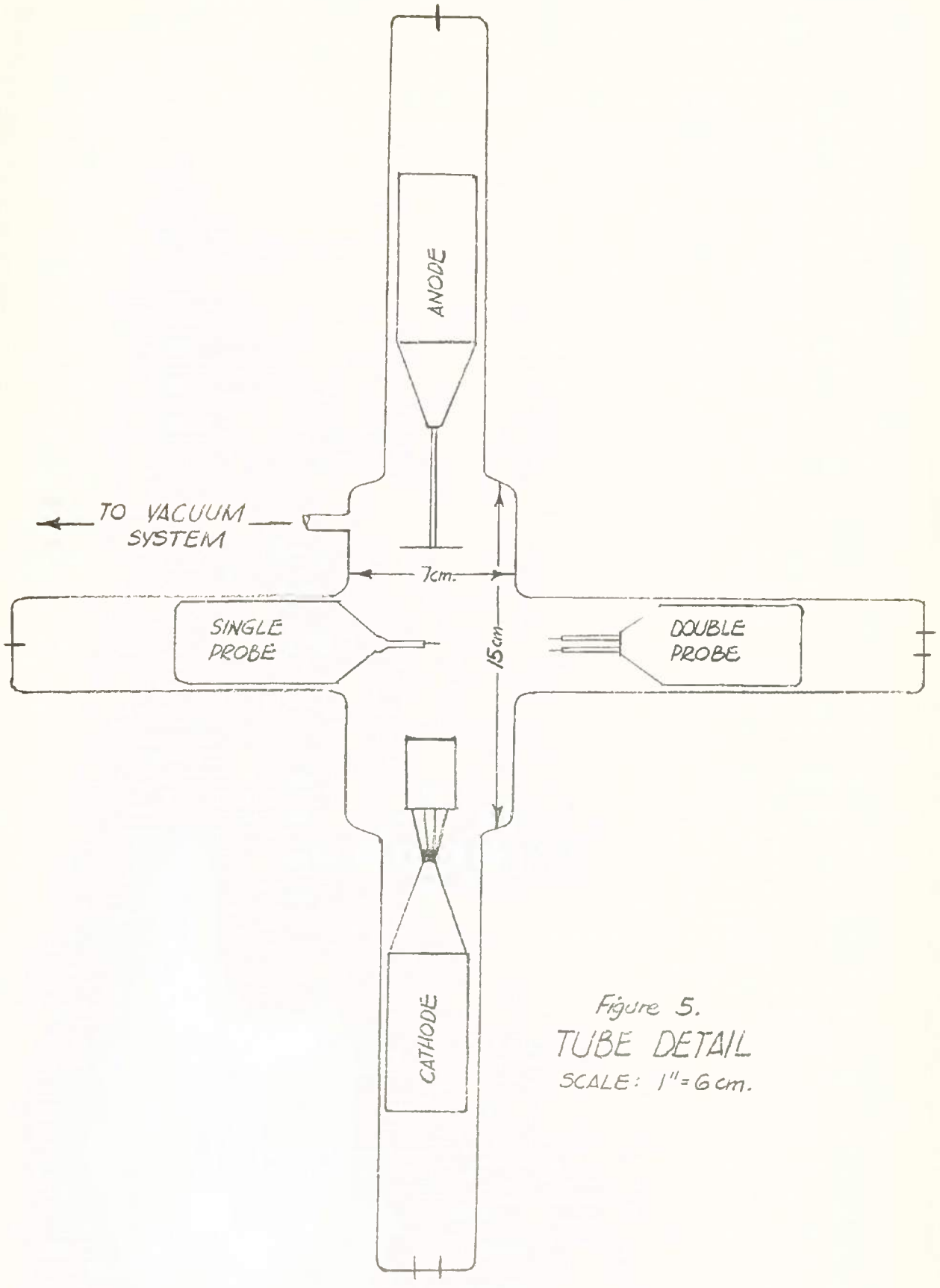

Figure 5.
TUBE DETAIL
SCALE: 1" = 6 cm.

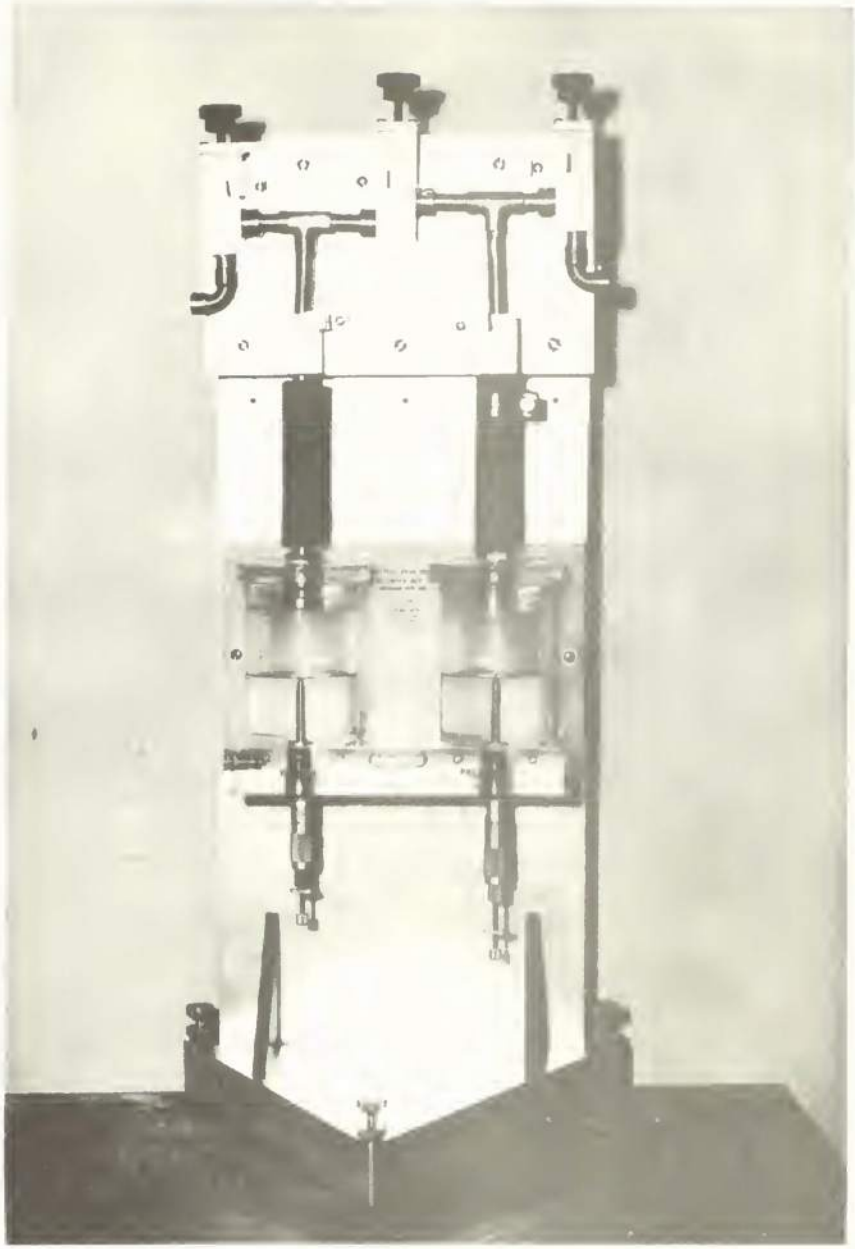

Figure 6. Photograph of Modified Hook Gauge

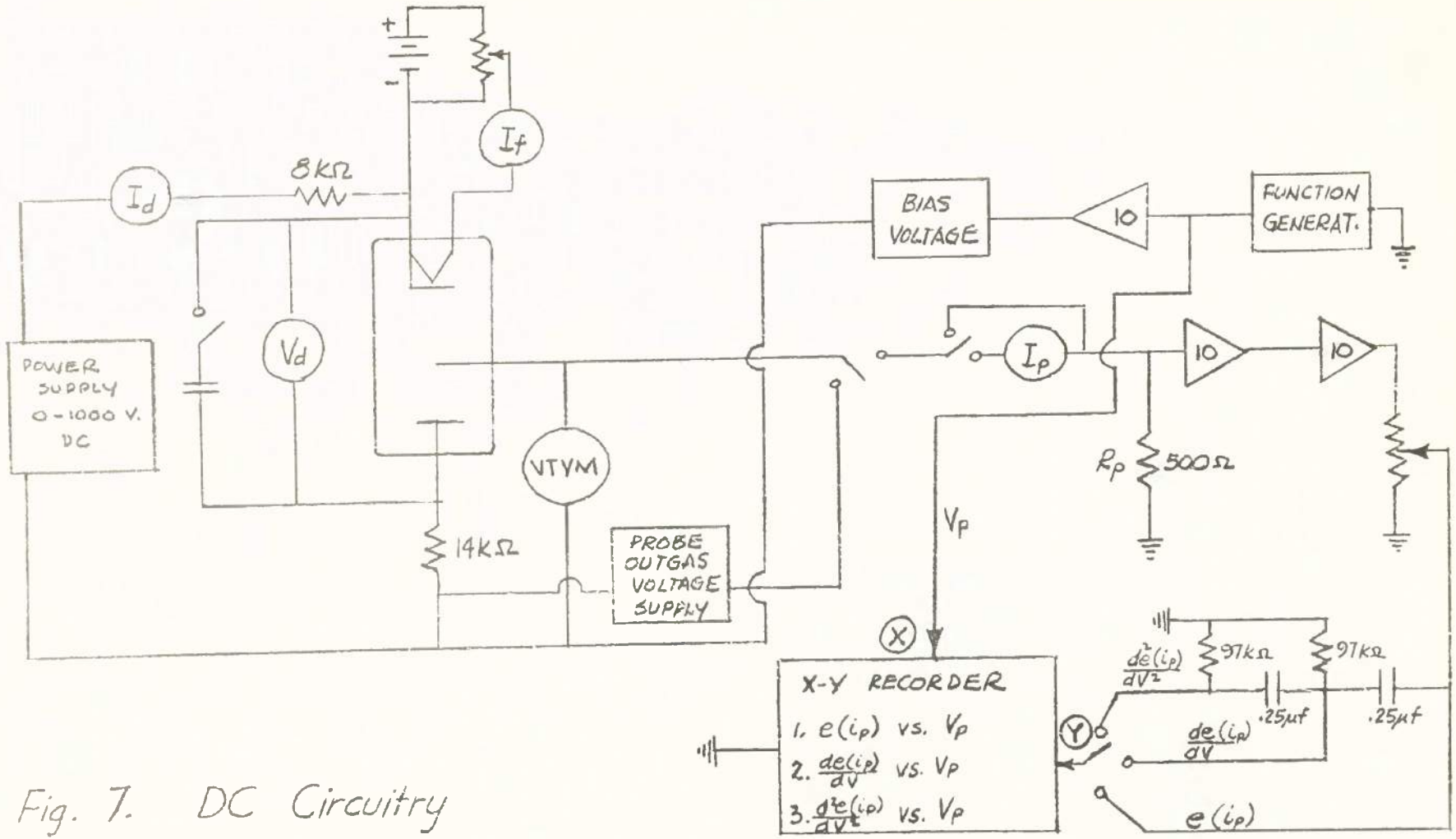

Fig. 7. DC Circuitry

SUB RUN	PROBE-ANODE SPACING (mm)	SPACE POTENTIAL			ELECTRON TEMPERATURE			ELECTRON DENSITY			ION DENSITY		ELECTRON OSCILLATIONS		ION OSCILLATIONS	
		$\frac{dI}{dV}$ max	$Ln I_p - V_p$ (break fm. linear)	Best Value	Slope $Ln I_p - V_p$	(eV) Druyv.	Best Value	Random E.C.	Druyv.	Calc. fm. Osc.	$\frac{dI^2}{dV_p}$	$\times k\sqrt{\frac{T_i}{T_e}}$	AMPLITUDE (AMPS)	FREQ (MC)	AMPLITUDE (MV)	FREQ (KC)
19.1	2	-2.0	+1.0	-0.7	5.95	5.07	5.45	4.94×10^{8}	4.43×10^{8}	5.16×10^{9}	4.92×10^{9}	3.72×10^{8}	3×10^{-12}	645	7	143
19.2	4	-2.0	-2.0	-2.0	5.54	3.98	5.10	4.22×10^{8}	5.35×10^{8}	5.08×10^{9}	8.1×10^{9}	6.31×10^{8}	1.5×10^{-12}	641	8	147
19.3	7	-2.0	-2.5	-2.2	4.37	4.88	4.60	4.04×10^{8}	3.83×10^{8}	—	8.69×10^{9}	7.15×10^{8}	-	-	8	143
19.4	9	-3.0	-5.0	-4.0	5.50	6.50	5.90	3.49×10^{8}	6.83×10^{8}	—	10.33×10^{9}	7.51×10^{8}	-	-	8	143
19.5	14.5	-3.0	-1.7	-2.3	6.40	5.05	5.80	3.79×10^{8}	5.50×10^{8}	5.10×10^{9}	9.67×10^{9}	7.09×10^{8}	1.6×10^{-12}	642	12	143
19.6	19.7	-3.5	-2.3	-2.7	5.95	5.46	5.70	3.51×10^{8}	5.45×10^{8}	5.06×10^{9}	9.63×10^{9}	7.11×10^{8}	1.0×10^{-12}	639	11	143
19.7	24.6	-4.0	-5.0	-4.5	5.96	6.60	6.30	3.64×10^{8}	6.90×10^{8}	—	8.72×10^{9}	6.12×10^{8}	-	-	2	125
19.8	29.8	-4.0	-6.0	-4.9	6.85	6.06	6.40	3.04×10^{8}	5.80×10^{8}	—	6.98×10^{9}	4.87×10^{8}	-	-	3	119
19.9	34.8	-4.0	-3.0	-3.5	10.92	-	10.92	1.96×10^{8}	—	—	4.29×10^{9}	2.29×10^{8}	-	-	8	119

PAGE 45

FIG. 8 RUN 19 / NEON / Pressure: 10 microns / Anode - Cathode Spacing: 40mm / I_d = 30 ma /

SUB RUN	PROBE-ANODE SPACING (mm)	SPACE POTENTIAL			ELECTRON TEMPERATURE			ELECTRON DENSITY			ION DENSITY		ELECTRON OSCILLATIONS		ION OSCILLATIONS	
		$\frac{dI}{dV}$ max	$\ln I_p - V_p$ (break in slope)	Best Value	Slope $\ln I_p - V_p$	(eV) Druyv.	Best Value	Random E.C.	Druyv.	Calc. fm. Osc.	$\frac{dI^2}{dV_p}$	$\times k\sqrt{\frac{T_i}{T_e}}$	AMPLITUDE (AMPS)	FREQ. (MC)	AMPLITUDE (MV.)	FREQ. (KC)
21.1	2	+5.0	+3.3	+4.2	4.47	3.02	3.70	4.88×10^{6}	5.05×10^{8}	4.33×10^{8}	4.15×10^{9}	3.81×10^{8}	1.0×10^{-8}	187	6	114
21.2	4	+6.0	+3.5	+4.75	4.67	4.95	4.85	6.0×10^{8}	9.68×10^{8}	—	6.25×10^{9}	4.98×10^{8}	—	—	6	114
21.3	5.8	+4.5	+3.0	+3.65	4.35	2.58	3.55	5.1×10^{8}	3.92×10^{8}	—	7.53×10^{9}	7.04×10^{8}	—	—	8	114
21.4	10	+5.2	+3.5	+4.40	5.36	4.31	4.80	4.69×10^{8}	6.35×10^{8}	—	7.37×10^{9}	5.21×10^{8}	—	—	10	147
21.5	16	+5.0	+2.0	+3.56	4.45	4.35	4.40	5.62×10^{8}	5.66×10^{8}	11.1×10^{8}	7.60×10^{9}	6.38×10^{8}	6×10^{-12}	300	10	143
21.6	22	+5.0	+1.5	+3.58	5.10	4.80	5.10	5.2×10^{8}	6.14×10^{8}	11.1×10^{8}	7.02×10^{9}	5.47×10^{8}	17×10^{-12}	300	6	119
21.7	29.8	+5.0	+2.5	+3.60	6.04	-	6.04	4.12×10^{8}	4.15×10^{8}	12.75×10^{8}	5.56×10^{9}	3.97×10^{8}	4×10^{-12}	321	2	122
21.8	35.7	+12.0	+5.5	+9.0	13.27	-	13.27	2.90×10^{8}	—	12.75×10^{8}	2.54×10^{9}	1.23×10^{8}	3×10^{-12}	321	3	125
21.9	37.7	—	+5.0	+9.0	17.85	—	17.85	2.20×10^{8}	—	—	2.83×10^{9}	1.17×10^{5}	-	-	16	147
21.10	11.6	+5.0	+2.0	+3.55	4.75	-	4.75	6.39×10^{8}	-	-	10.53×10^{9}	8.59×10^{8}	-	-	6	119
21.11*	51.6	-	+3.4	+3.4	4.48	-	4.48	7.95×10^{8}	-	-	9.41×10^{9}	7.83×10^{8}	-	-	8	116
21.12**	1.6	-	+4.0	+4.0	5.81	-	5.81	5.59×10^{8}	-	-	5.37×10^{9}	3.92×10^{8}	-	-	8	115

NOTE — ANODE - CATHODE SPACING, 80mm.
** ANODE - CATHODE SPACING, 30mm.

FIG. 9 RUN 21 / NEON / Pressure: 10 microns / Anode - Cathode Spacing: 40 mm / I_d = 30 ma /

RUN	ANODE SPACING (mm)	SPACE POTENTIAL $\frac{dI}{dV}$ max.	SPACE POTENTIAL $\ln I_p - V_p$ (break fm. linear)	SPACE POTENTIAL Best Value	ELECTRON TEMPERATURE Slope $\ln I_p - V_p$	ELECTRON TEMPERATURE (eV) Druyv.	ELECTRON TEMPERATURE Best Value	ELECTRON DENSITY Random E.C.	ELECTRON DENSITY Druyv.	ELECTRON DENSITY Calc. fm. Osc.	ION DENSITY $\frac{dI^2}{dV_p}$	ION DENSITY $\times k\sqrt{T_i/T_e}$	ELECTRON OSCILLATIONS AMPLITUDE (AMPS)	ELECTRON OSCILLATIONS FREQ. (MC)	ION OSCILLATIONS AMPLITUDE (MV)	ION OSCILLATIONS FRLQ. (KC)
39.1	2.0	-2.5	-2.5	-2.5	2.77	2.70	2.73	4.62×10^{9}	3.36×10^{9}	–	–	–	–	–	6	147
39.2	4.8	-2.0	-2.0	-2.0	2.86	3.10	3.00	5.56×10^{9}	5.10×10^{9}	–	2.46×10^{10}	5.19×10^{9}	–	–	7	147
39.3	7.5	-2.0	-2.5	-2.2	2.54	3.32	2.92	6.21×10^{9}	5.92×10^{9}	–	2.54×10^{10}	5.46×10^{9}	–	–	10	147
39.4	9.9	-2.0	-2.5	-2.2	2.66	3.17	2.90	6.78×10^{9}	6.34×10^{9}	–	2.51×10^{10}	5.42×10^{9}	–	–	11	143
39.5	12.5	-1.6	-2.5	-2.1	2.56	3.12	2.85	7.70×10^{9}	6.81×10^{9}	–	2.92×10^{10}	6.35×10^{9}	–	–	14	143
39.6	15.4	-1.5	-1.5	-1.5	2.94	3.22	3.08	8.51×10^{9}	7.32×10^{9}	9.05×10^{9}	3.70×10^{10}	7.75×10^{9}	7×10^{-12}	855	16	143
39.7	18.0	-1.6	-2.0	-1.8	2.89	3.01	3.00	8.48×10^{9}	7.09×10^{9}	8.92×10^{9}	3.97×10^{10}	8.40×10^{9}	3×10^{-11}	843	24	143
39.8	20.4	-1.7	-1.7	-1.7	3.18	3.66	3.40	8.09×10^{9}	7.40×10^{9}	8.72×10^{9}	4.19×10^{10}	8.35×10^{9}	8×10^{-10}	839	35	143
39.9	22.7	-1.5	-2.5	-2.0	2.94	3.54	3.25	7.74×10^{9}	6.70×10^{9}	7.36×10^{9} 8.33×10^{9} 6.85×10^{9}	4.04×10^{10}	8.33×10^{9}	4×10^{-8} 4×10^{-7} 2×10^{-7}	771 820 845	70	143
39.10	24.6	-1.5	-2.5	-2.0	3.53	3.92	3.80	7.19×10^{9}	6.94×10^{9}	8.09×10^{9}	3.65×10^{10}	6.85×10^{9}	3×10^{-6}	808	90	143
39.11	27.4	-1.5	-0.8	-2.0	4.25	5.18	4.70	7.0×10^{9}	7.85×10^{9}	6.66 7.22×10^{9}	4.36×10^{10}	7.36×10^{9}	4×10^{-7} 3×10^{-6}	733 800	80	147
39.12	30.3	-2.0	-3.0	-2.4	4.35	3.25	3.75	6.84×10^{9}	5.69×10^{9}	6.09 8.14×10^{9}	4.22×10^{10}	8.0×10^{9}	3×10^{-7} 1×10^{-6}	699 810	80	147
39.13	32.5	-1.8	-1.8	-1.8	3.05	2.97	3.00	8.75×10^{9}	6.01×10^{9}	–	4.44×10^{10}	9.4×10^{9}	–	–	70	143
39.14	35.6	-2.0	-2.5	-2.2	3.04	2.65	2.85	7.12×10^{9}	4.21×10^{9}	–	3.44×10^{10}	7.49×10^{9}	–	–	70	143

PAGE 47

FIG. 10 RUN 39 / ARGON / Pressure: 10 microns / Anode - Cathode Spacing: 40 mm / I_d = 99.5 ma /

SUB RUN	PROBE-ANODE SPACING (mm)	SPACE POTENTIAL			ELECTRON TEMPERATURE (eV)			ELECTRON DENSITY			ION DENSITY		ELECTRON OSCILLATIONS		ION OSCILLATIONS		
		$\frac{dI}{dV}$ max.	$\ln I_p - V_p$ (break fm. linear)	Best Value	Slope $\ln I_p - V_p$	Druyv.	Best Value	Random E.C.	Druyv.	Calc. fm. Osc.	$\frac{dI^2}{dV_p} \times k\sqrt{\frac{T_i}{T_e}}$		AMPLITUDE (AMPS)	FREQ (Mc)	AMPLITUDE (MV)	FREQ (KC)	
40.1 *	37.2	-10	-10.5	-10.2	5.59	-	5.59	2.41×10^{8}	—	—	4.69×10^{10}	5.84×10^{9}	-	-	900	119	
40.2 *	35.5	+1.0	-6.0	-2.5	6.75	-	6.75	4.55×10^{9}	—	—	1.03×10^{10}	1.17×10^{9}	—	-	600	147	
40.3	33.4	+1.0	0	+0.5	3.11	5.74	4.50	6.59×10^{9}	11.2×10^{9}	5.47×10^{9}	5.01×10^{10}	6.93×10^{9}	3×10^{-12}	665	16	122	
40.4	31.6	+2.0	0	+1.1	3.19	6.52	4.70	7.86×10^{9}	14.03×10^{9}	6.59×10^{9} 8.04×10^{9}	4.09×10^{10}	5.54×10^{9}	5×10^{-9} 2×10^{-8}	729 806	16	119	
40.5	29.6	+2.0	+1.4	+1.7	4.34	6.00	5.20	8.75×10^{9}	12.7×10^{9}	8.77×10^{9}	5.06×10^{10}	6.65×10^{9}	2×10^{-6}	841	90	147	
40.6	27.6	+2.0	+1.3	+1.8	3.83	3.58	3.70	10.62×10^{9}	8.89×10^{9}	12.2×10^{9}	6.32×10^{10}	9.63×10^{9}	1.5×10^{-7}	992	50	147	
40.7	24.9	+2.5	+1.5	+2.0	3.40	3.85	3.65	11.8×10^{9}	11.6×10^{9}	7.73×10^{9} 9.02×10^{9}	5.95×10^{10}	9.14×10^{9}	3×10^{-7} 1.6×10^{-6}	790 854	35	147	
40.8	22.6	+2.2	+1.3	+1.9	2.97	3.29	3.10	12.57×10^{9}	10.46×10^{9}	12.51×10^{9}	5.78×10^{10}	9.58×10^{9}	1×10^{-9}	1004	24	143	
40.9	18.8	+2.0	+1.5	+1.8	3.06	3.39	3.25	12.02×10^{9}	10.48×10^{9}	—	7.1×10^{10}	11.57×10^{9}	—	—	18	143	
40.10	11.4	+2.0	+1.5	+1.8	2.96	3.14	3.05	10.32×10^{9}	8.61×10^{9}	—	3.88×10^{10}	6.52×10^{9}	—	—	7	147	
40.11	2.8	0	0	0	2.40	2.75	2.60	5.82×10^{9}	5.46×10^{9}	—	3.68×10^{10}	6.70×10^{9}	—	—	7	147	

NOTE * $T_i = 90.5$ ev.

FIG. 11 RUN 40 / KRYPTON / Pressure: 10 microns / Anode - Cathode Spacing: 40 mm / I_d = 115 ma /

Fig 12. NEON RUN 19.1

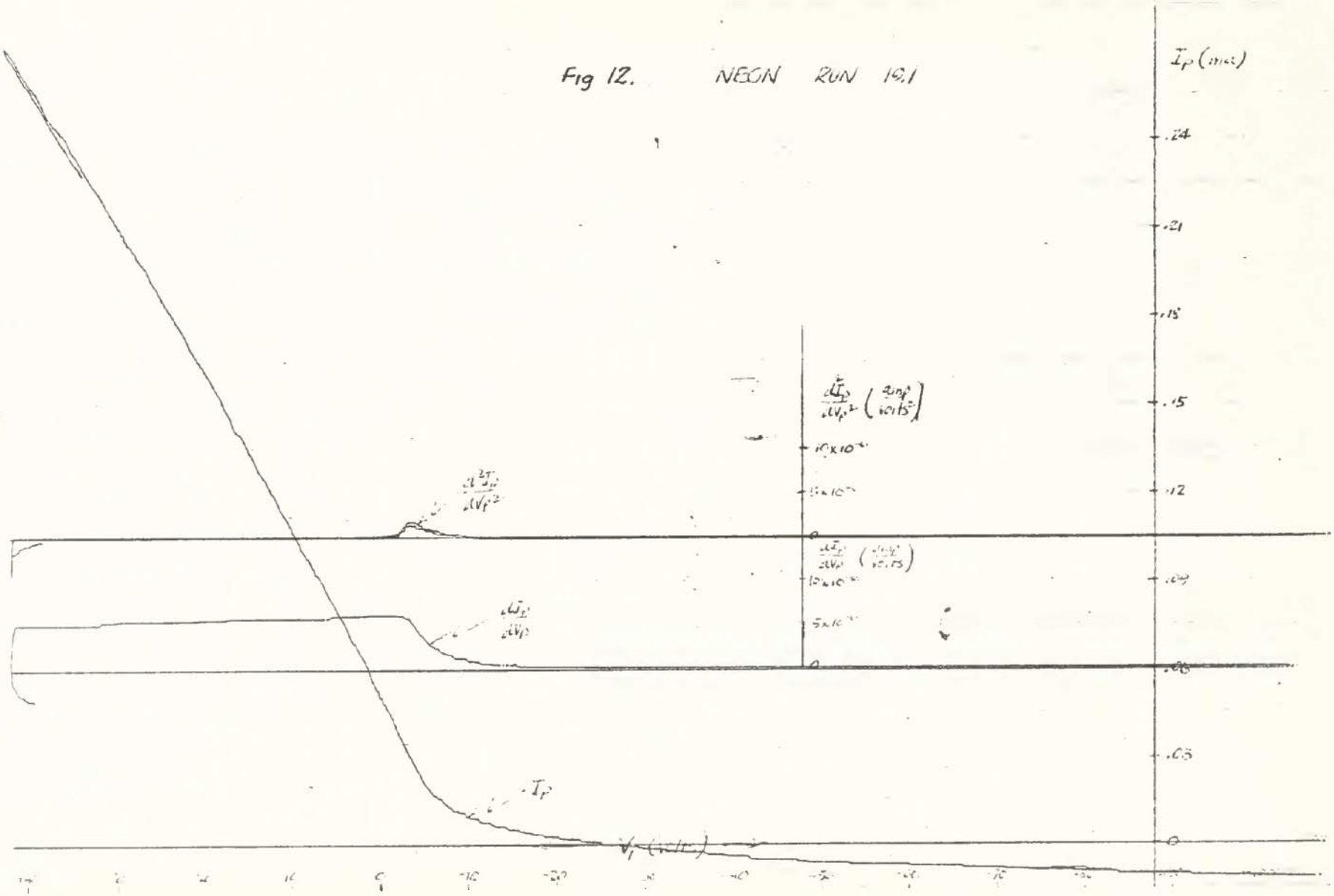

Fig. 13 NEON RUN 19.4

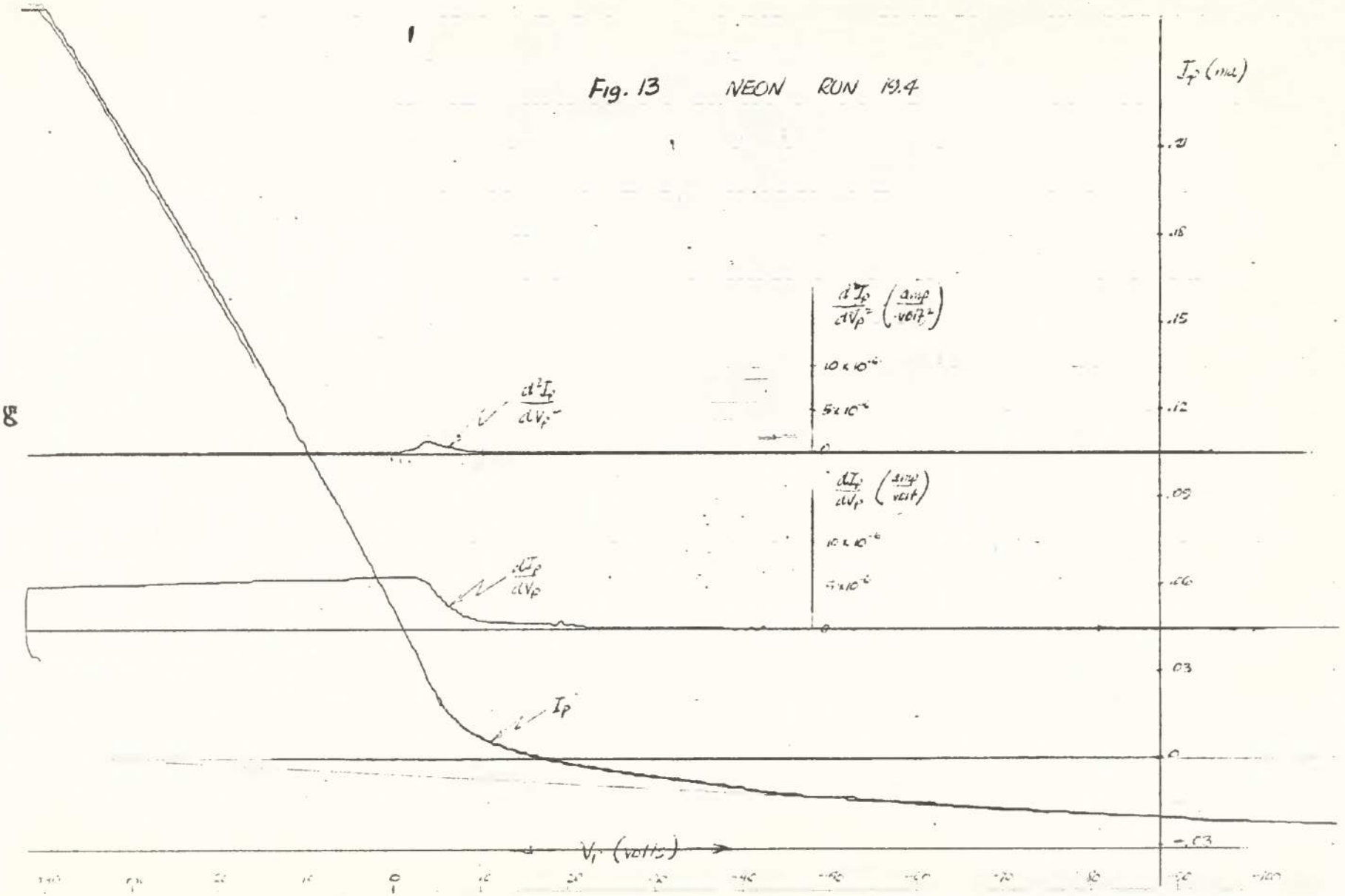

Fig. 14 NEON RUN 19.7

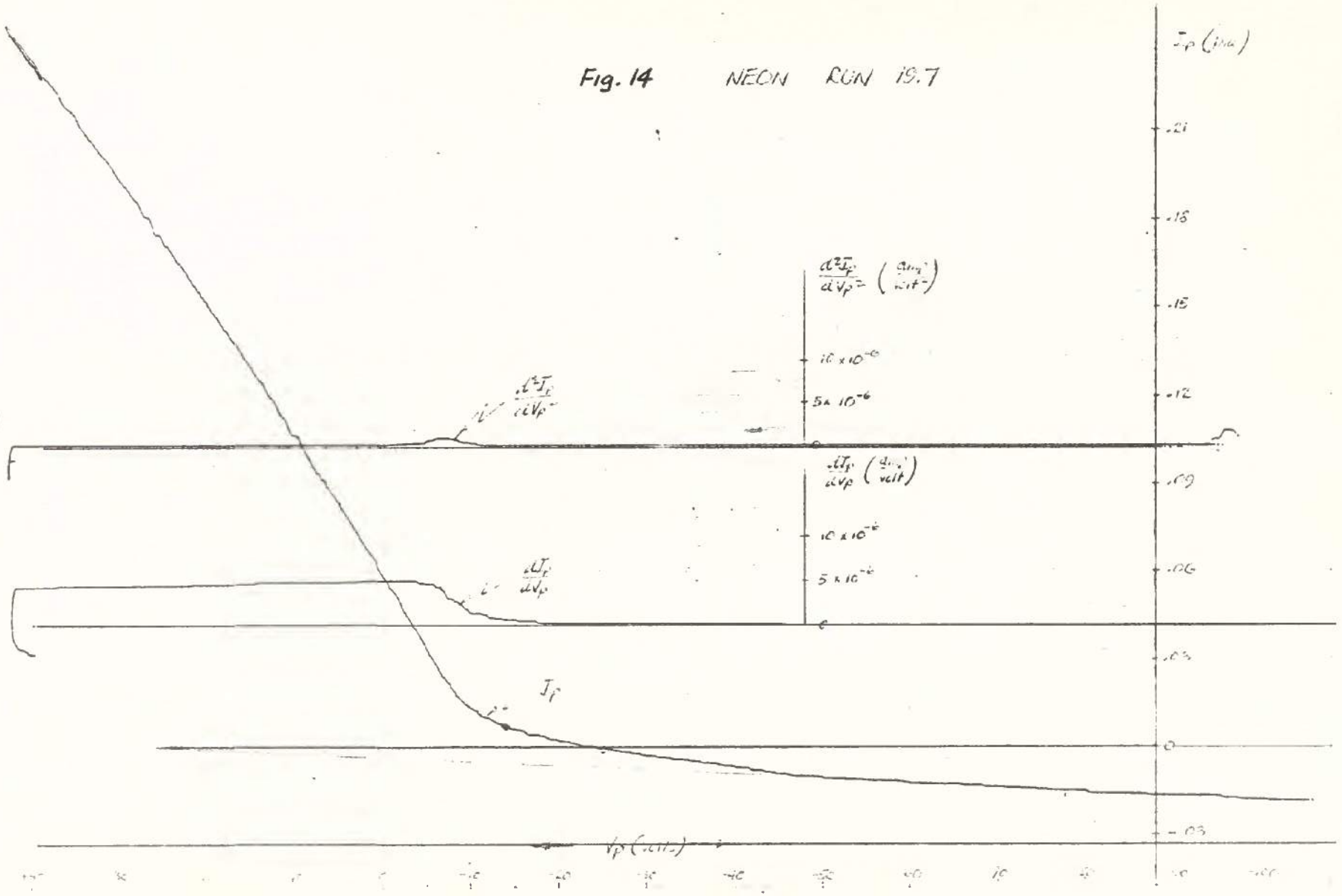

Fig. 15 NEON RUN 19.9

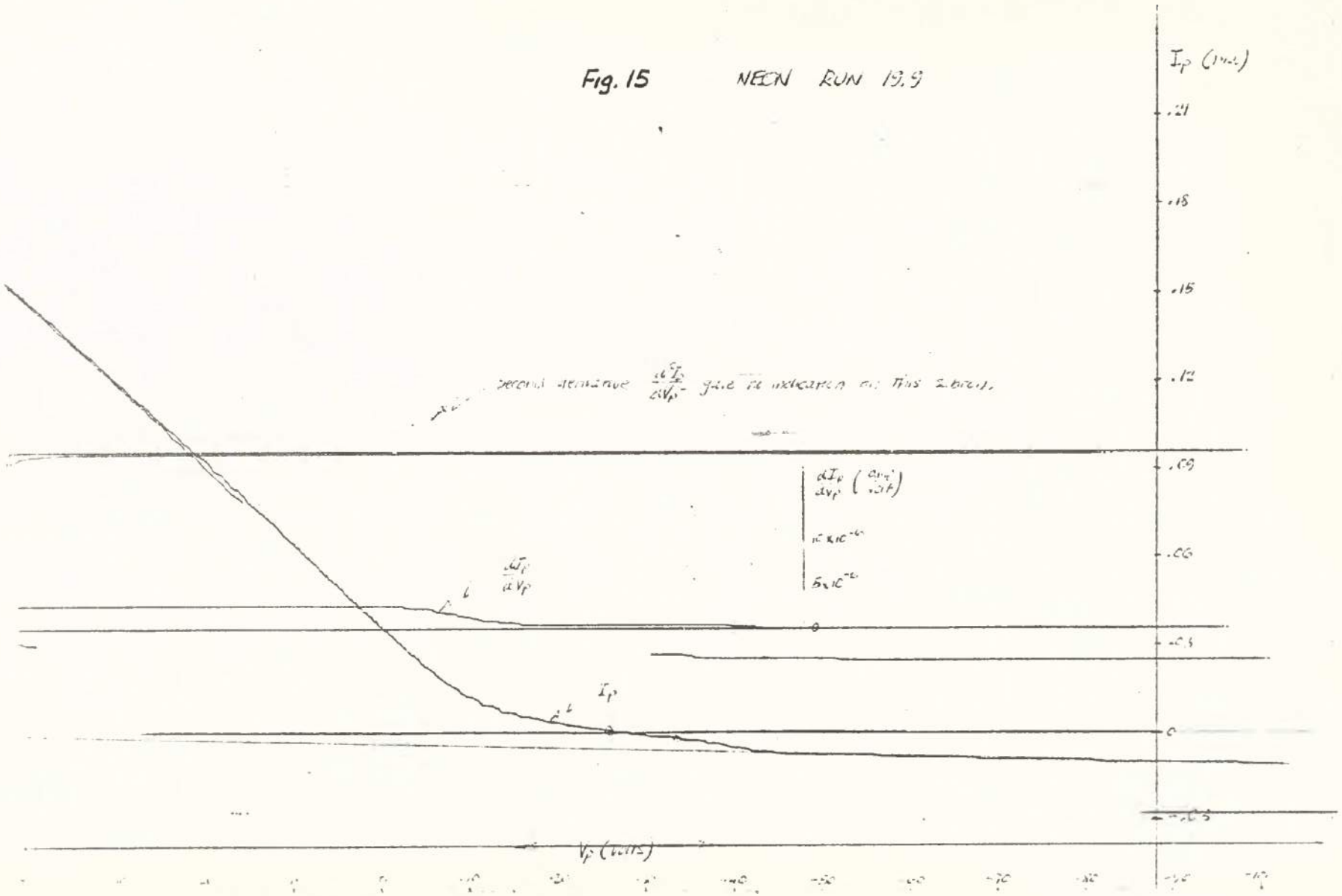

Fig. 16 NEON RUN 21.1

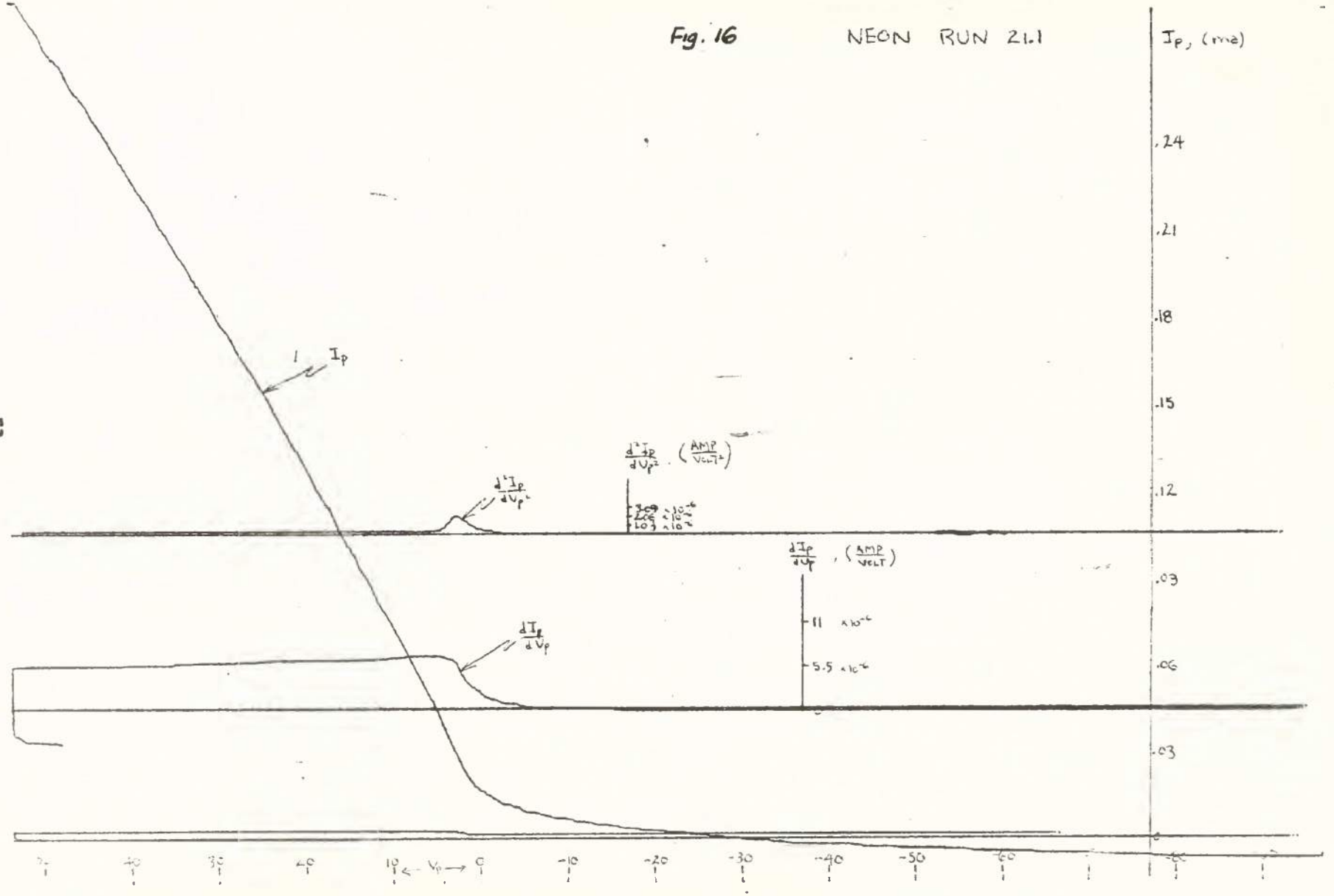

Fig. 17 NEON RUN 21.4

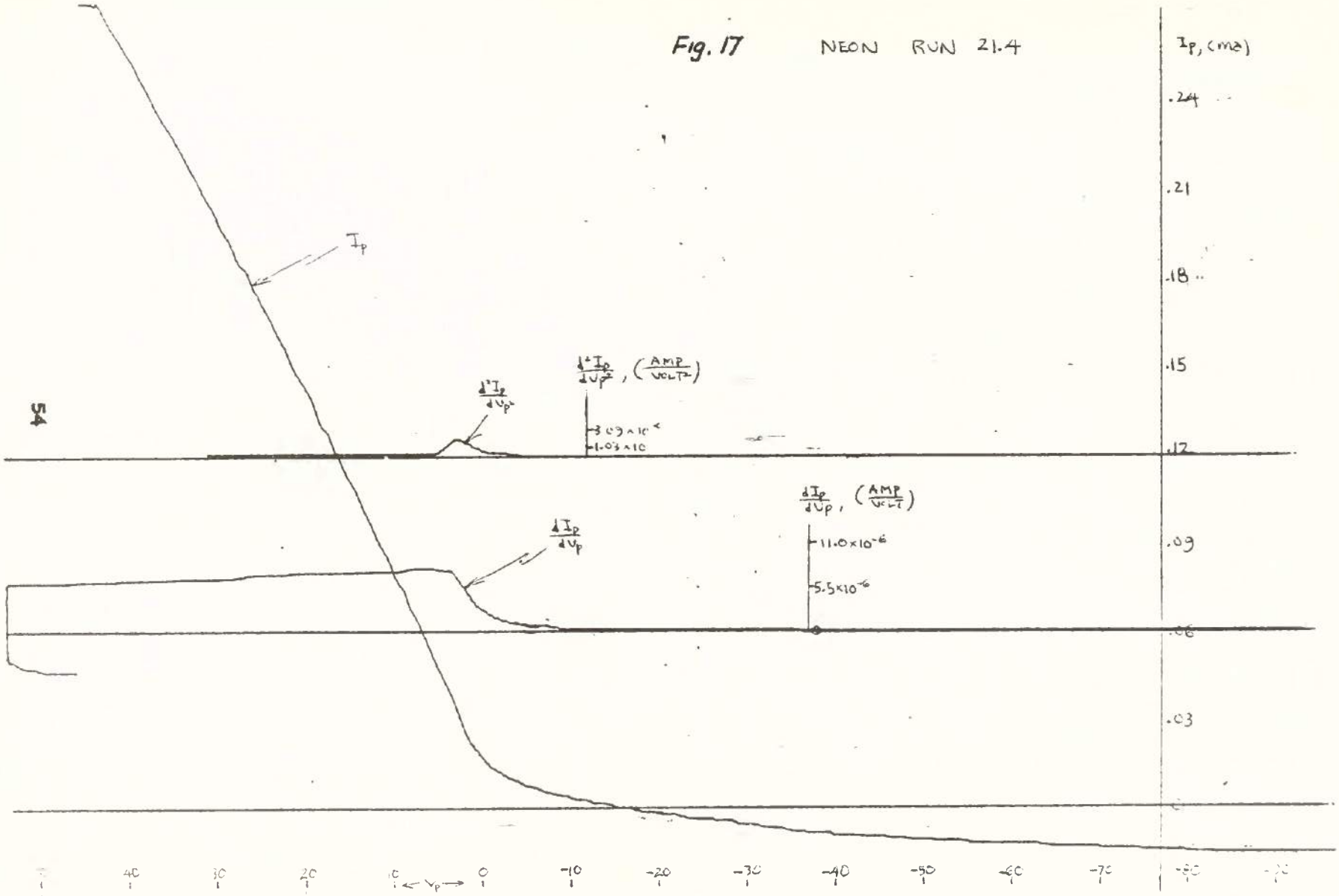

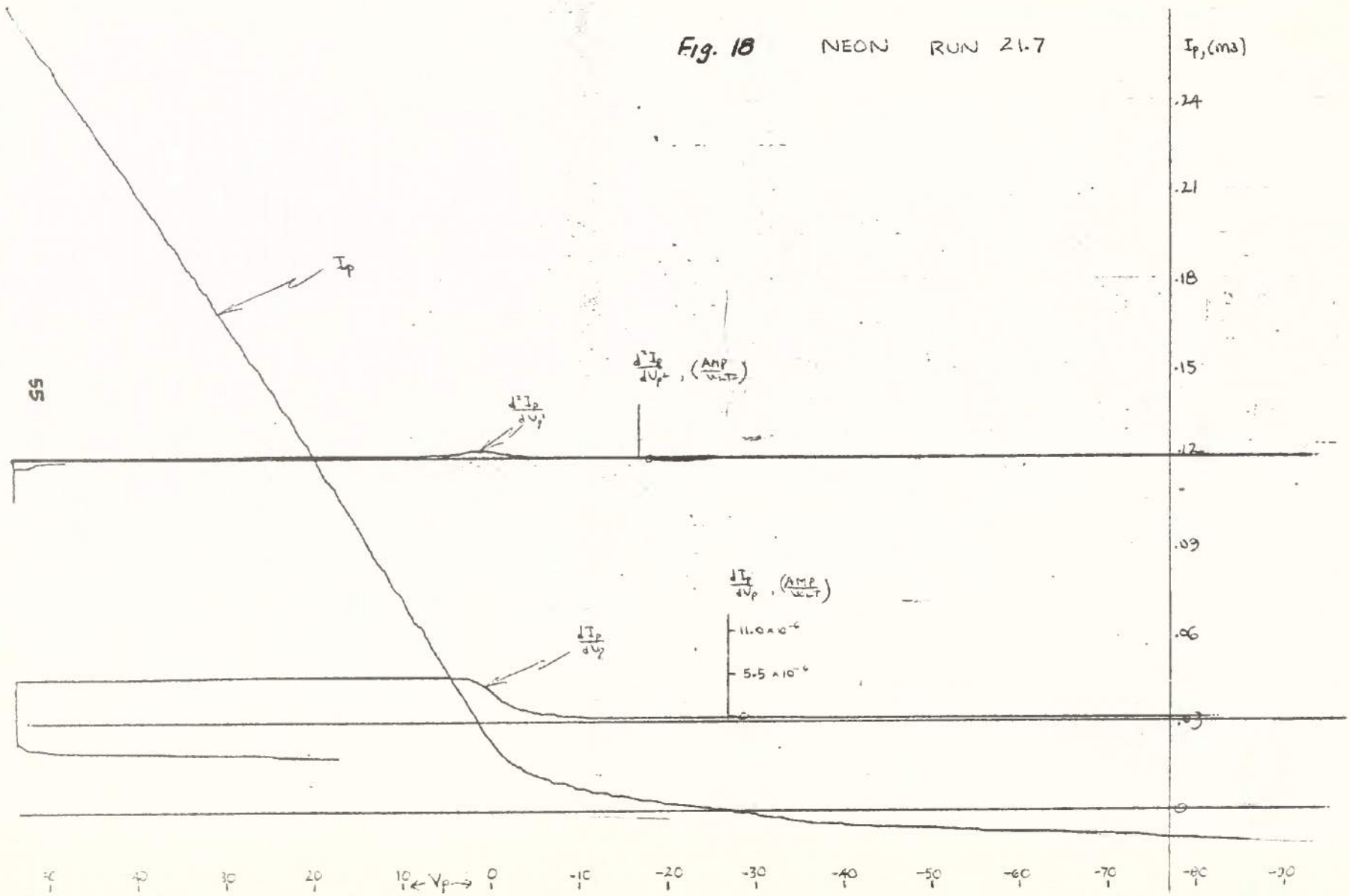
Fig. 18 NEON RUN 21.7
I_p, (ma)
.24
.21
.18
.15
.12
.09
.06
.03
0
SS
I_p
$\frac{d^2 I_p}{dV_p^2}$, $\left(\frac{AMP}{VOLT}\right)$
$\frac{d^2 I_p}{dV_p^2}$
$\frac{dI_p}{dV_p}$, $\left(\frac{AMP}{VOLT}\right)$
11.0×10^{-6}
5.5×10^{-6}
$\frac{dI_p}{dV_p}$
40 30 20 10 $\leftarrow V_p \rightarrow$ 0 -10 -20 -30 -40 -50 -60 -70 -80 -90

Fig. 19 NEON RUN 21.8

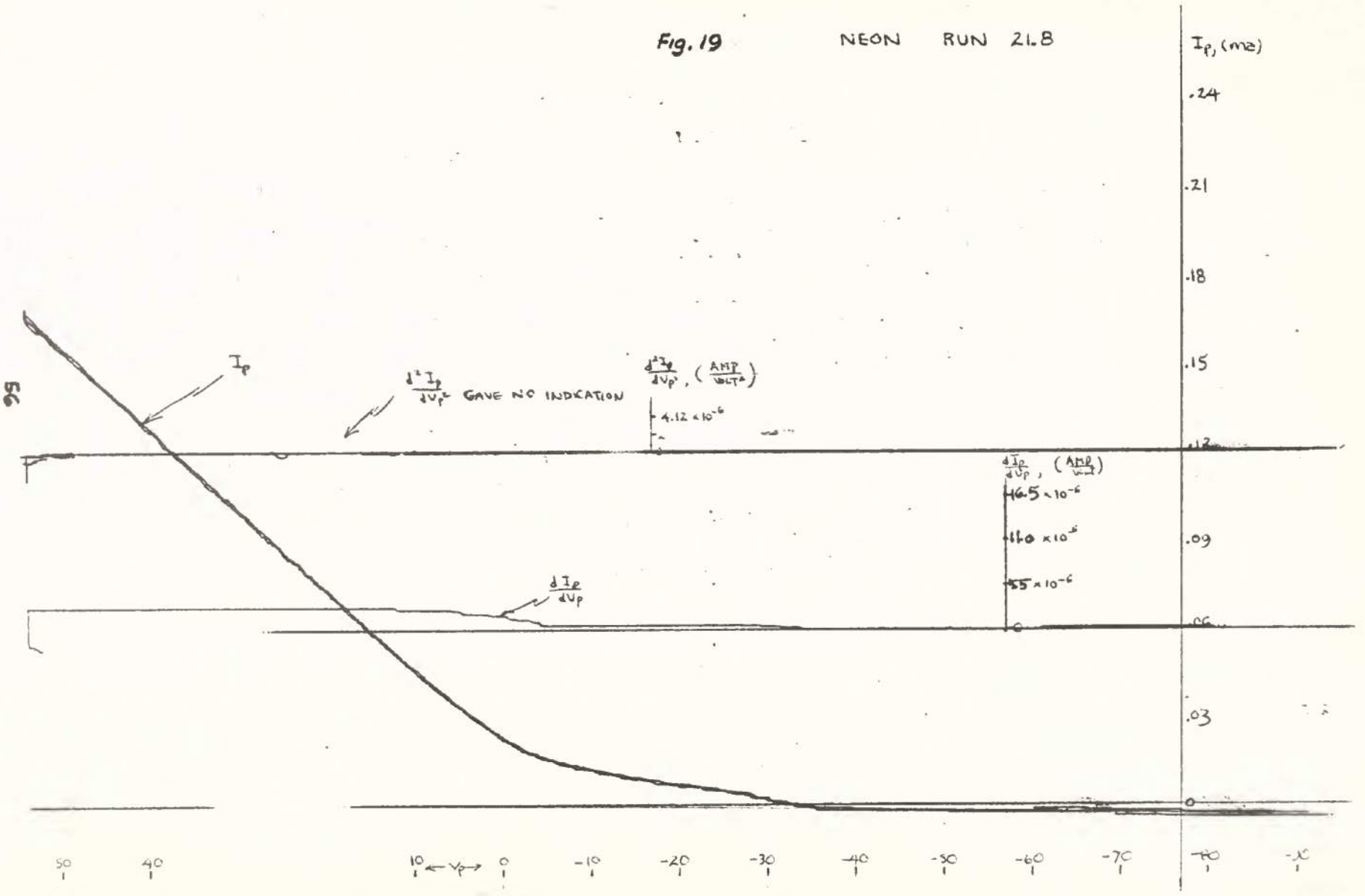

Fig. 20 ARGON RUN 39.1

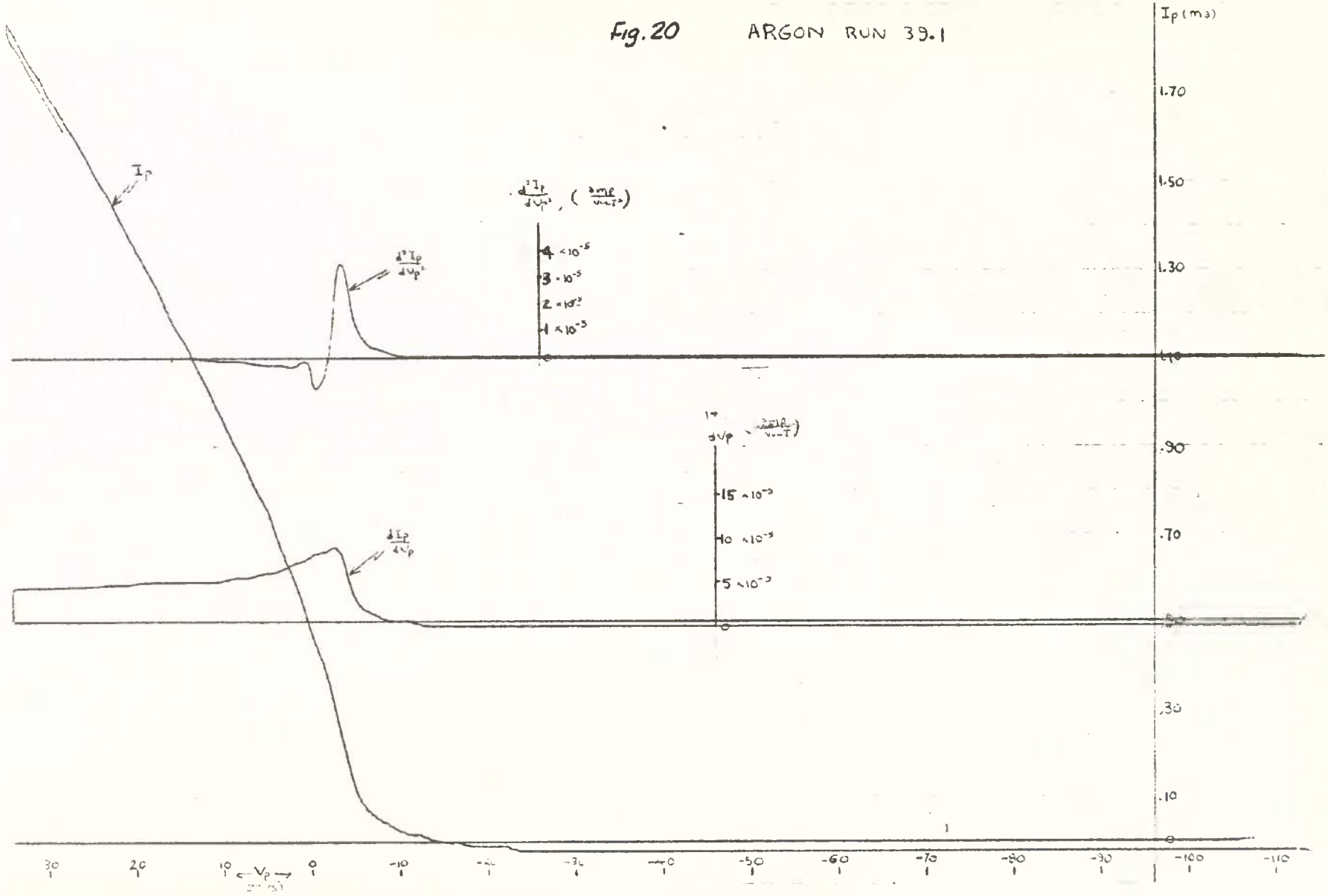

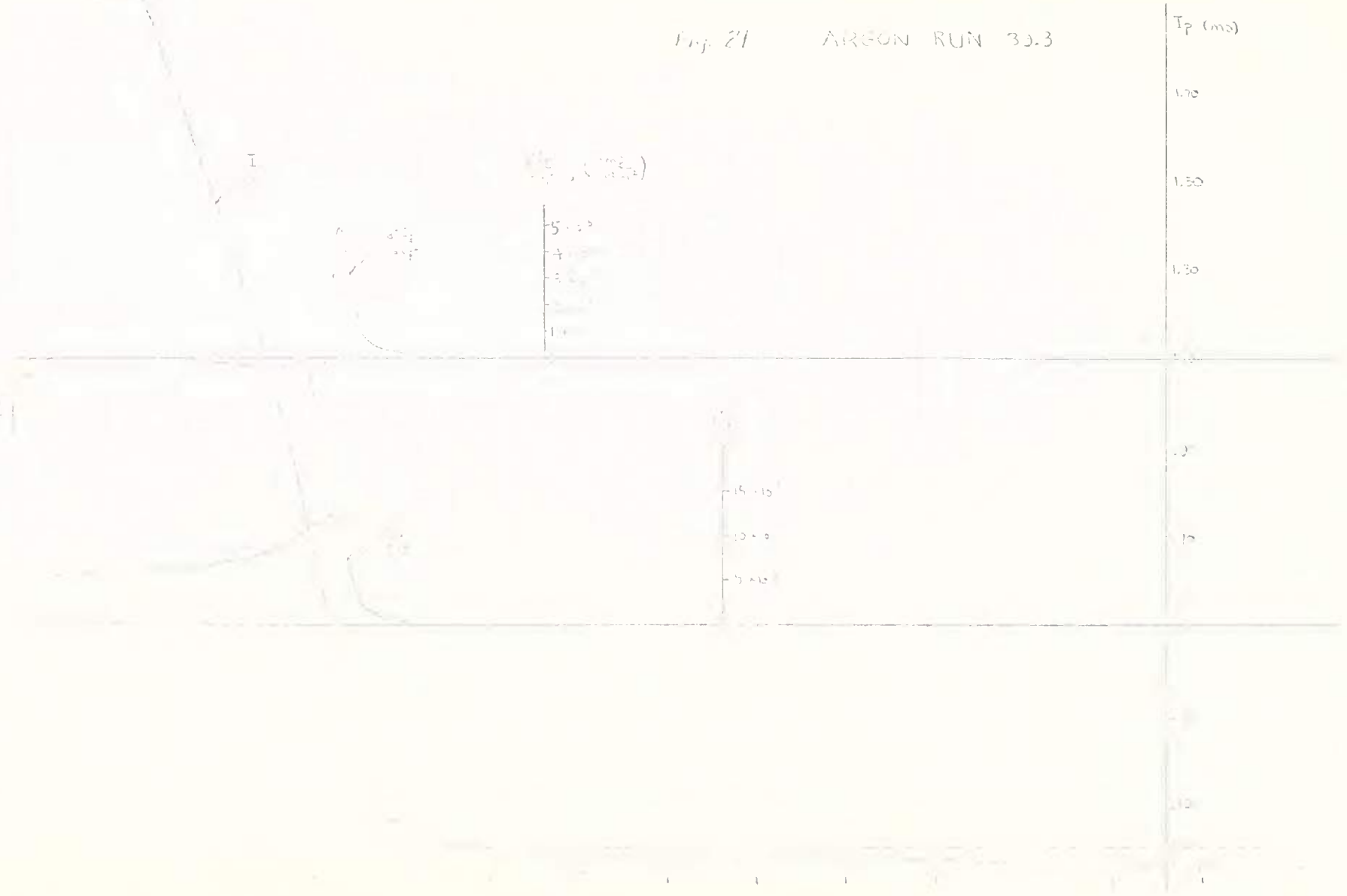
Fig. 21 ARGON RUN 30.3
T_P (ms)
1.70
1.50
1.30

Fig. 22 ARGON RUN 39.5

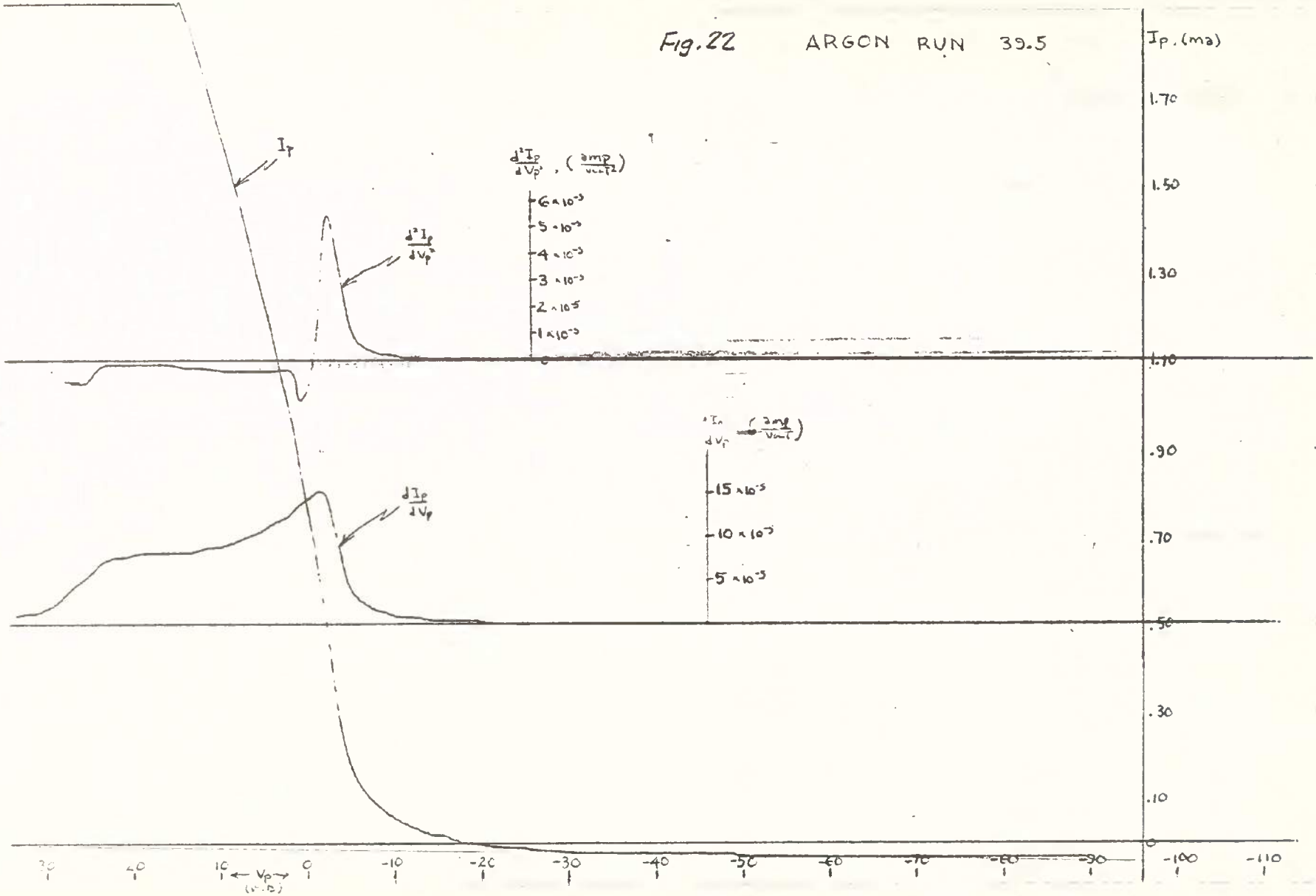

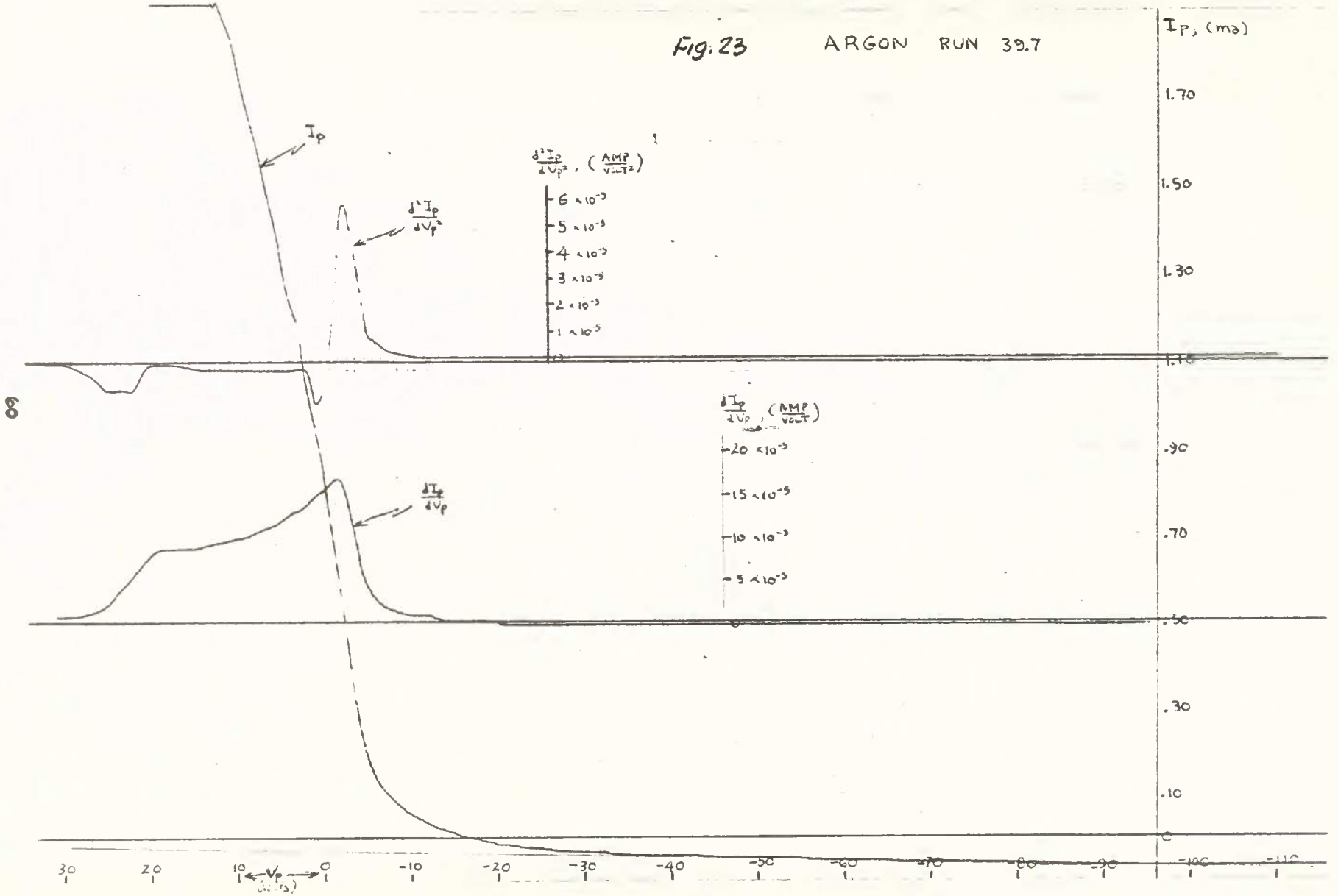
Fig. 23 ARGON RUN 39.7
I_p, (ma)
1.70
1.50
1.30
.90
.70
.50
.30
.10
0
I_p
$\frac{d^2 I_p}{dV_p^2}$
$\frac{d^2 I_p}{dV_p^2}$, $\left(\frac{AMP}{VOLT^2}\right)$
6×10^{-5}
5×10^{-5}
4×10^{-5}
3×10^{-5}
2×10^{-5}
1×10^{-5}
$\frac{dI_p}{dV_p}$
$\frac{dI_p}{dV_p}$, $\left(\frac{AMP}{VOLT}\right)$
20×10^{-5}
15×10^{-5}
10×10^{-5}
5×10^{-5}
30
20
10
V_p
0
-10
-20
-30
-40
-50
-60
-70
-80
-90
-100
-110

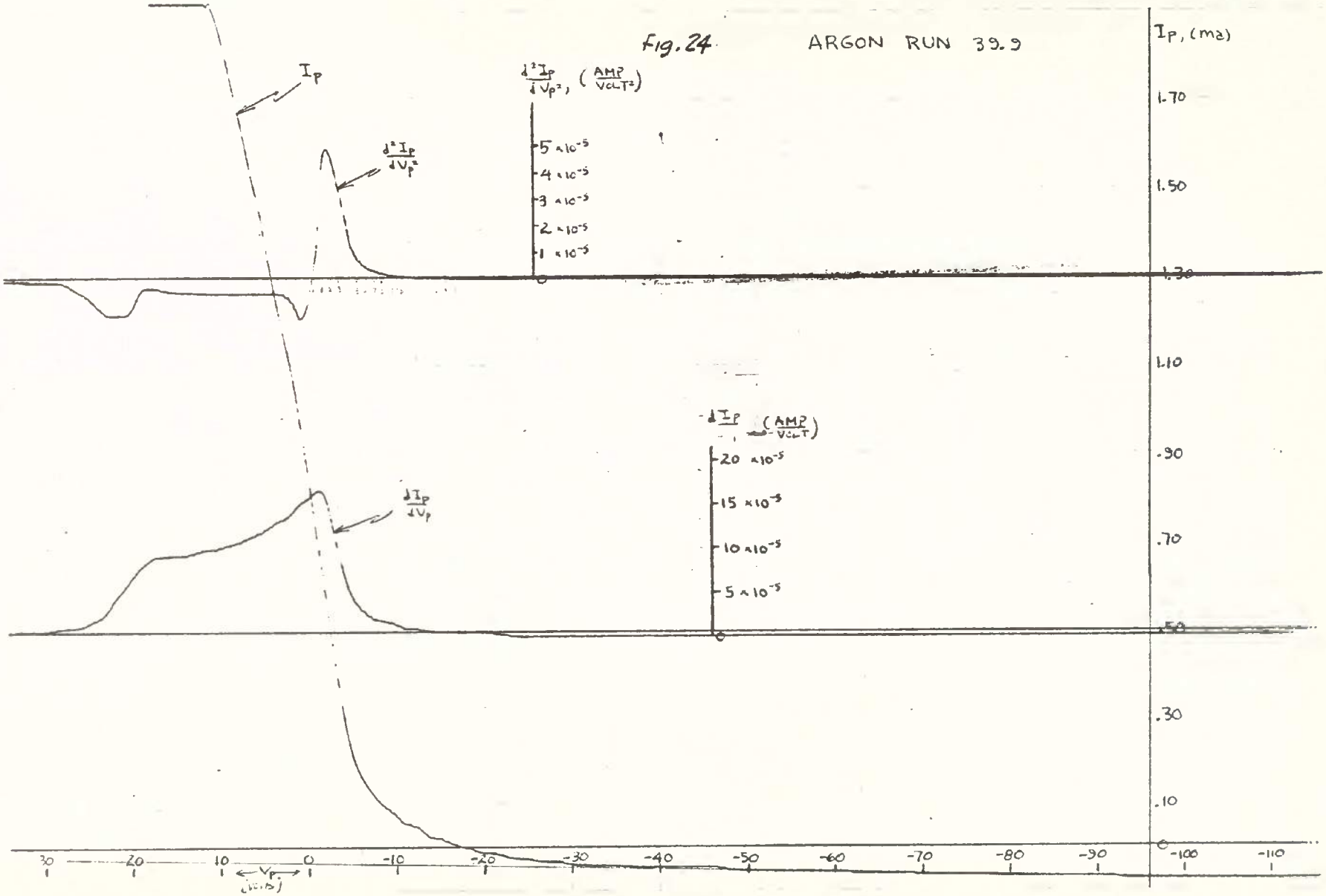
Fig. 24
ARGON RUN 39.9
I_P
$\frac{d^2I_P}{dV_P^2}$, $(\frac{AMP}{VOLT^2})$
$\frac{dI_P}{dV_P}$ $(\frac{AMP}{VOLT})$
I_P, (ma)
1.70
1.50
1.30
1.10
.90
.70
.50
.30
.10
0
5×10^{-5}
4×10^{-5}
3×10^{-5}
2×10^{-5}
1×10^{-5}
20×10^{-5}
15×10^{-5}
10×10^{-5}
5×10^{-5}
30 20 10 0 -10 -20 -30 -40 -50 -60 -70 -80 -90 -100 -110
V_P (VOLTS)

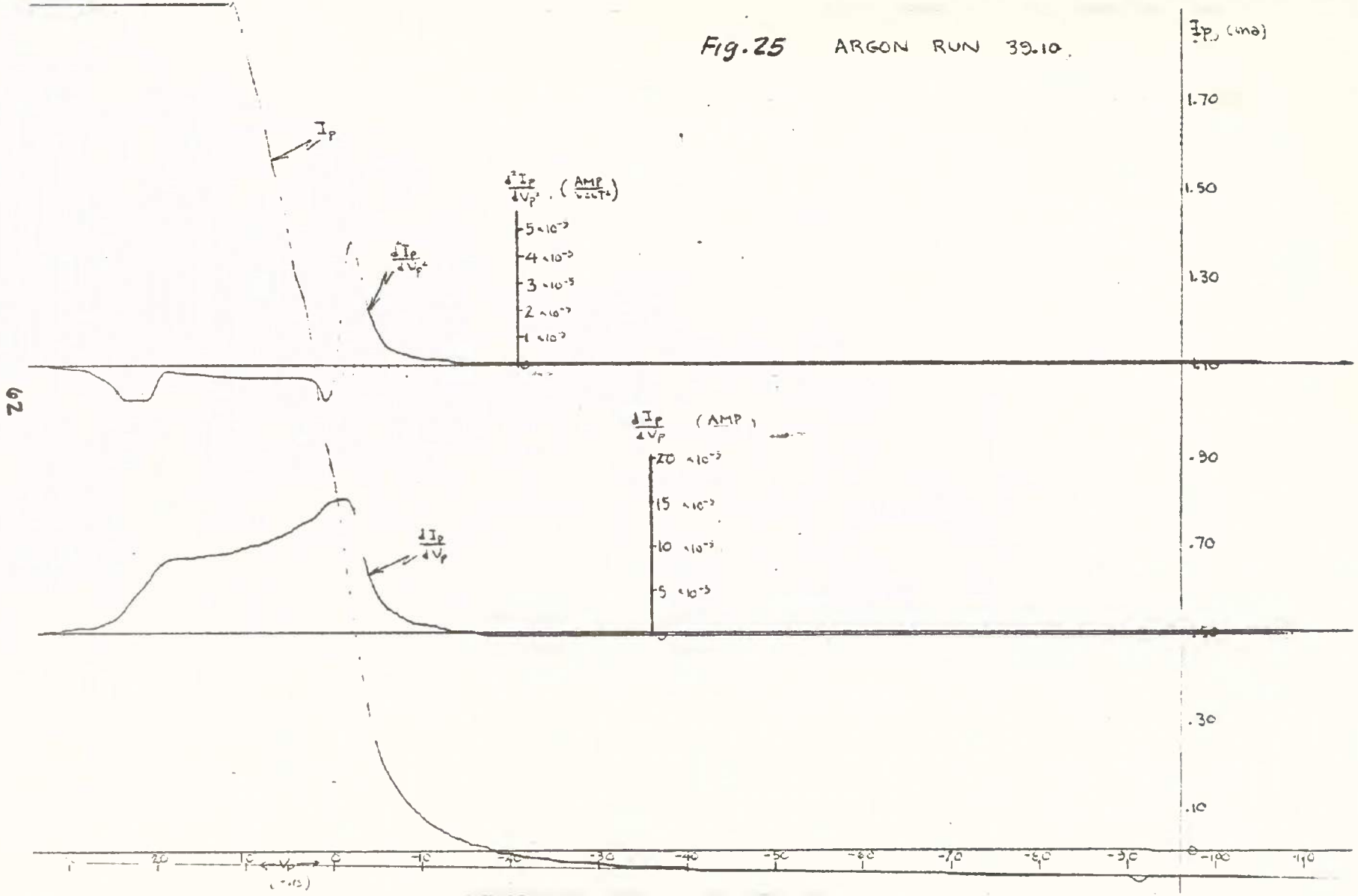
Fig. 25 ARGON RUN 39.10
I_p (ma)
1.70
1.50
1.30
1.10
.90
.70
.50
.30
.10
I_p
$\frac{d^2 I_p}{dV_p^2}$. ($\frac{AMP}{volt^2}$)
5×10^{-3}
4×10^{-3}
3×10^{-3}
2×10^{-3}
1×10^{-3}
$\frac{dI_p}{dV_p}$
$\frac{dI_p}{dV_p}$ (AMP)
20×10^{-3}
15×10^{-3}
10×10^{-3}
5×10^{-3}
V_p
20
10
0
-10
-20
-30
-40
-50
-60
-70
-80
-90
-100
-110

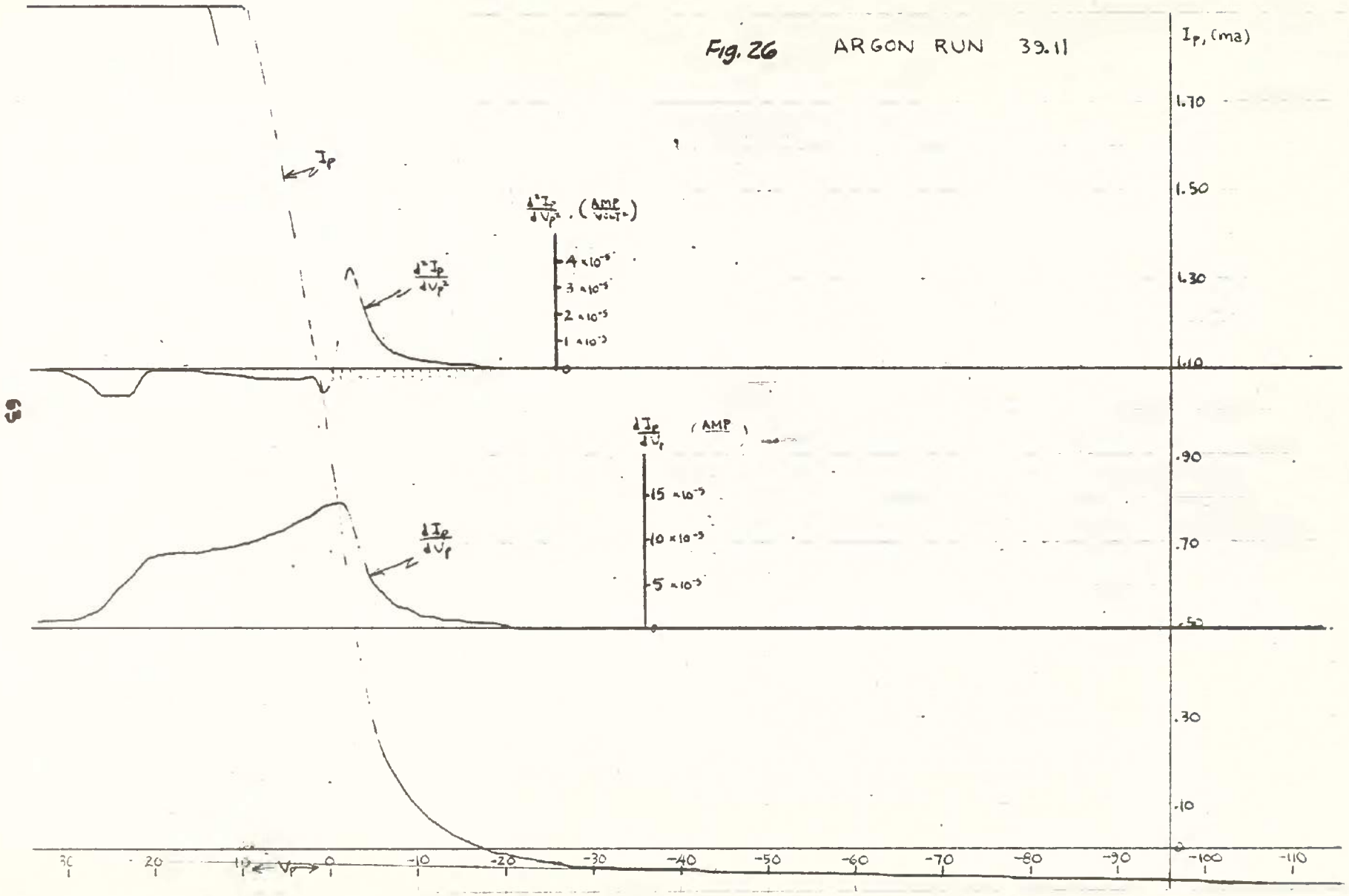
Fig. 26 ARGON RUN 39.11
I_p, (ma)
1.70
1.50
1.30
1.10
.90
.70
.50
.30
.10
0
I_p
$\frac{d^2 I_p}{dV_p^2}$. (AMP/volt)
4×10^{-5}
3×10^{-5}
2×10^{-5}
1×10^{-5}
$\frac{dI_p}{dV_p}$ (AMP)
15×10^{-5}
10×10^{-5}
5×10^{-5}
30
20
10
V_p
0
-10
-20
-30
-40
-50
-60
-70
-80
-90
-100
-110

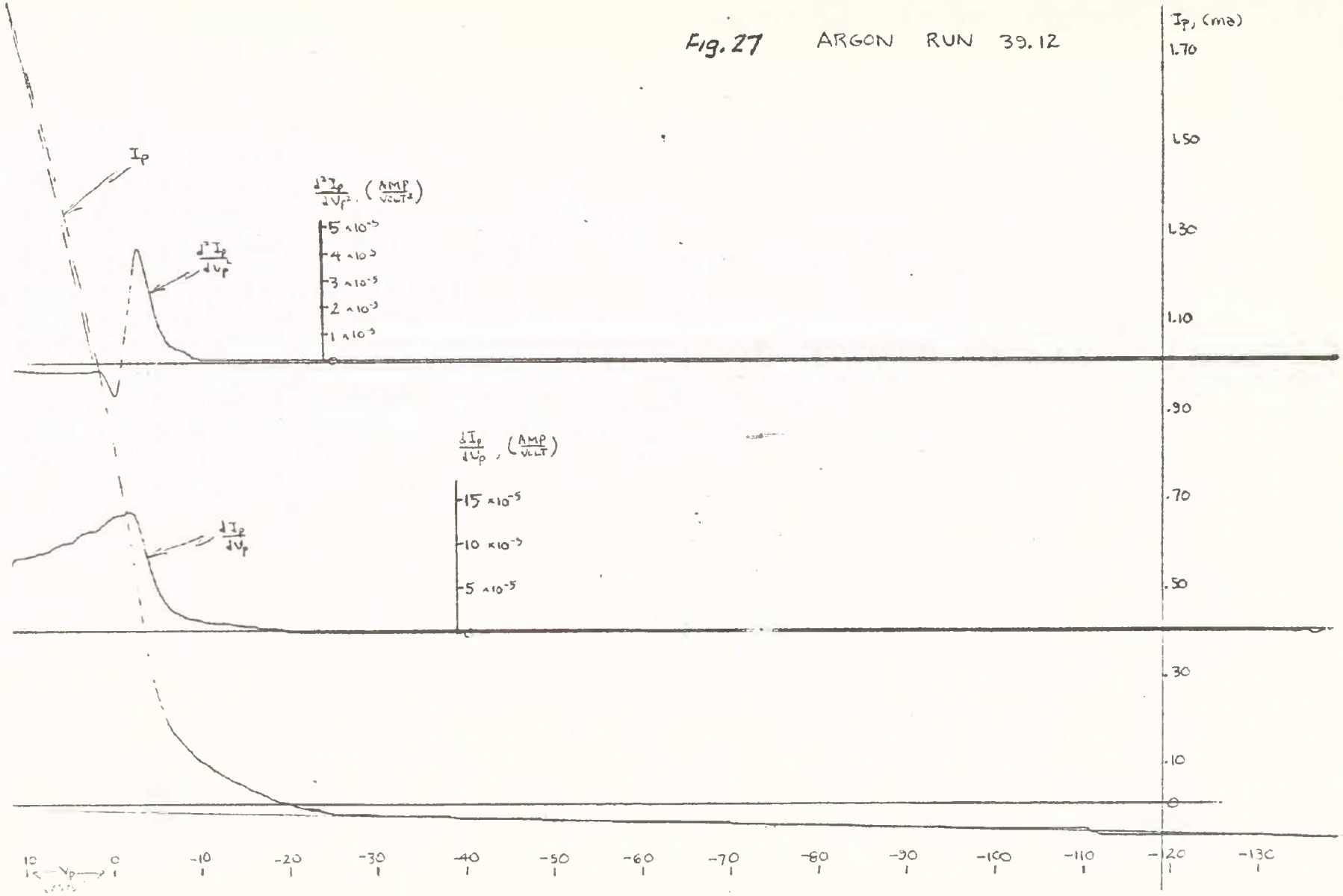
Fig. 27 ARGON RUN 39.12
I_p, (ma)
1.70
1.50
1.30
1.10
.90
.70
.50
.30
.10
I_p
$\frac{d^2 I_p}{dV_p^2}$, $\left(\frac{AMP}{VOLT^2}\right)$
5×10^{-5}
4×10^{-5}
3×10^{-5}
2×10^{-5}
1×10^{-5}
$\frac{d^2 I_p}{dV_p}$
$\frac{dI_p}{dV_p}$, $\left(\frac{AMP}{VOLT}\right)$
15×10^{-5}
10×10^{-5}
5×10^{-5}
$\frac{dI_p}{dV_p}$
10
0
V_p
-10
-20
-30
-40
-50
-60
-70
-80
-90
-100
-110
-120
-130

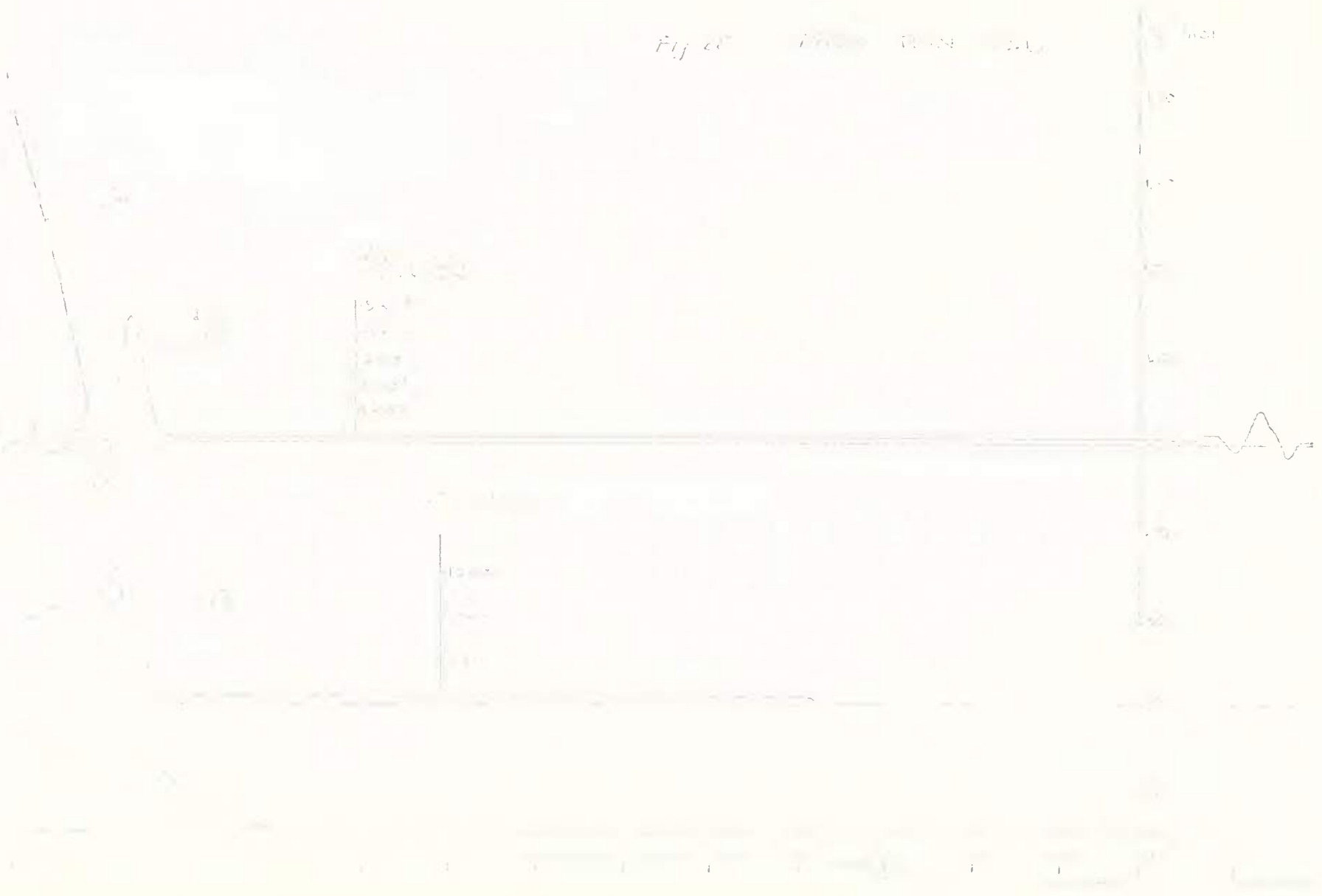

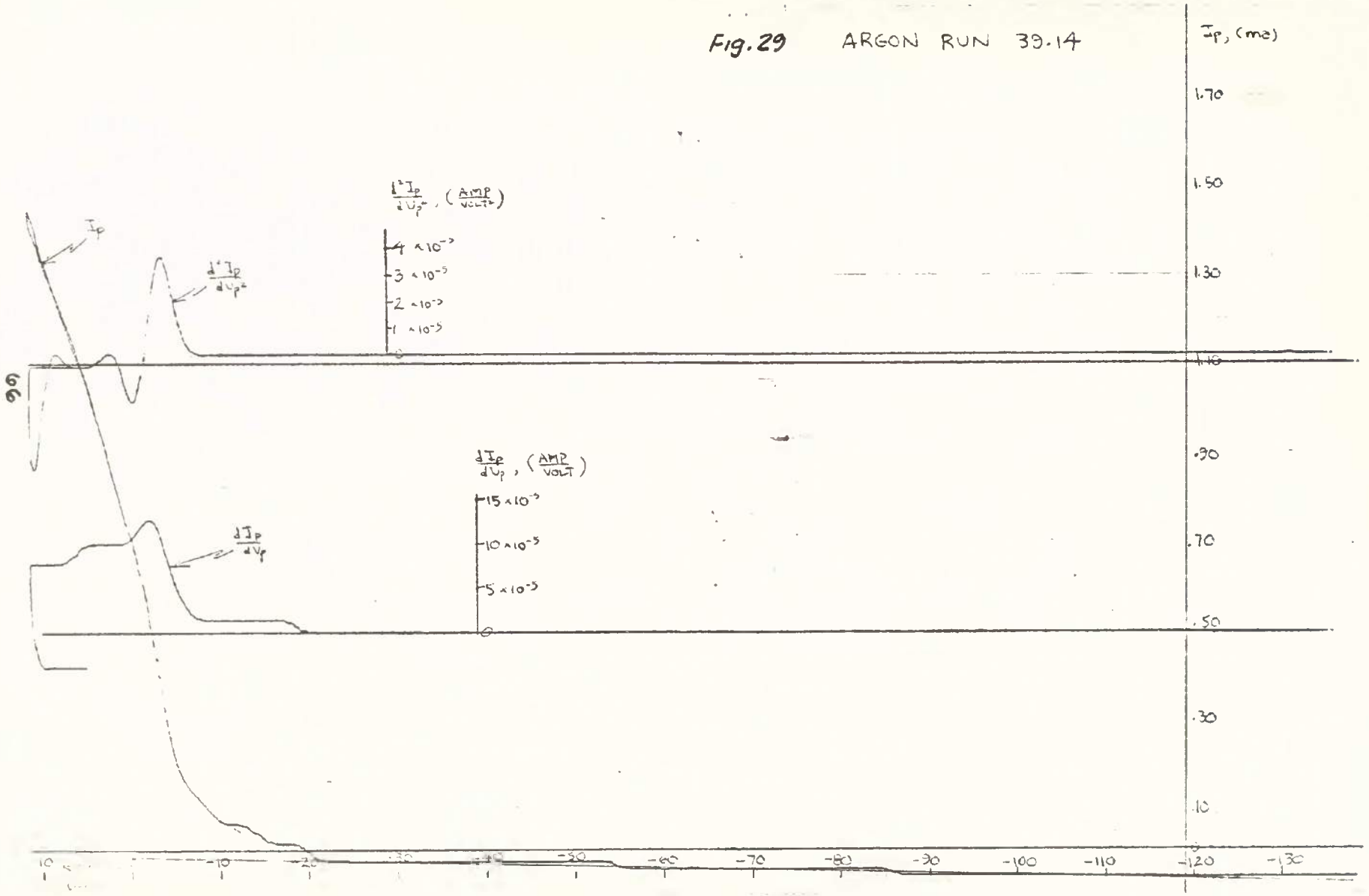
Fig. 29 ARGON RUN 39.14
I_p, (ma)
1.70
1.50
1.30
1.10
.90
.70
.50
.30
.10
0
$\frac{d^2 I_p}{dV_p^2}$, $\left(\frac{AMP}{VOLT^2}\right)$
4 ×10⁻⁵
3 ×10⁻⁵
2 ×10⁻⁵
1 ×10⁻⁵
0
I_p
$\frac{d^2 I_p}{dV_p^2}$
$\frac{dI_p}{dV_p}$, $\left(\frac{AMP}{VOLT}\right)$
15 ×10⁻³
10 ×10⁻³
5 ×10⁻³
0
$\frac{dI_p}{dV_p}$
10
-10
-20
-30
-40
-50
-60
-70
-80
-90
-100
-110
-120
-130

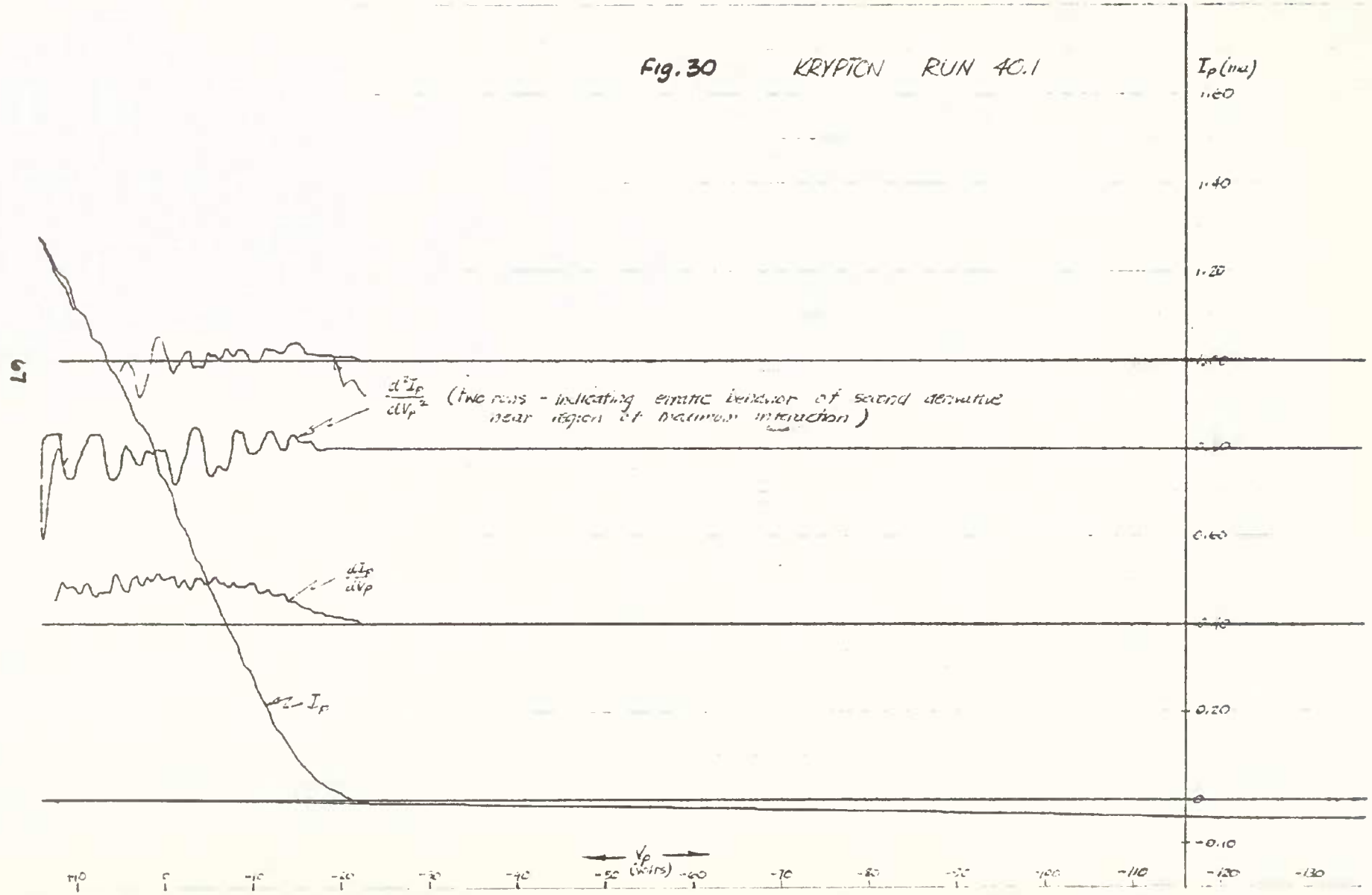
Fig. 30 KRYPTON RUN 40.1
I_p (ma)
1.60
1.40
1.20
0.60
0.20
0
-0.10
$\frac{d^2 I_p}{dV_p^2}$ (two roots - indicating erratic behavior of second derivative near region of beam-ion interaction)
$\frac{dI_p}{dV_p}$
I_p
V_p (volts)
+10
0
-10
-20
-30
-40
-50
-60
-70
-80
-90
-100
-110
-120
-130
67

Fig. 31 KRYPTON RUN #0.3

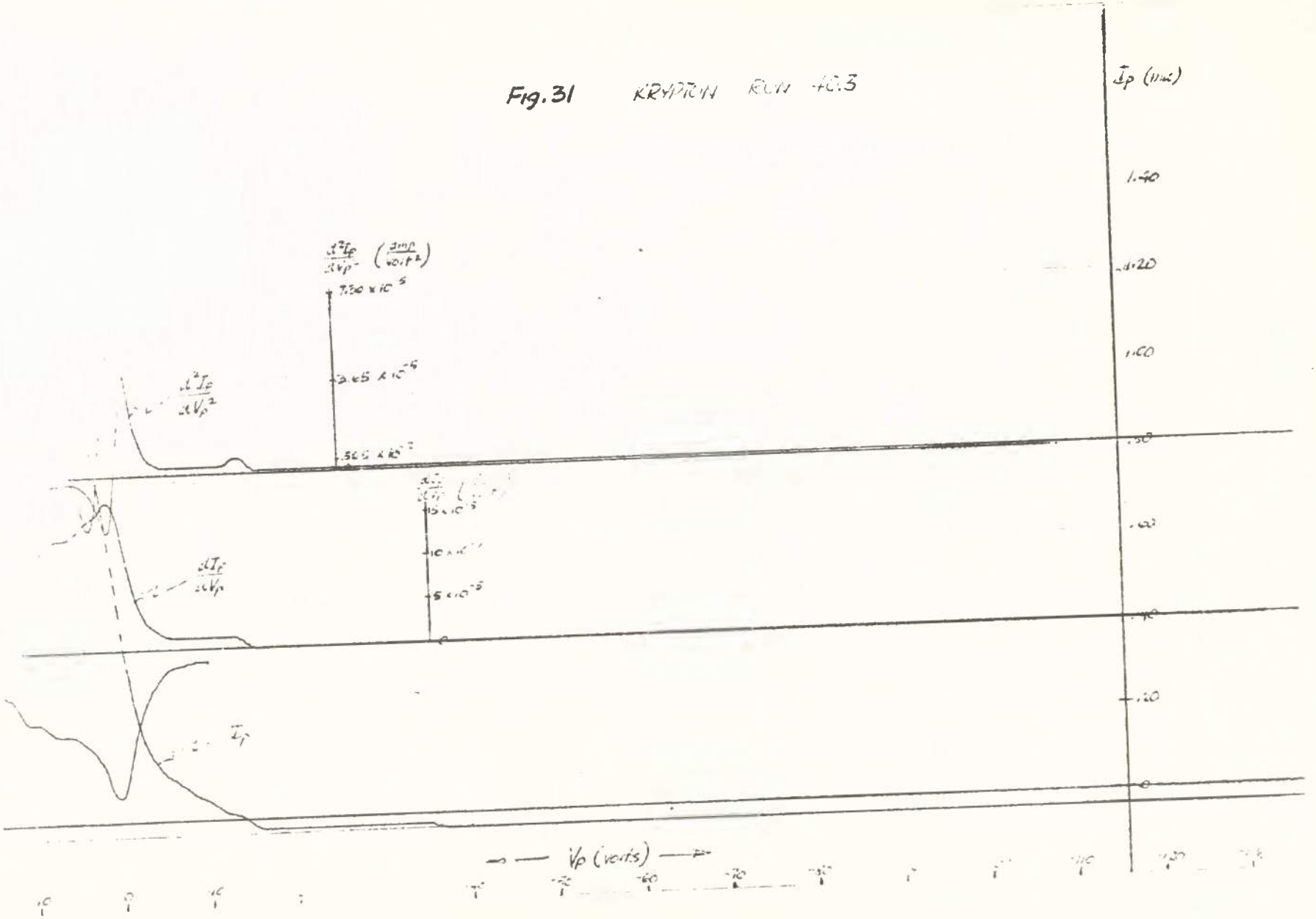

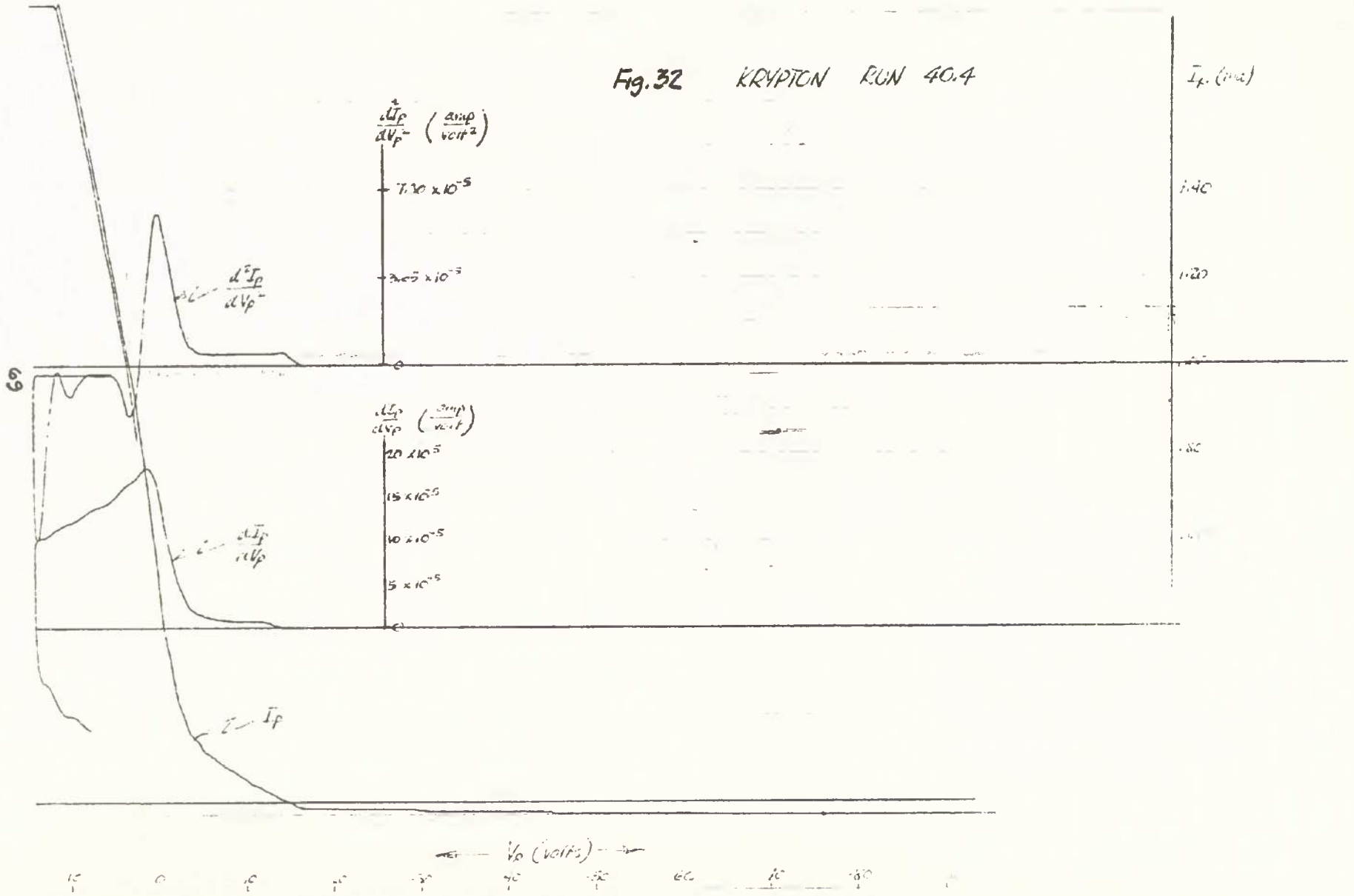
Fig. 32 KRYPTON RUN 40.4
$\frac{d^2 I_p}{dV_p^2}$ (amp/volt²)
7.70 x 10⁻⁵
3.85 x 10⁻⁵
$\frac{d^2 I_p}{dV_p^2}$
$\frac{dI_p}{dV_p}$ (amp/volt)
20 x 10⁻⁵
15 x 10⁻⁵
10 x 10⁻⁵
5 x 10⁻⁵
$\frac{dI_p}{dV_p}$
I_p
I_p (ma)
1.40
1.20
.80
V_p (volts)
69

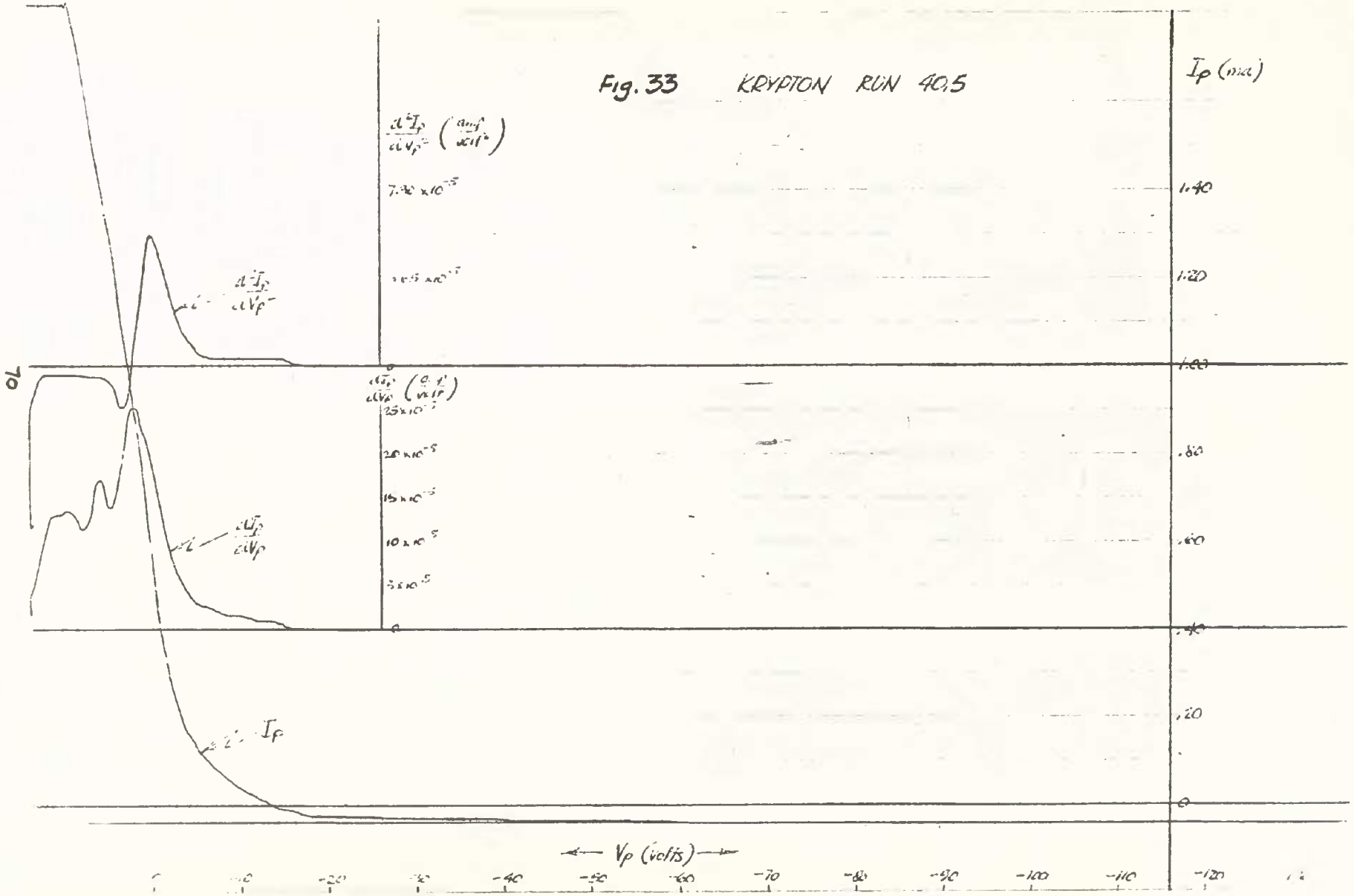
Fig. 33 KRYPTON RUN 40.5
I_p (ma)
$\frac{d^2 I_p}{dV_p^2}$ $\left(\frac{amp^2}{volt^2}\right)$
$\frac{dI_p}{dV_p}$ $\left(\frac{amp}{volt}\right)$
I_p
V_p (volts)
1.40
1.20
1.00
.80
.60
.40
.20
0
-10
-20
-30
-40
-50
-60
-70
-80
-90
-100
-110
-120

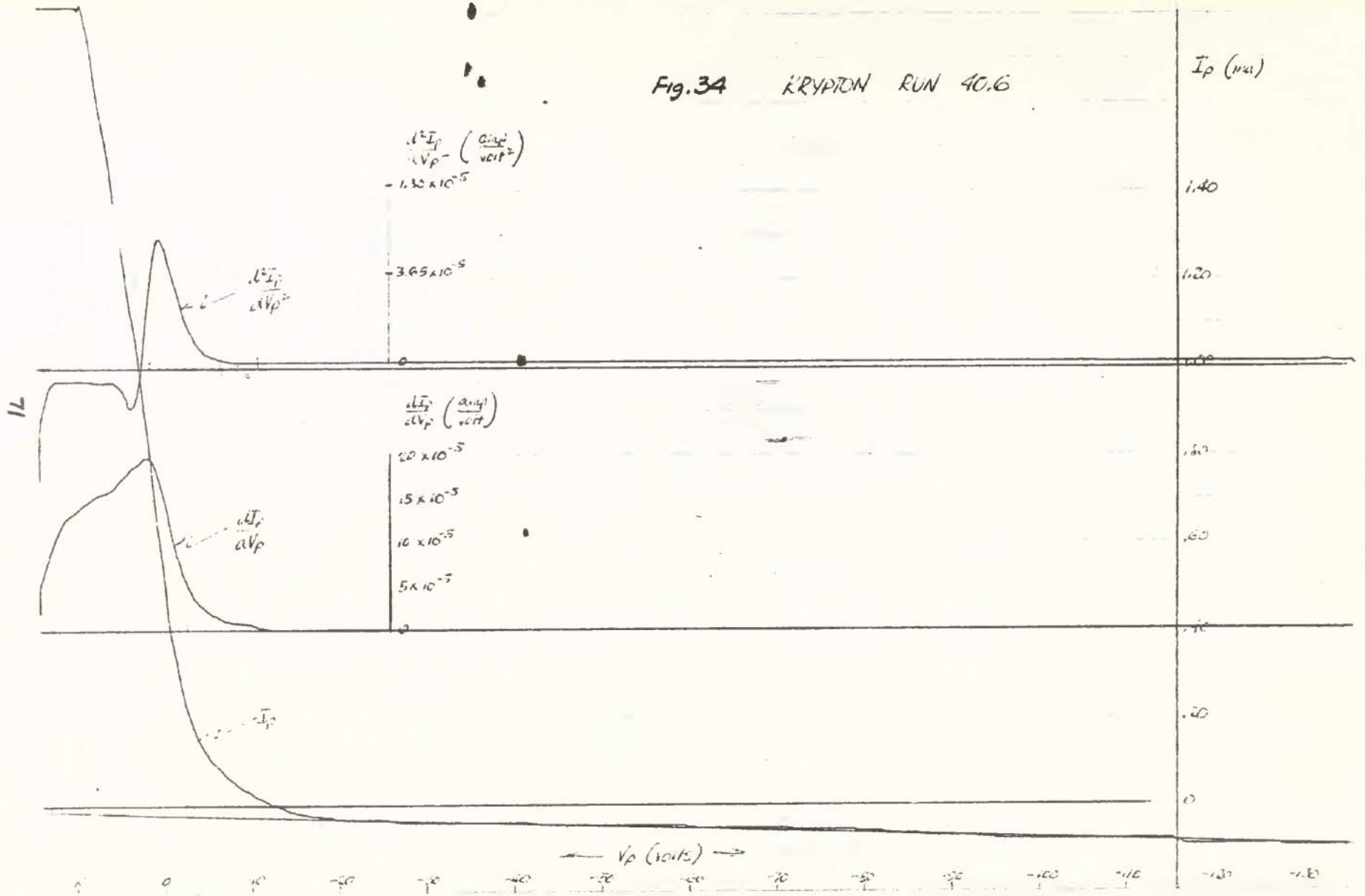
Fig. 34 KRYPTON RUN 40.6
I_p (ma)
$\frac{d^2 I_p}{dV_p}$ $\left(\frac{amp}{volt^2}\right)$
-1.30×10^{-5}
-3.95×10^{-5}
1.40
1.20
$\frac{d^2 I_p}{dV_p^2}$
$\frac{dI_p}{dV_p}$ $\left(\frac{amp}{volt}\right)$
20×10^{-5}
15×10^{-5}
10×10^{-5}
5×10^{-5}
.60
.40
.20
0
$-I_p$
V_p (volts)
0
-10
-20
-30
-40
-50
-60
-70
-80
-90
-100
-110
-120
-130
IL

Fig. 35. KRYPTON RUN 40.9

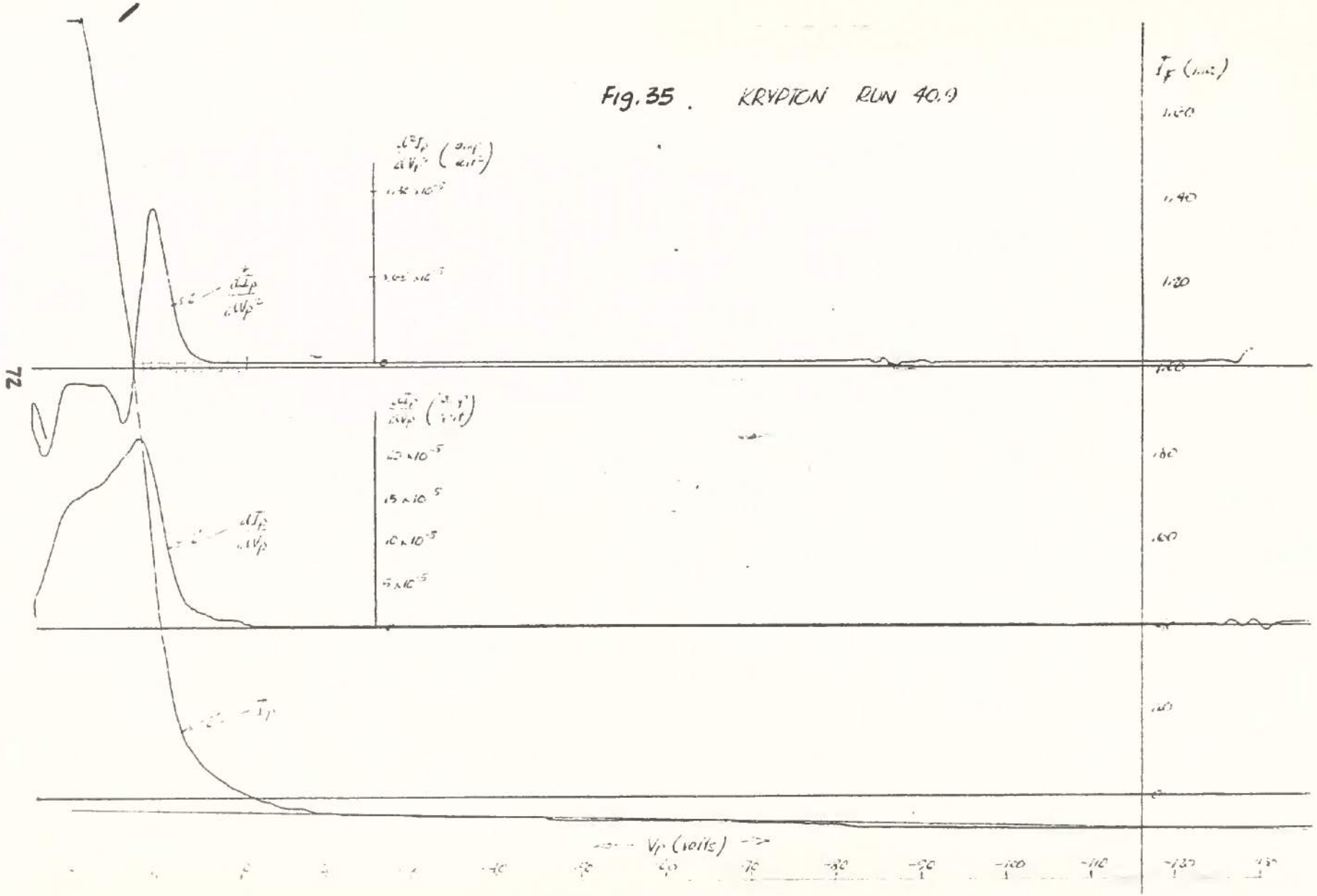

Fig. 36 KRYPTON RUN 46.11

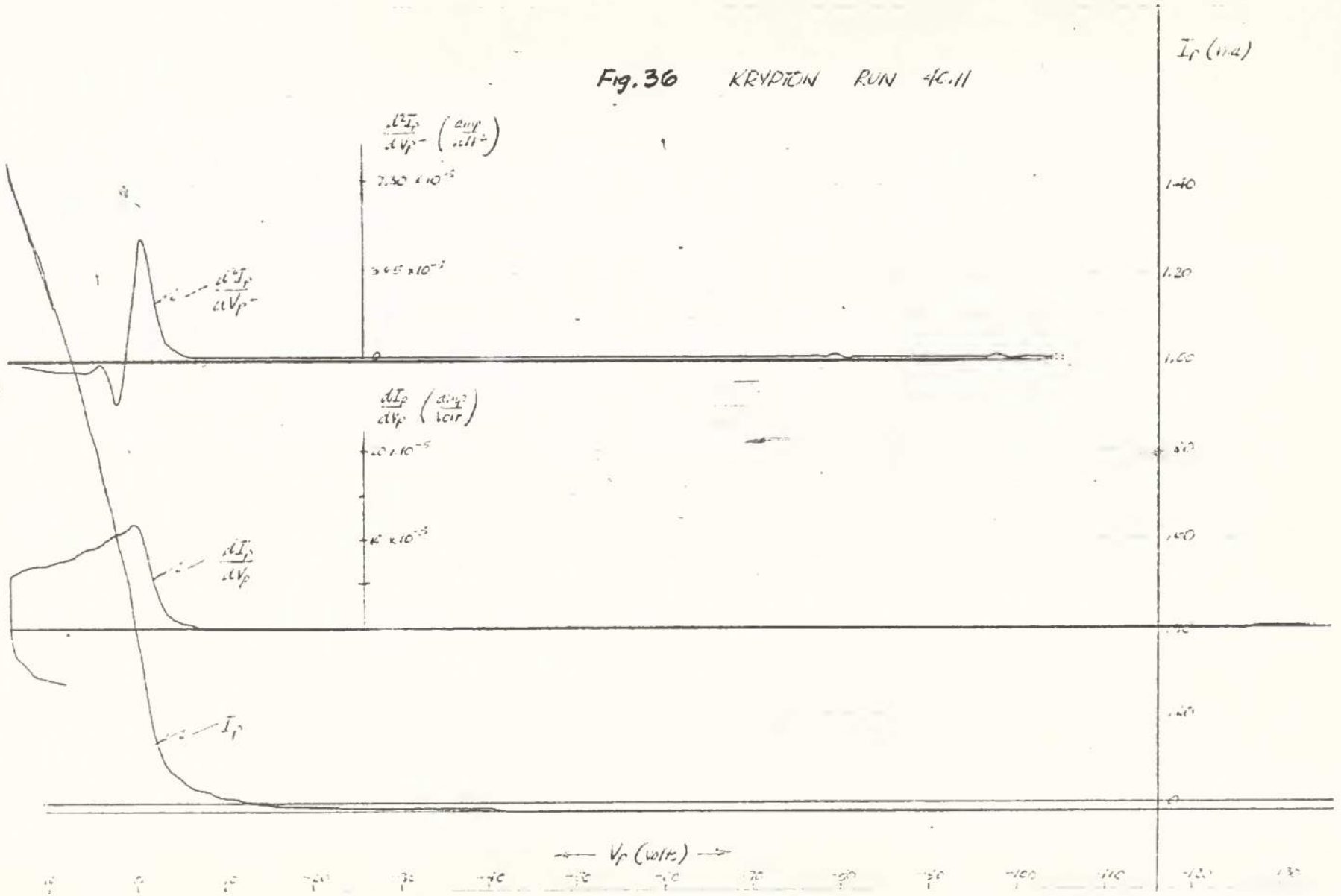

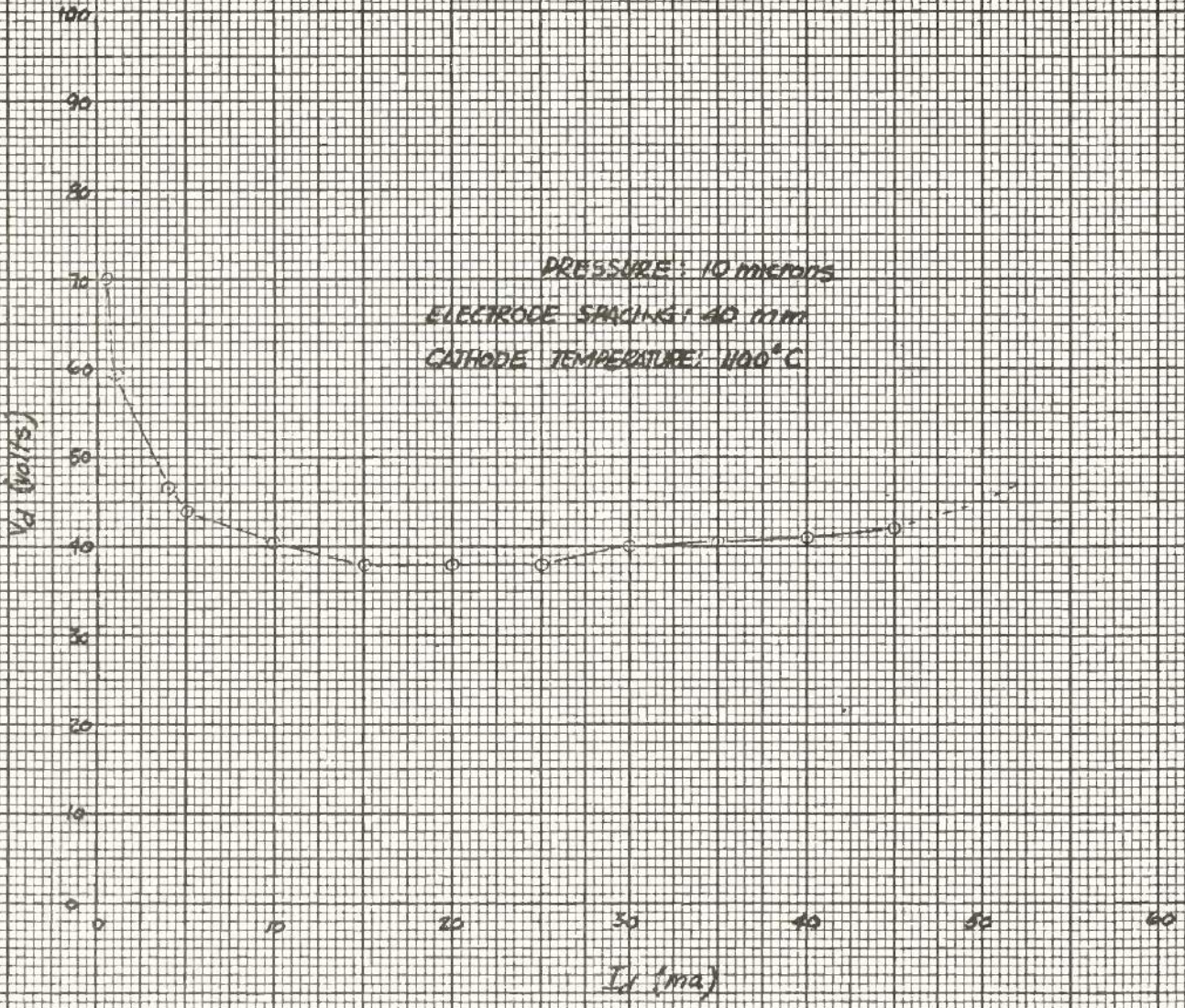

Figure 37. I_d-V_d Characteristic Curve, Neon, Runs 19 & 21.

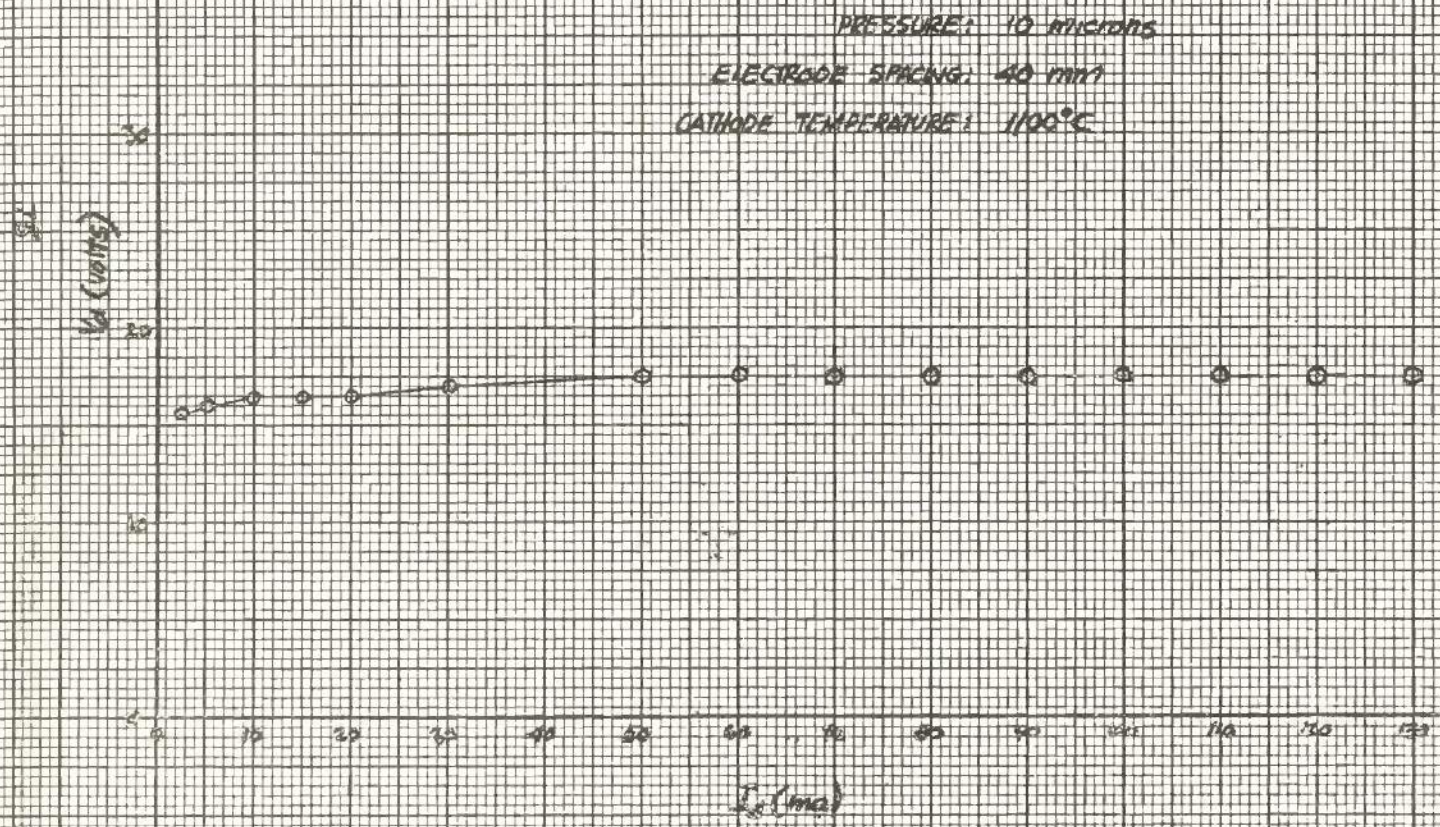

Figure 38. I_d-V_d Characteristic Curve, Argon, Run 39.

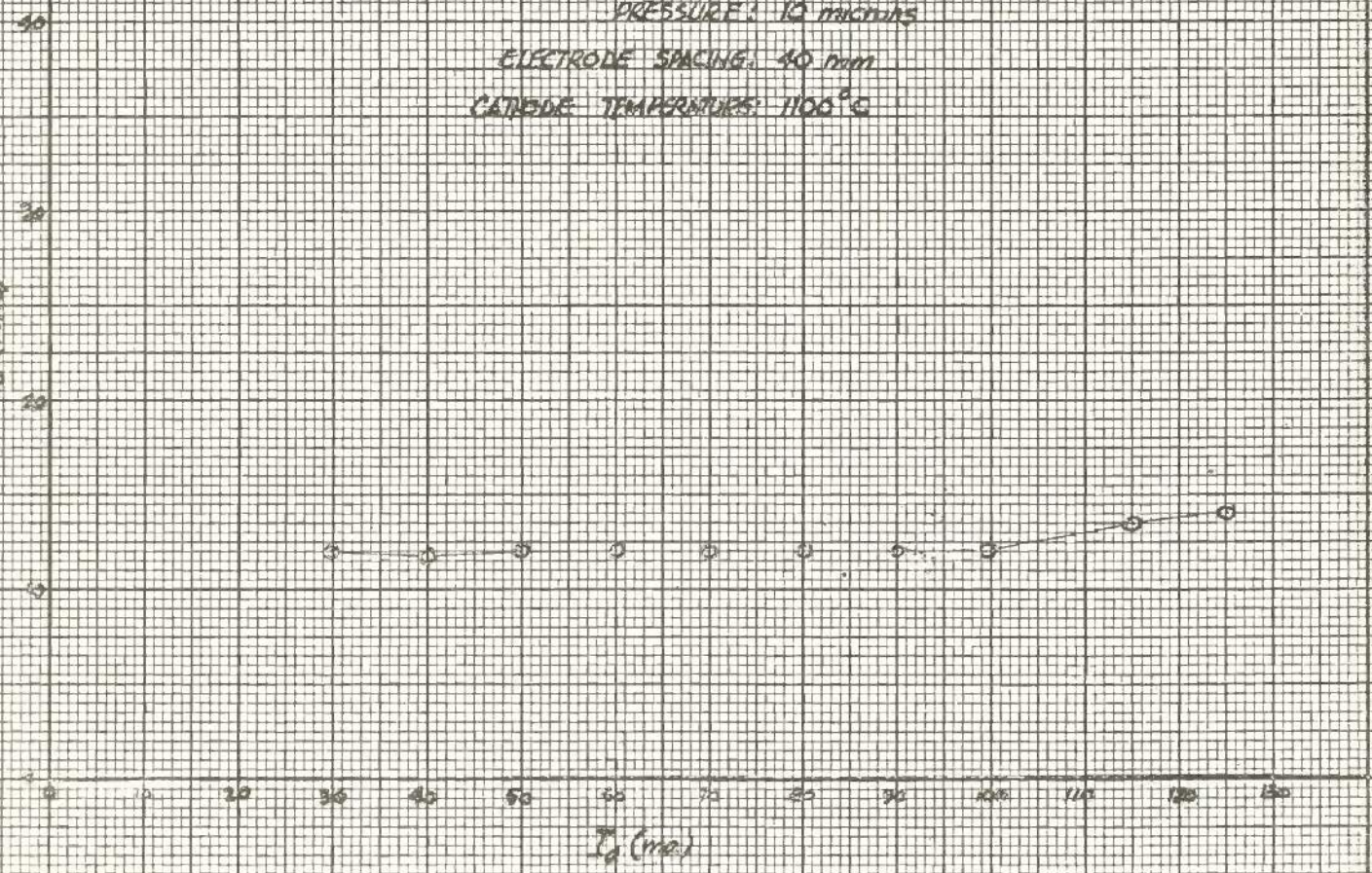

Figure 39. I_d-V_d Characteristic Curve, Krypton, Run 40.

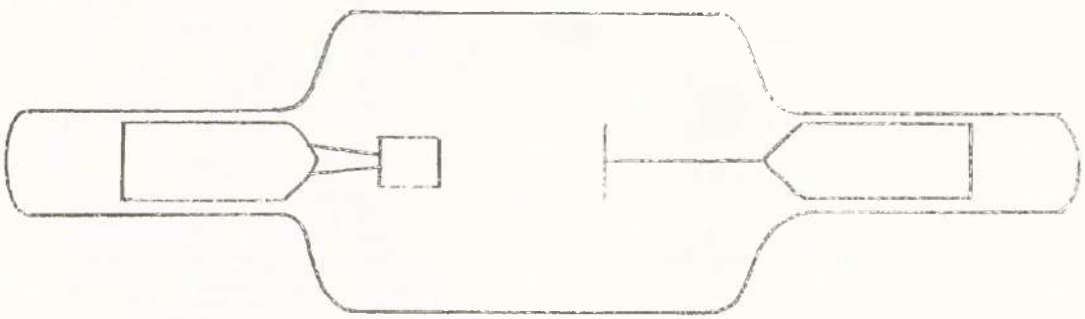

Figure 40. Sketch of Normal Diffuse
Discharge - 10 microns
Neon 30ma - Argon 100ma - Krypton 115ma

Frequencies Detected: ① 212/691 mc
② 211/354 mc
③ 462 mc

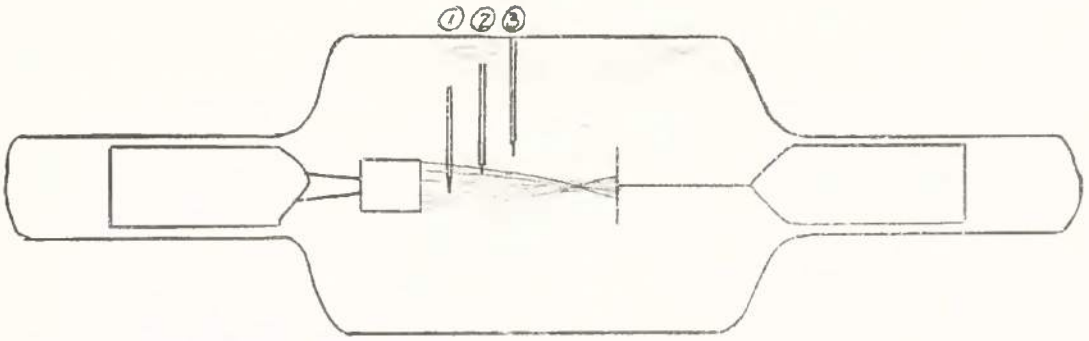

NEON - 32 microns - 50 ma.

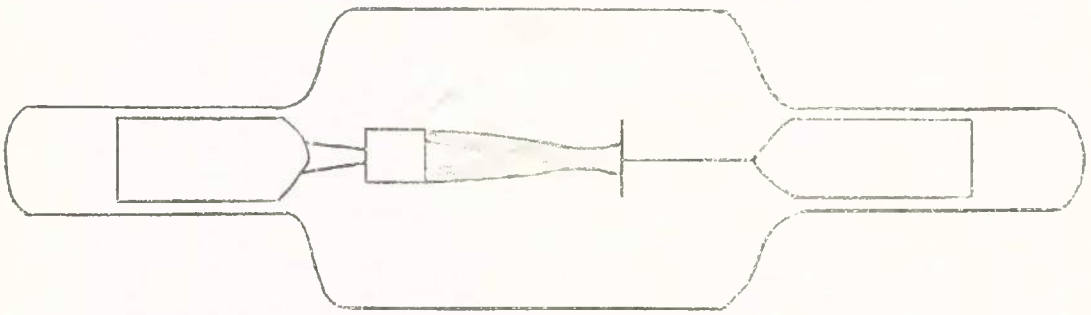

ARGON - 22 microns - 100 ma.

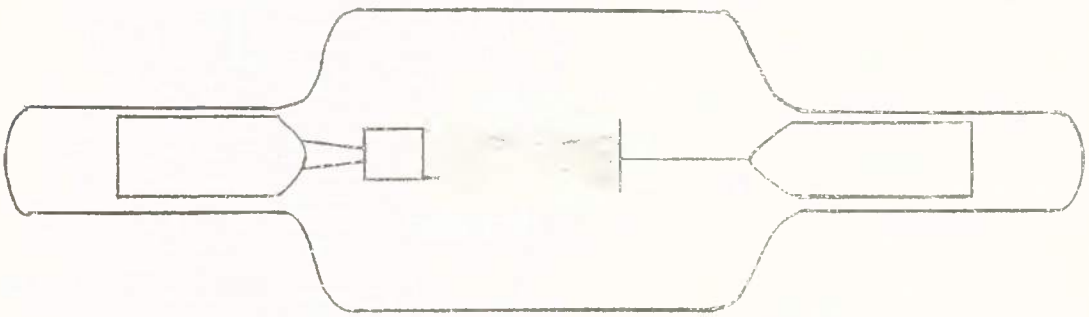

ARGON - 10 microns - 50 ma. - Reinitiated After Collapse

Figure 41. Sketches of Various Types of Discharges

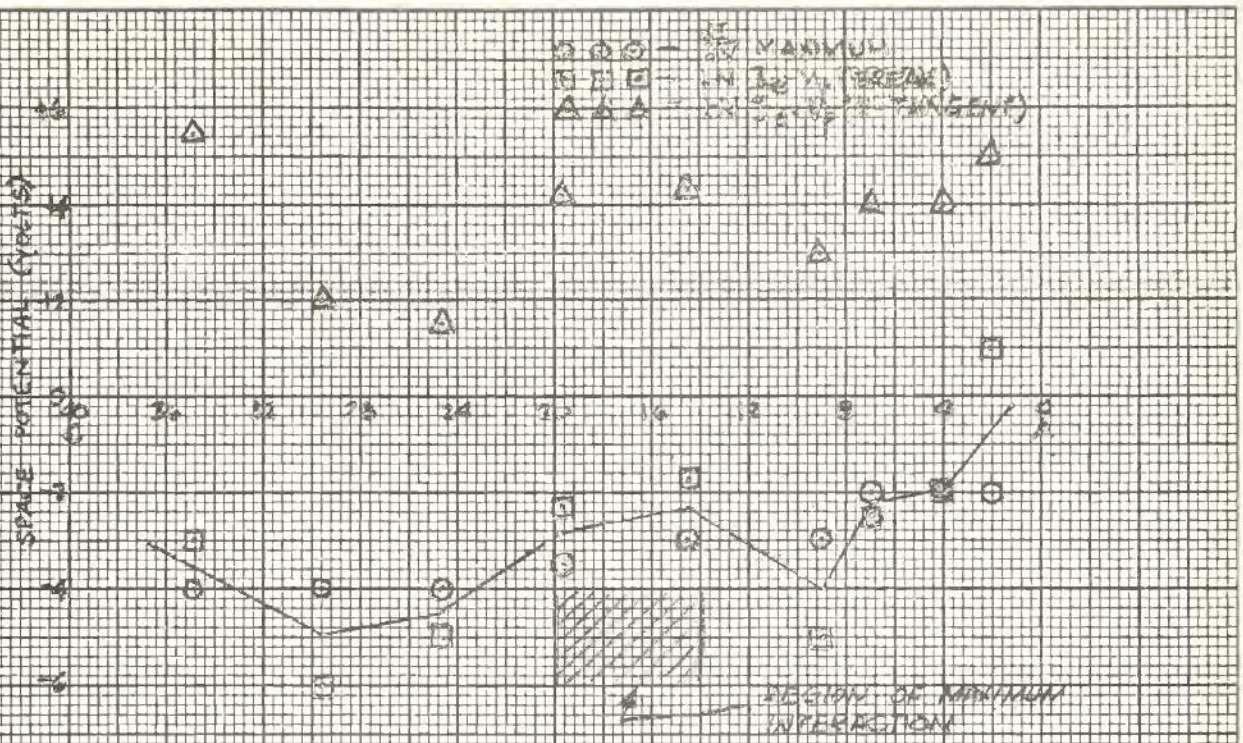

FIG. 42 SPACE POTENTIAL VS. PROBE POSITION, RUN 19 NEON

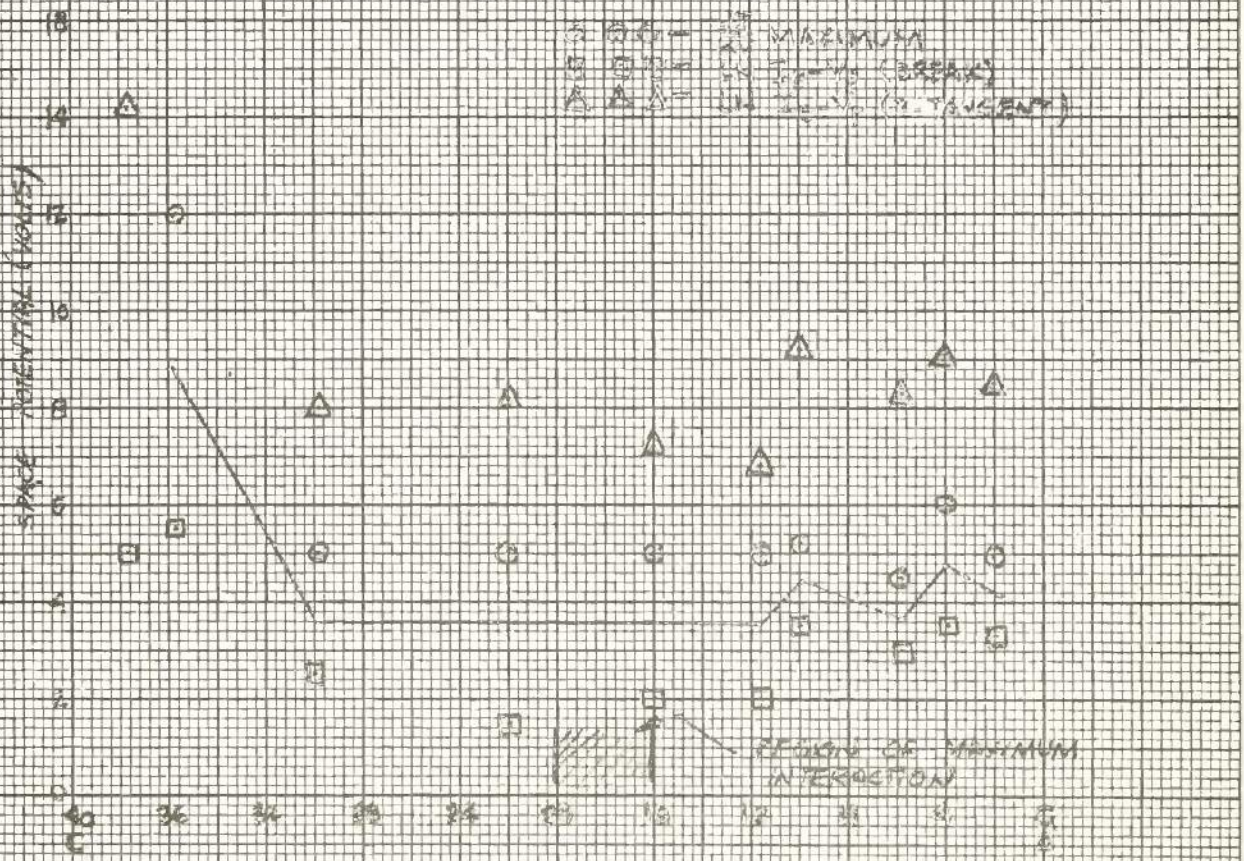

FIG. 43 SPACE POTENTIAL VS. PROBE POSITION, RUN 21 NEON

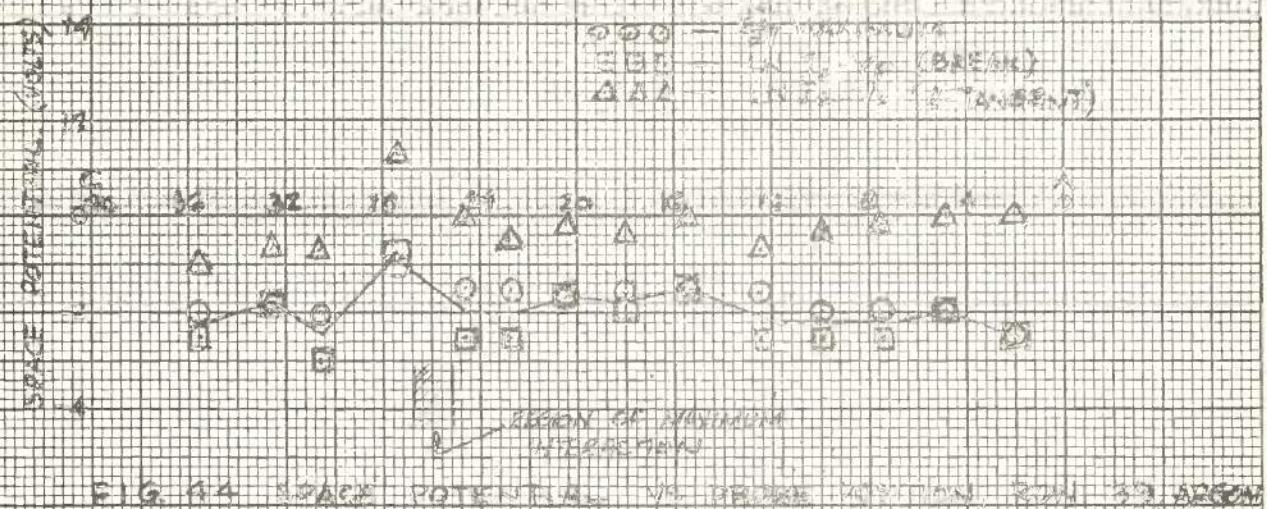

FIG. 44 [illegible]

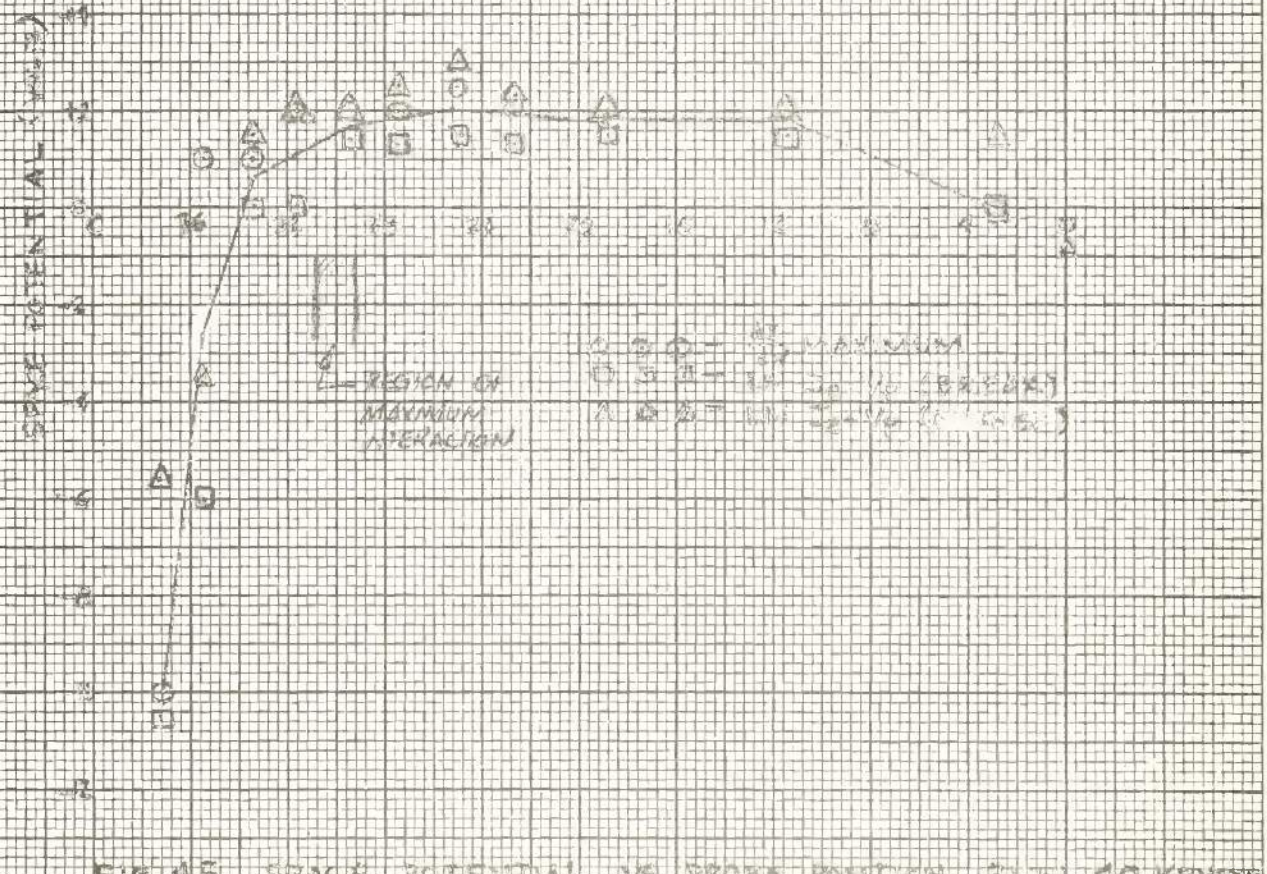

FIG. 45 [illegible]

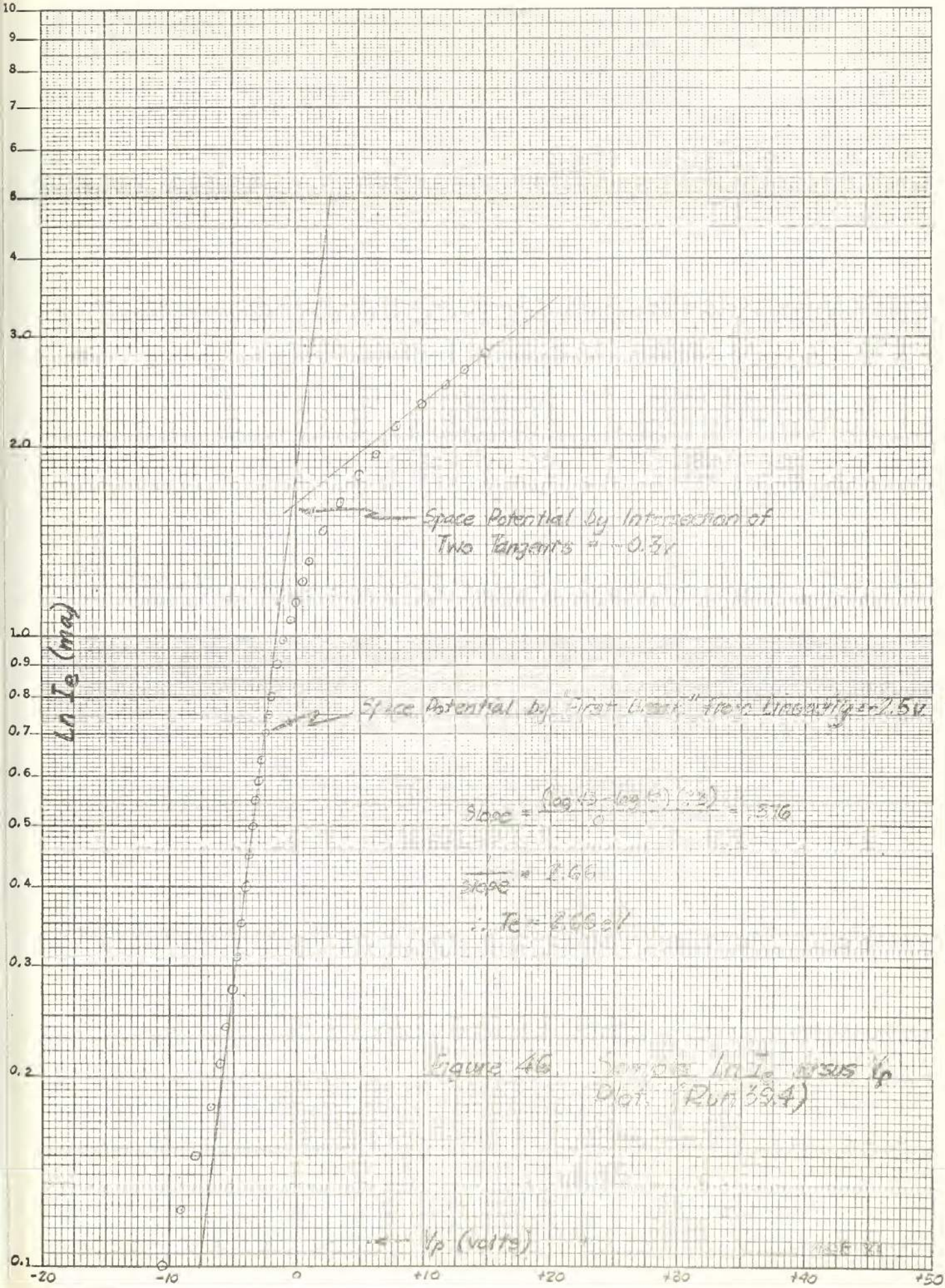

Figure 46 Semi-log Ie versus Vp Plot (Run 394)

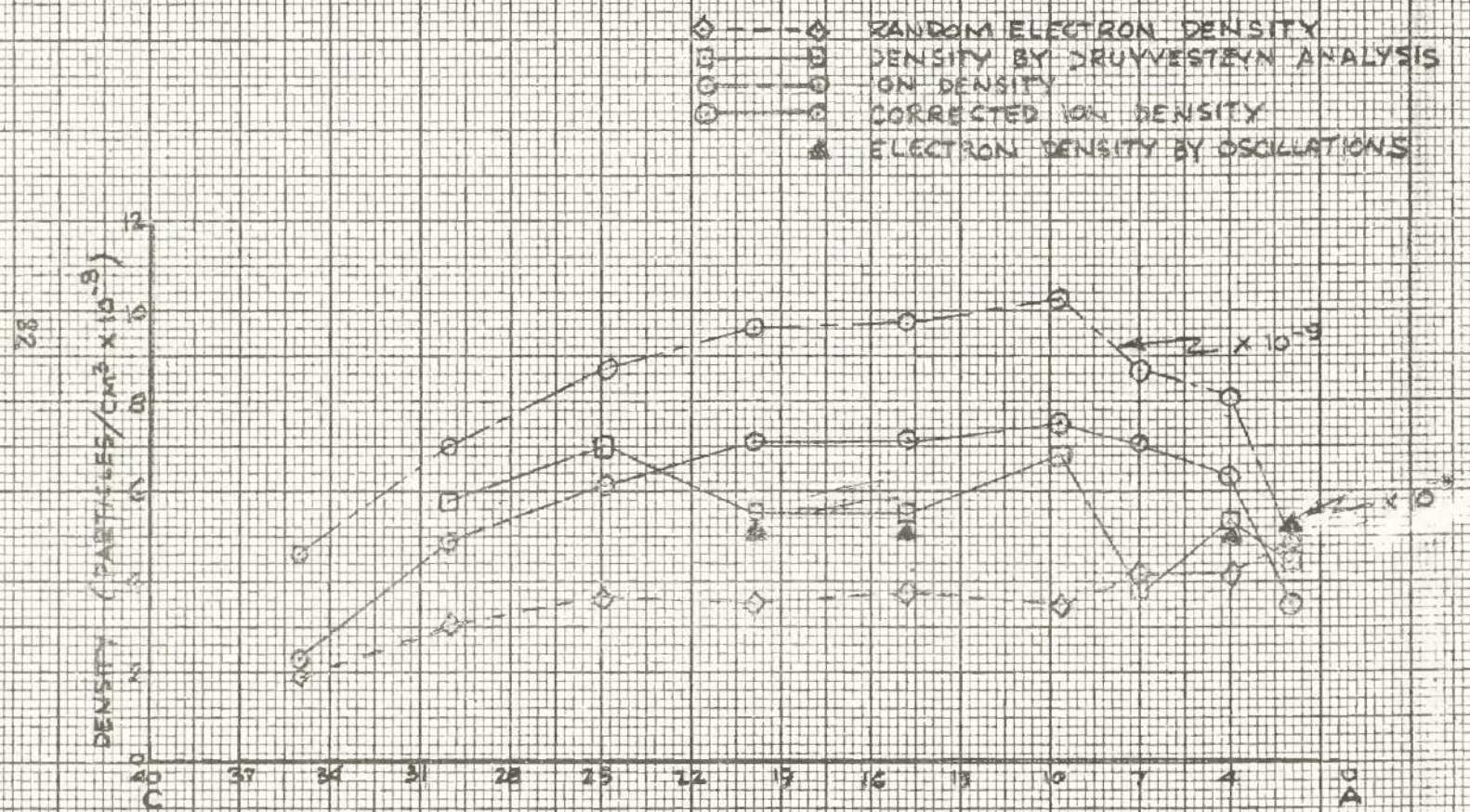

FIG 47 ELECTRON AND ION DENSITIES VS PROBE POSITION RUN 19 NEON

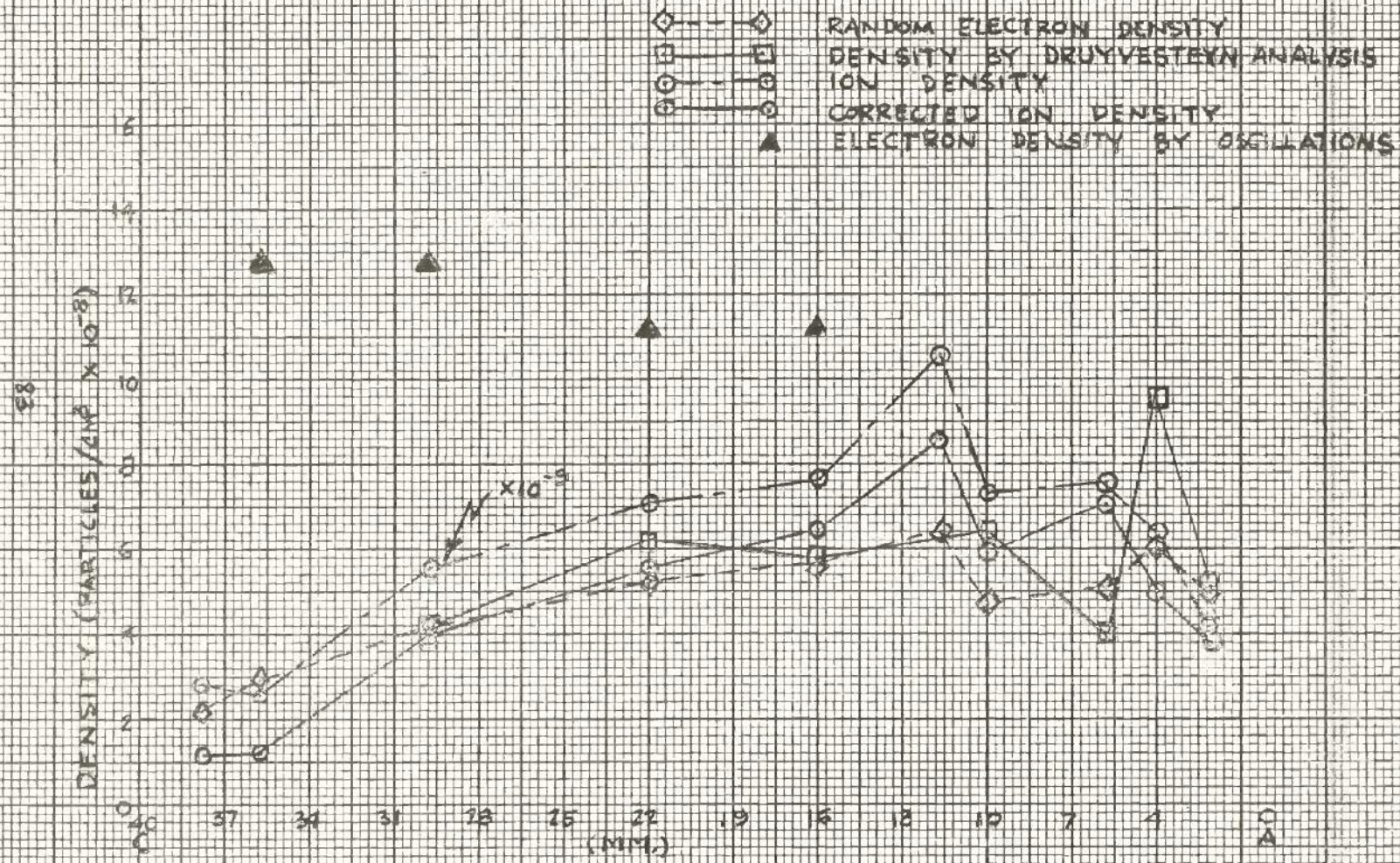

FIG. 48 ELECTRON AND ION DENSITIES VS PROBE POSITION, RUN 21, NEON

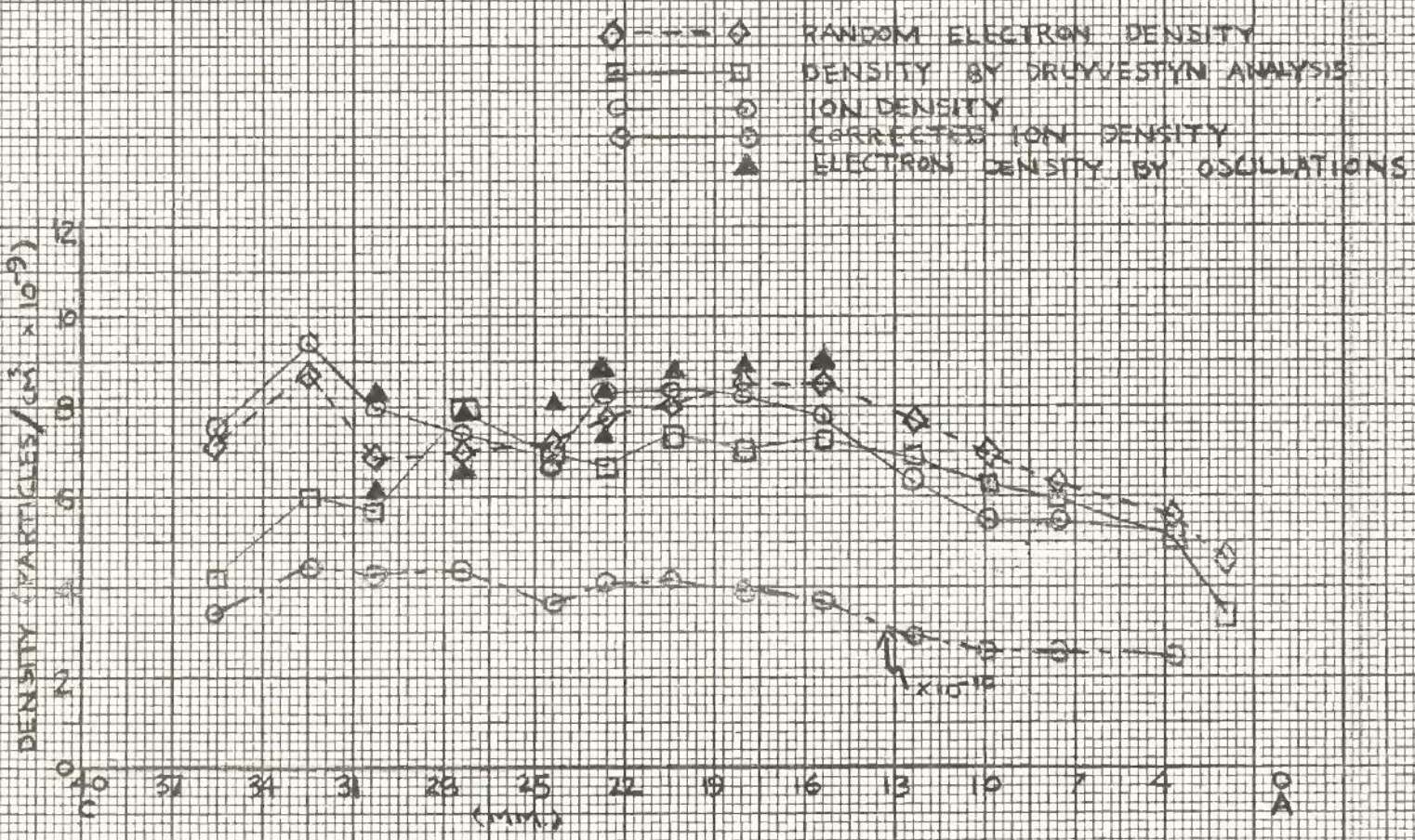

FIG. 49 ELECTRON AND ION DENSITIES VS PROBE POSITION, RUN 39 ARGON

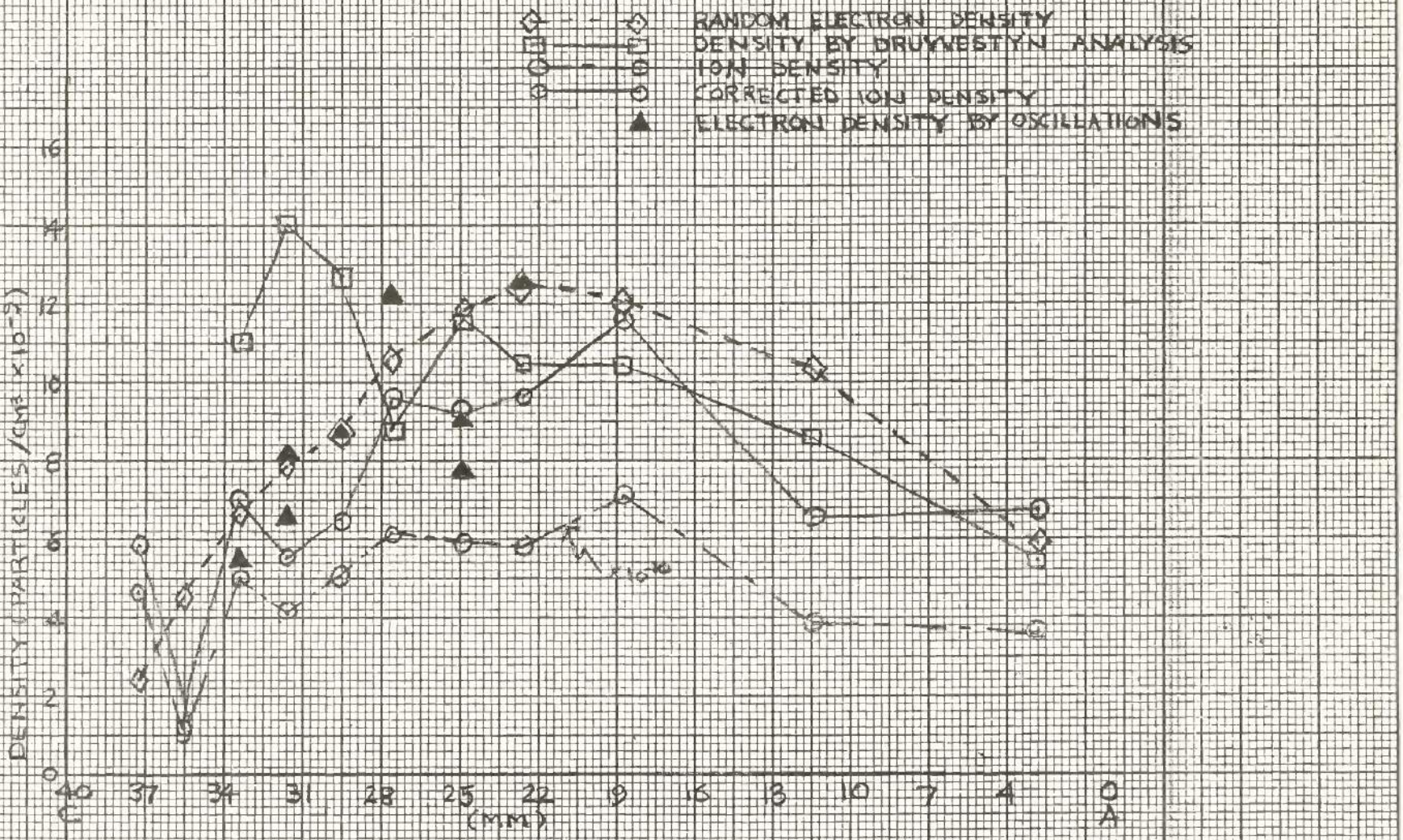

FIG. 50 ELECTRON AND ION DENSITIES VS PROBE POSITION, RUN 40 KRYPTON

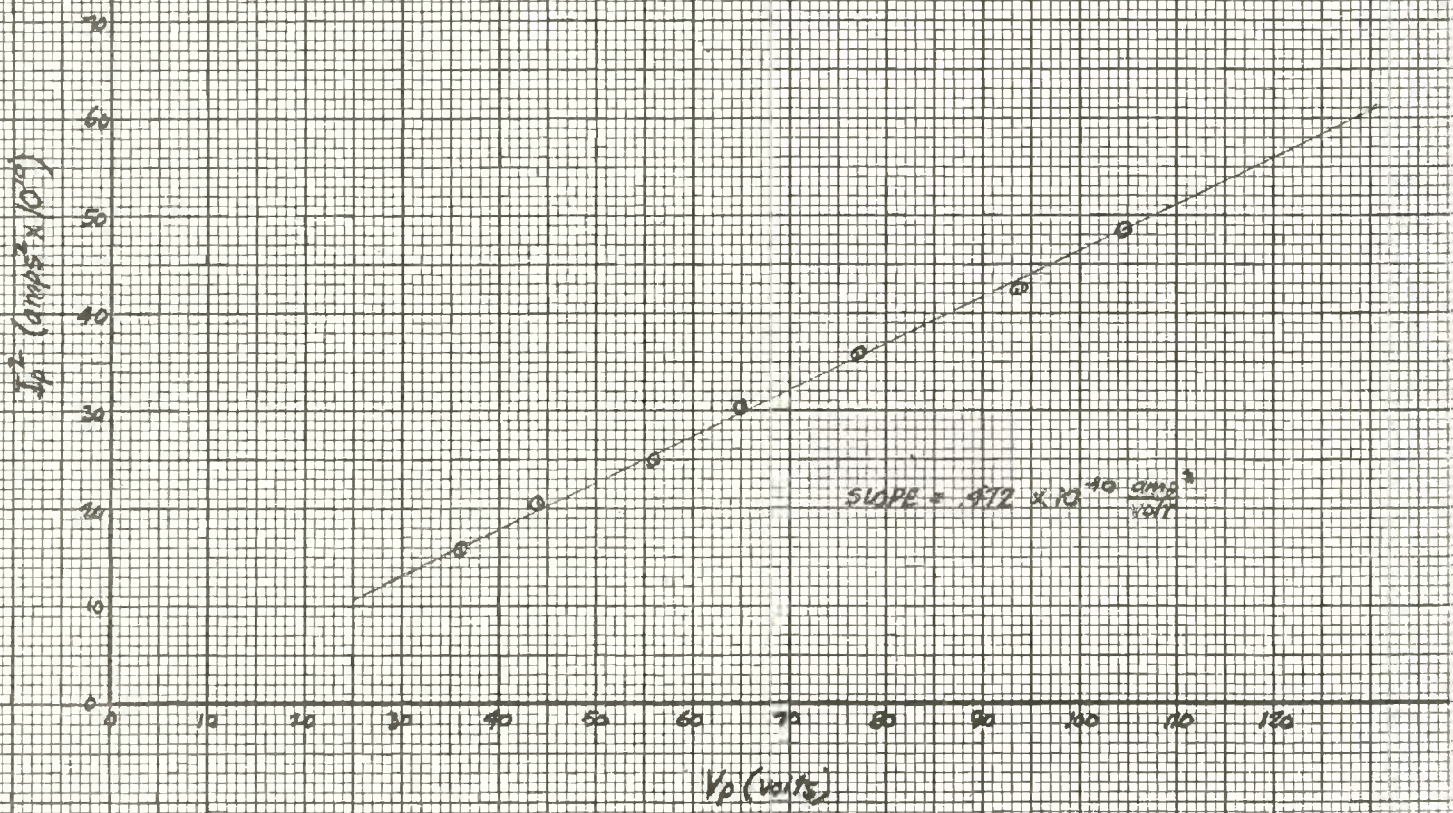

Figure 51. Sample I_p^2 versus V_p Plot (Run 39.7)

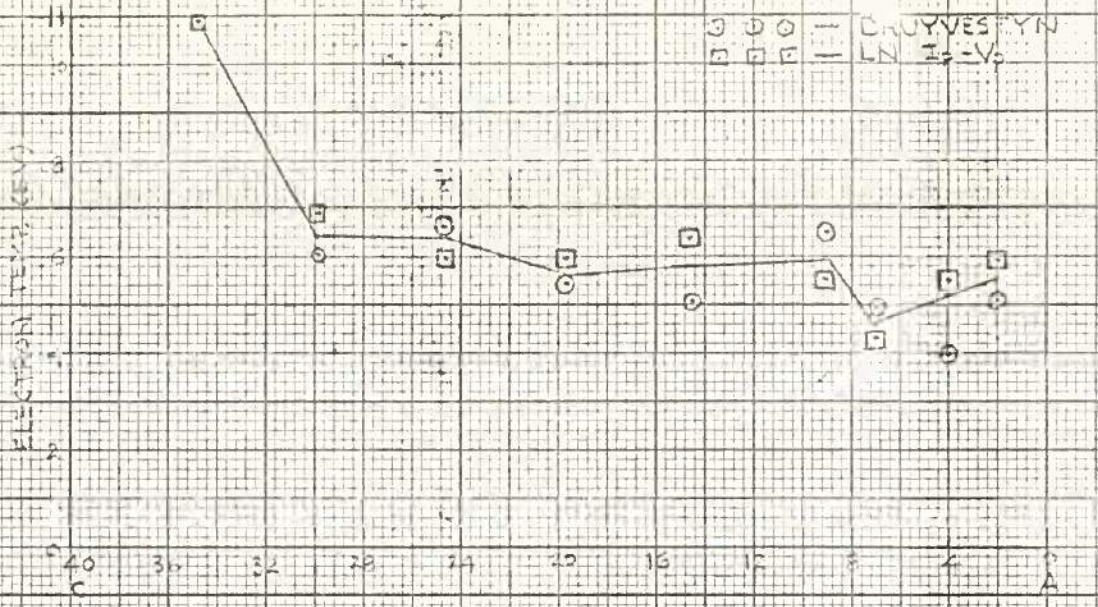

FIG. 52 ELECTRON TEMPERATURE VS. PROBE POSITION, RUN 19 NEON

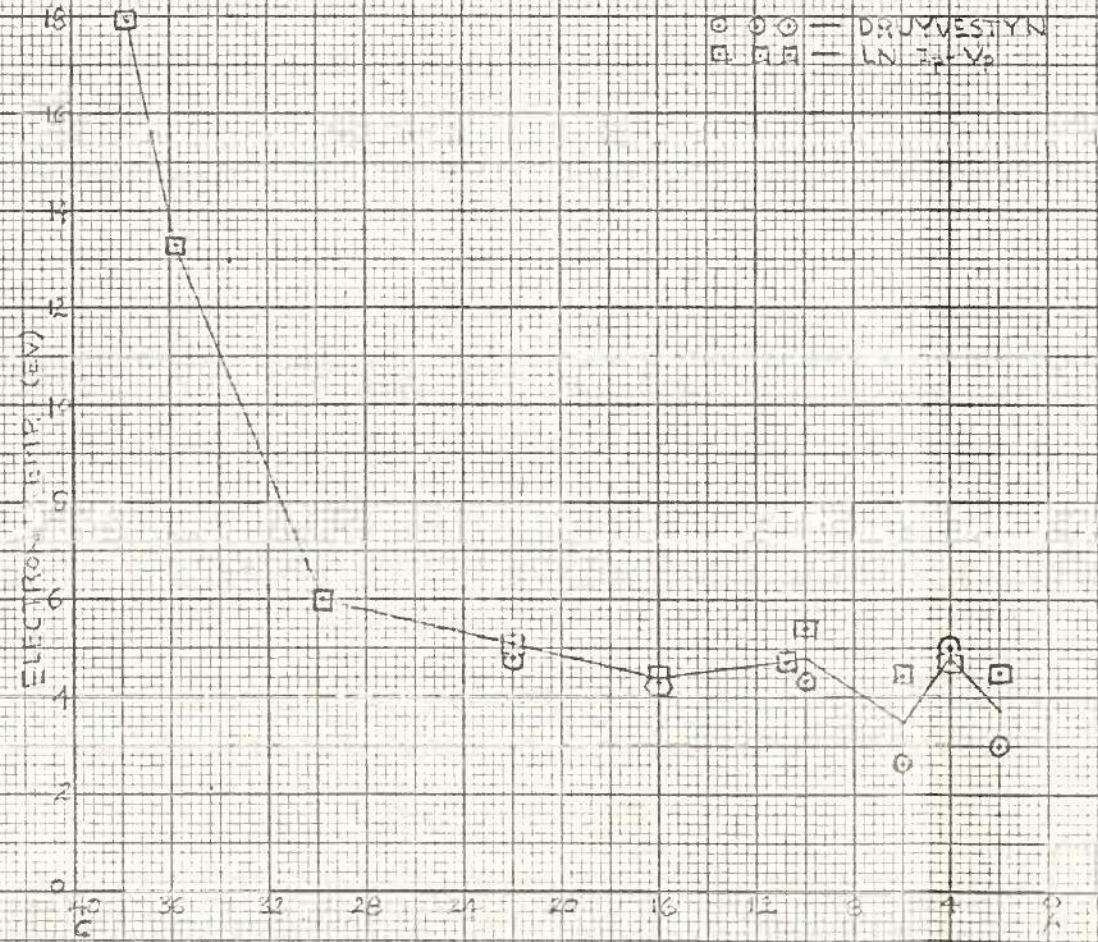

FIG. 53 ELECTRON TEMPERATURE VS. PROBE POSITION, RUN 21 NEON

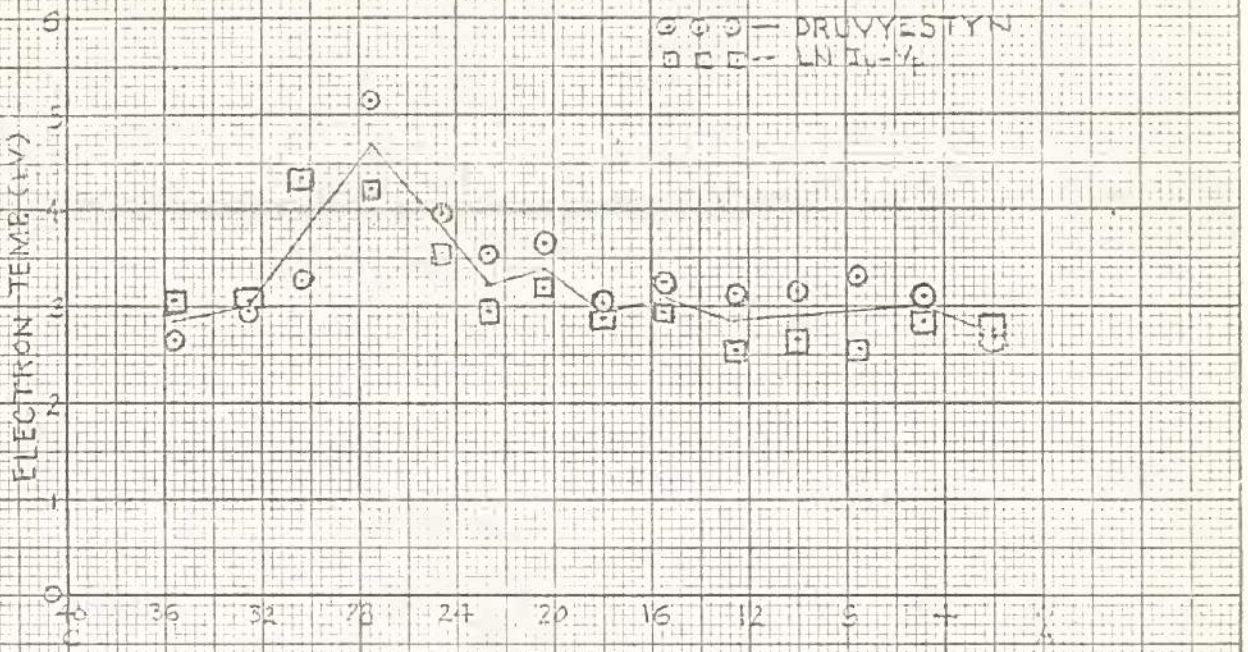

FIG. 54 ELECTRON TEMPERATURE VS. PROBE POSITION, RUN 39 ARGON

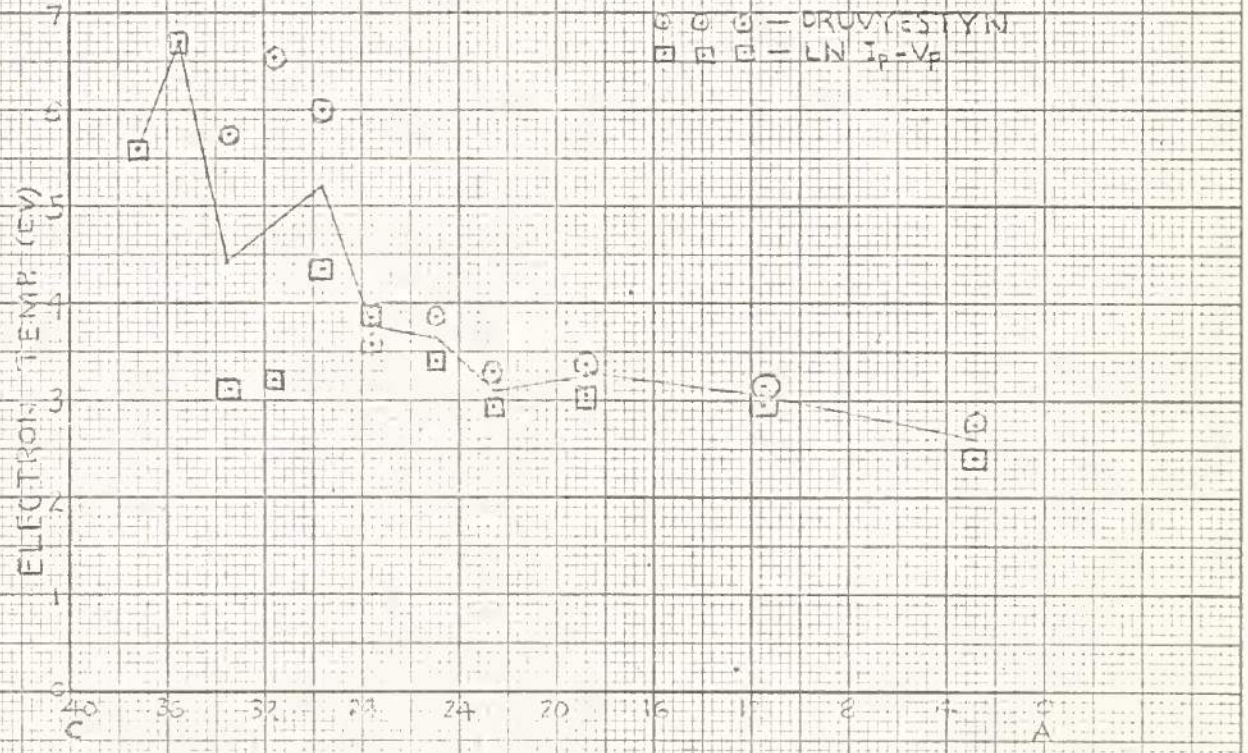

FIG. 55 ELECTRON TEMPERATURE VS. PROBE POSITION, RUN 40 KRYPTON

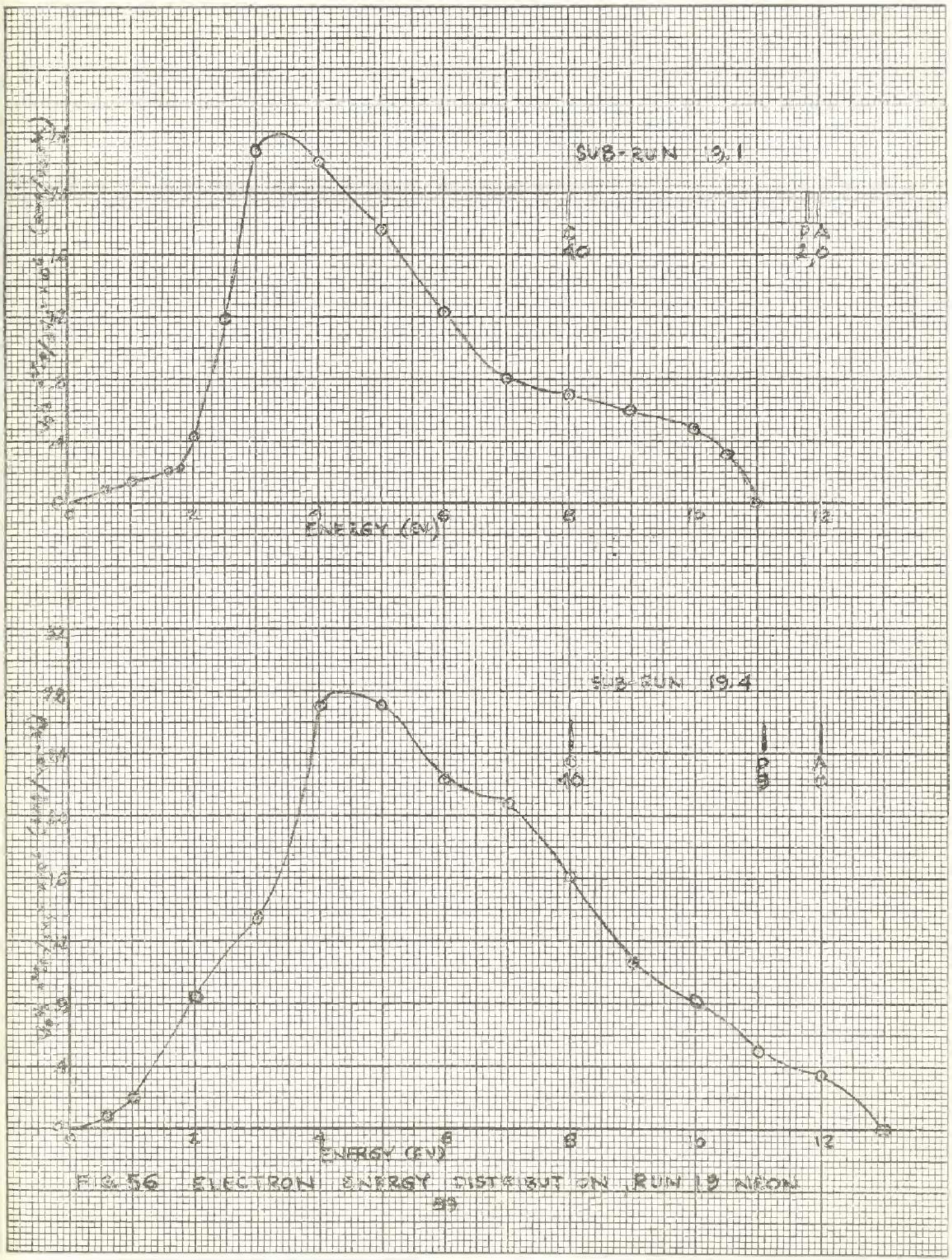

FIG 56 ELECTRON ENERGY DISTRIBUTION, RUN 19 NEON

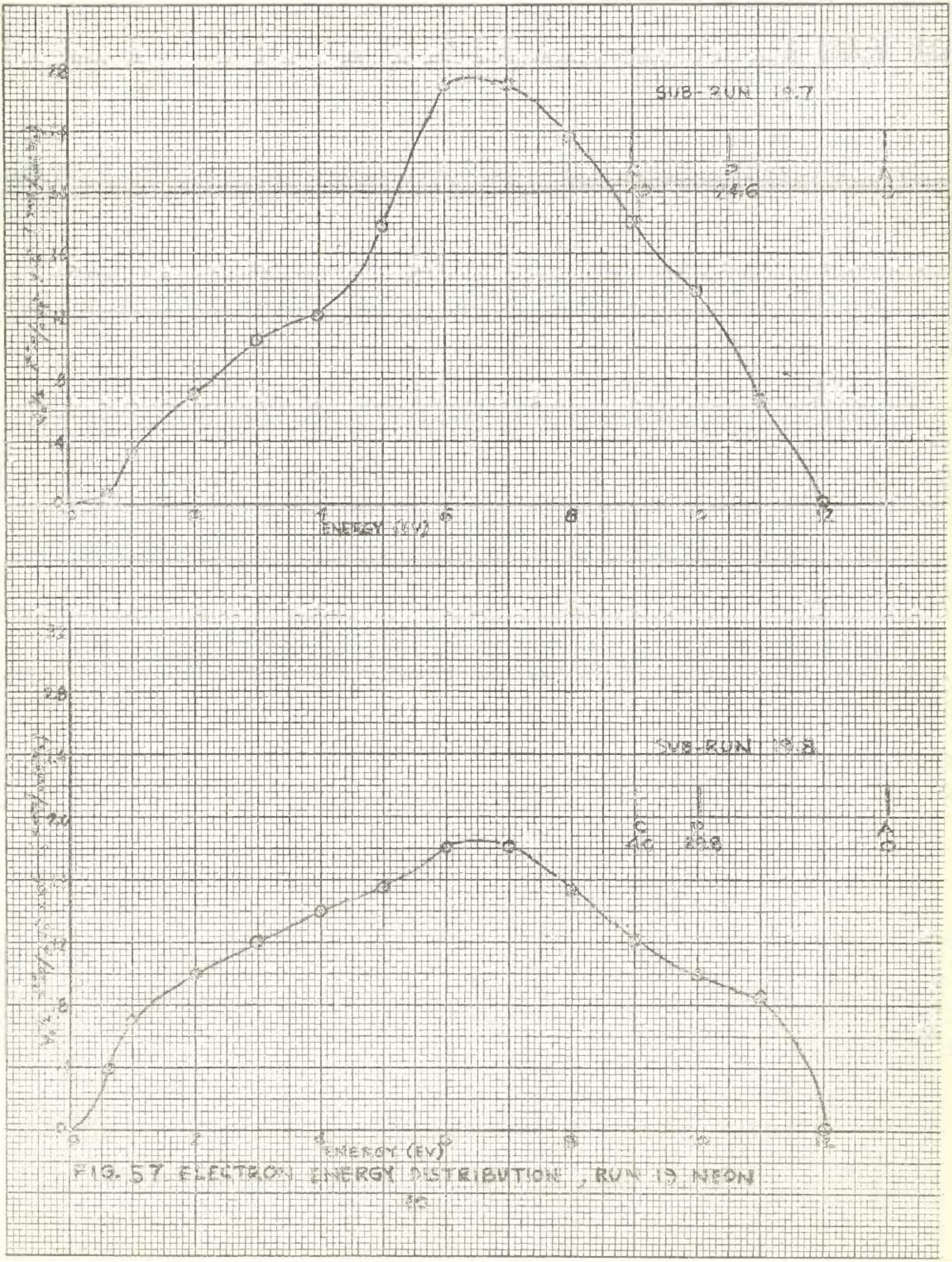

FIG. 57 ELECTRON ENERGY DISTRIBUTION, RUN 19 NEON

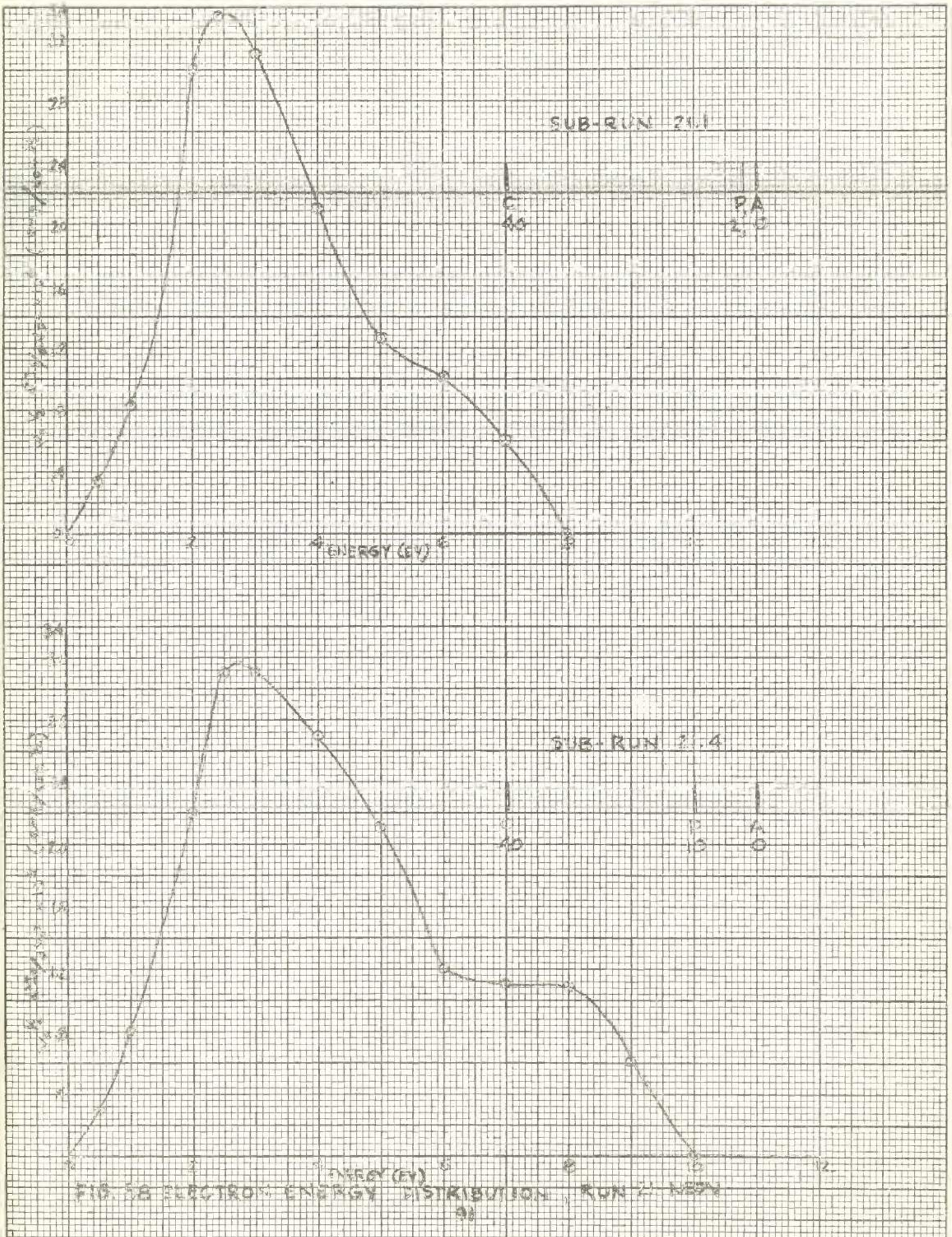

FIG. 5B ELECTRON ENERGY DISTRIBUTION, RUN 21, NEON

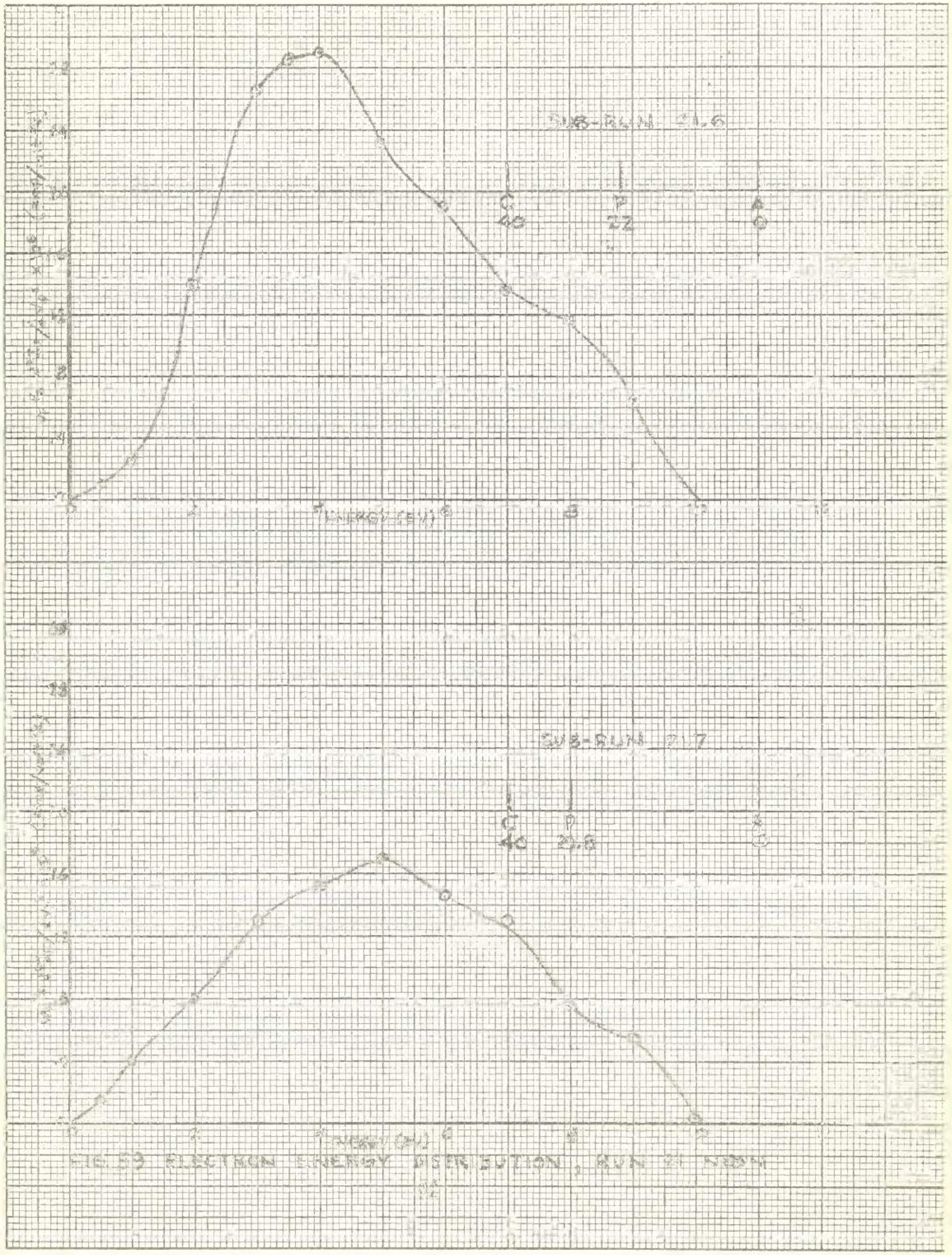

FIG. 23 ELECTRON ENERGY DISTRIBUTION, RUN 21 NEON

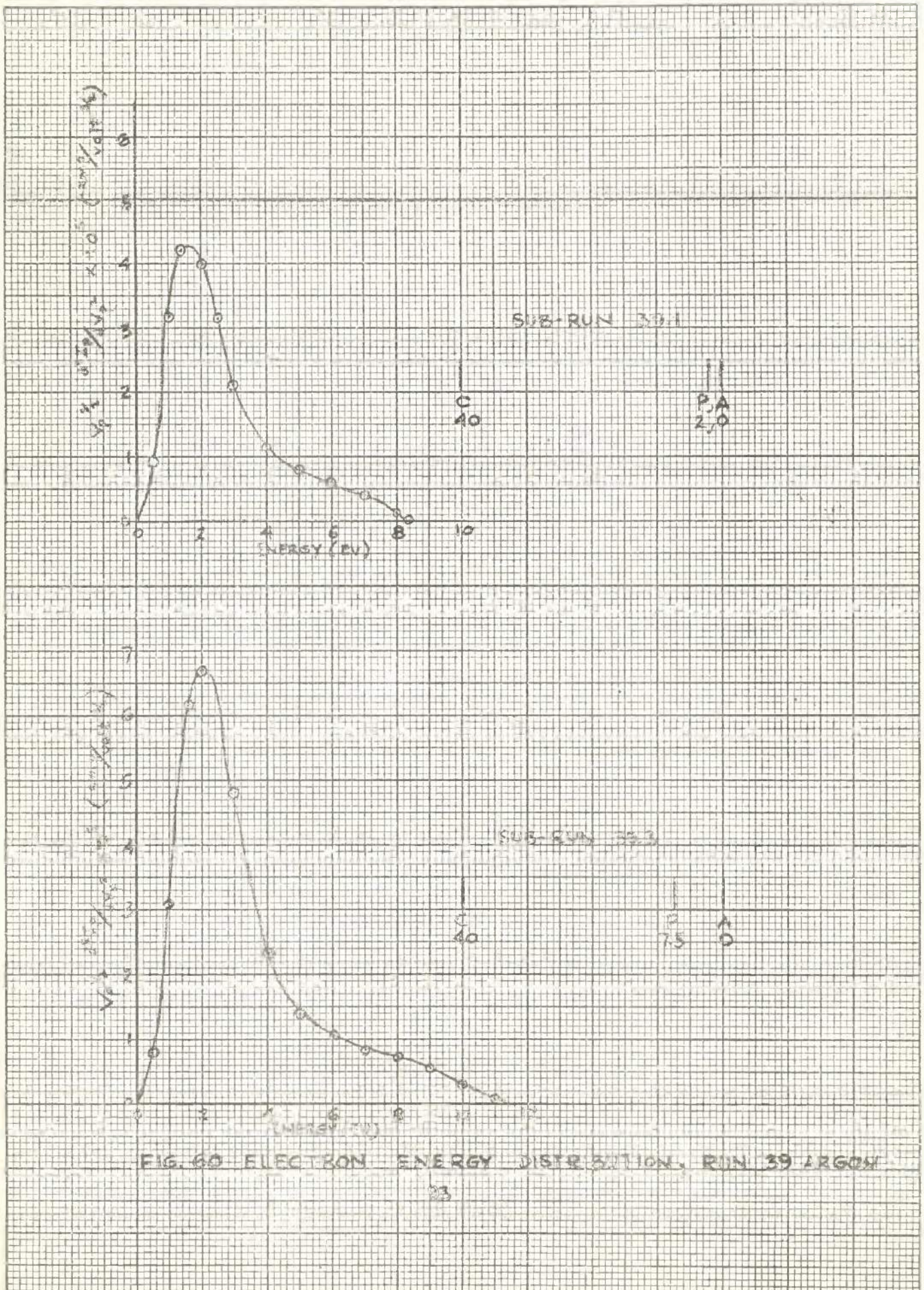

FIG. 60 ELECTRON ENERGY DISTRIBUTION, RUN 39 ARGON

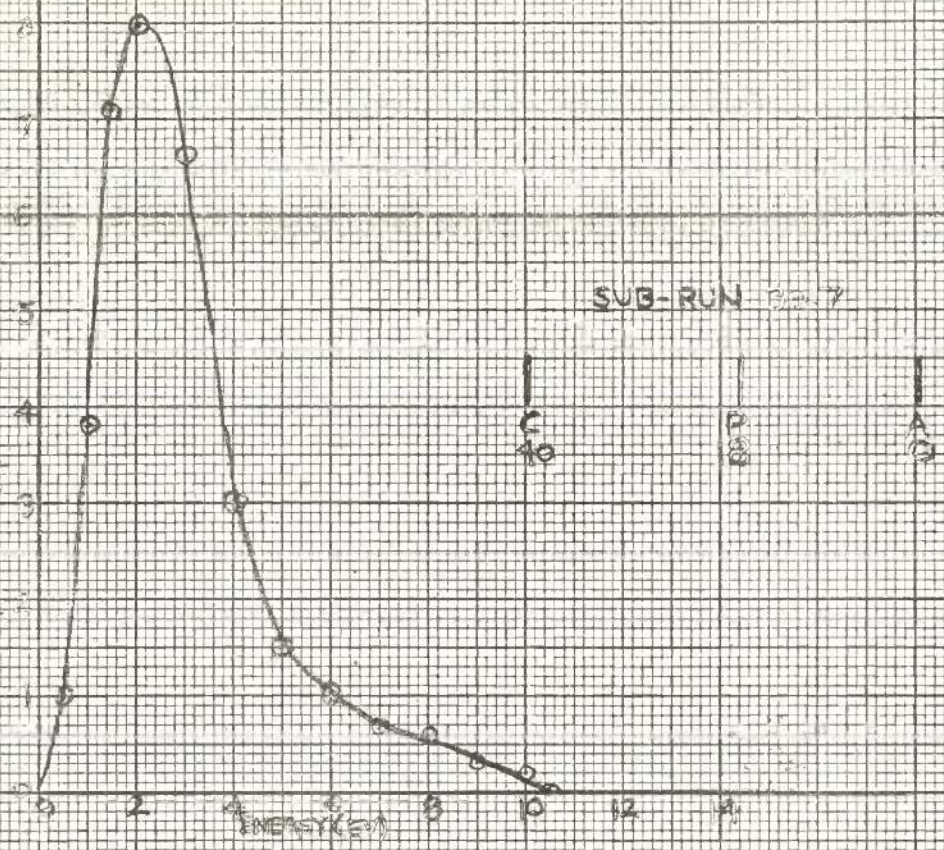

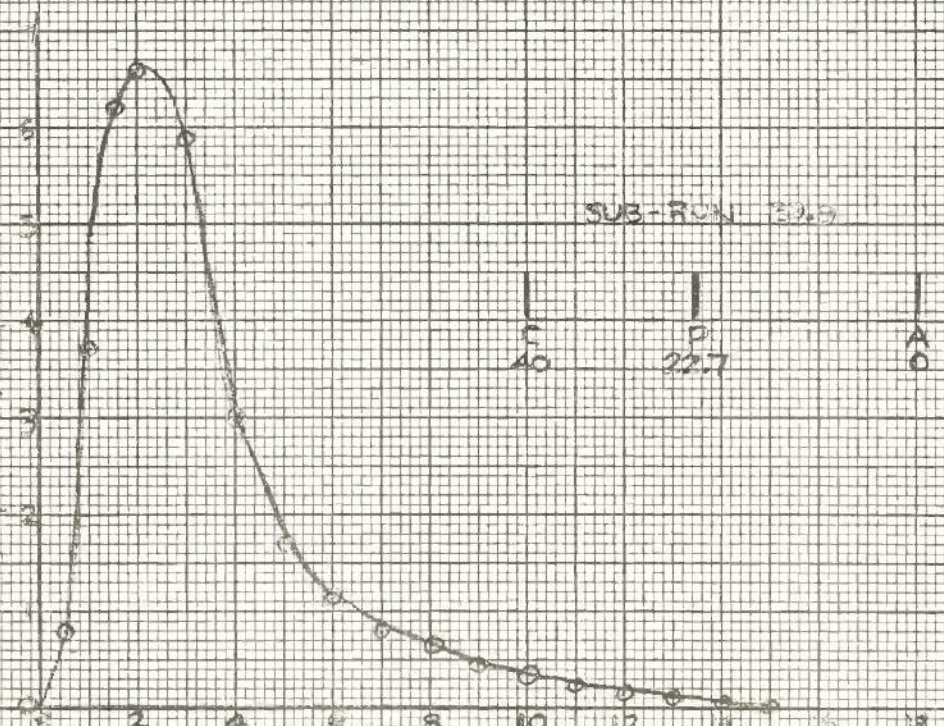

FIG 61 ELECTRON ENERGY DISTRIBUTION, RUN 29 ARGON

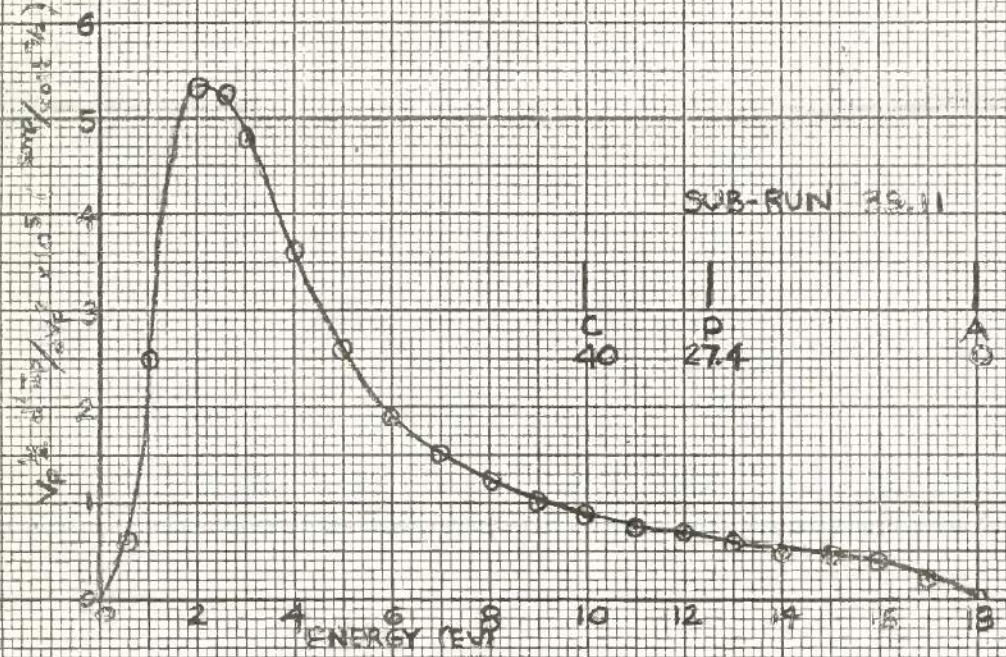

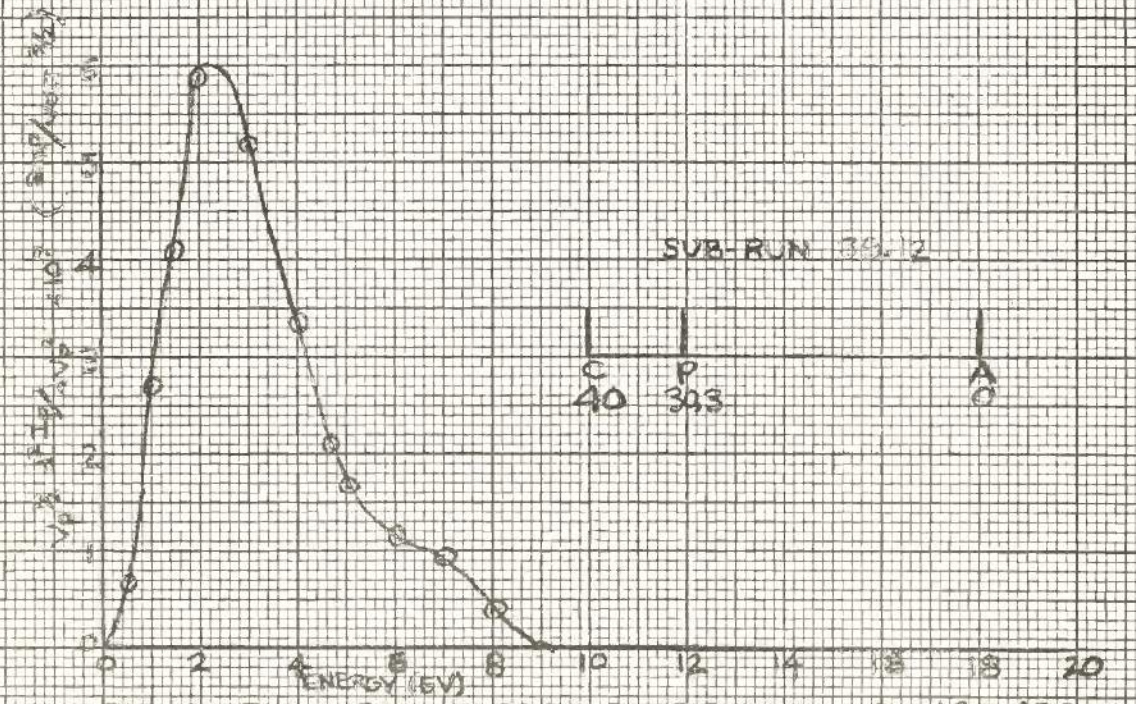

FIG. 62 ELECTRON ENERGY DISTRIBUTION, RUN 39 ARGON

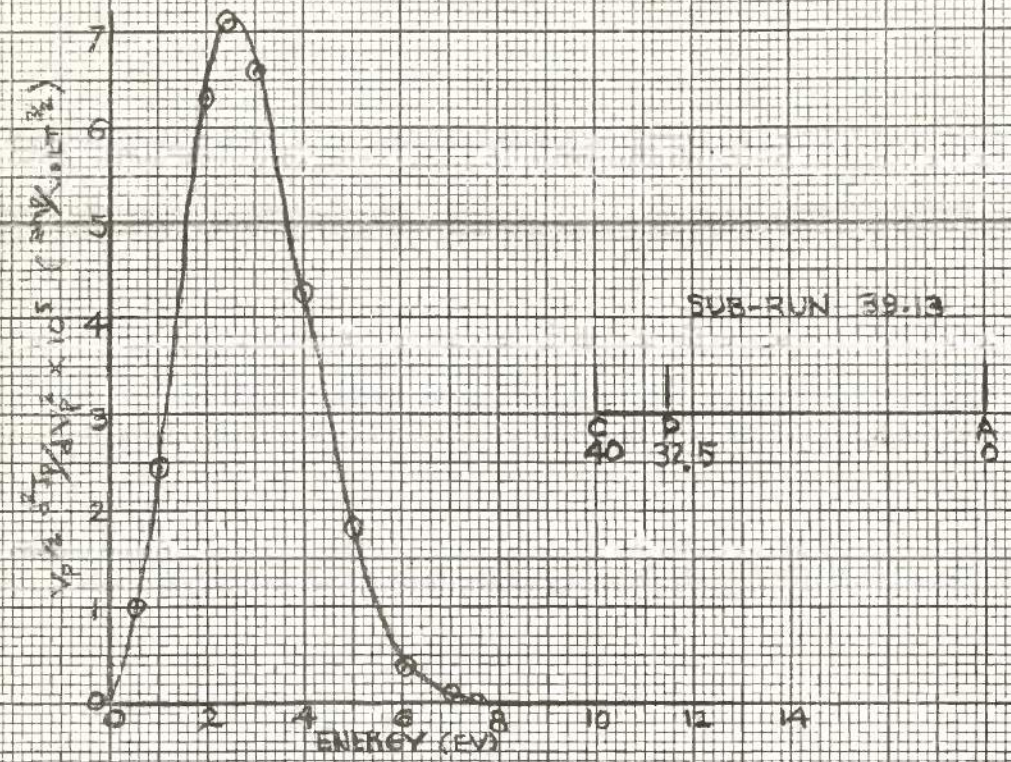

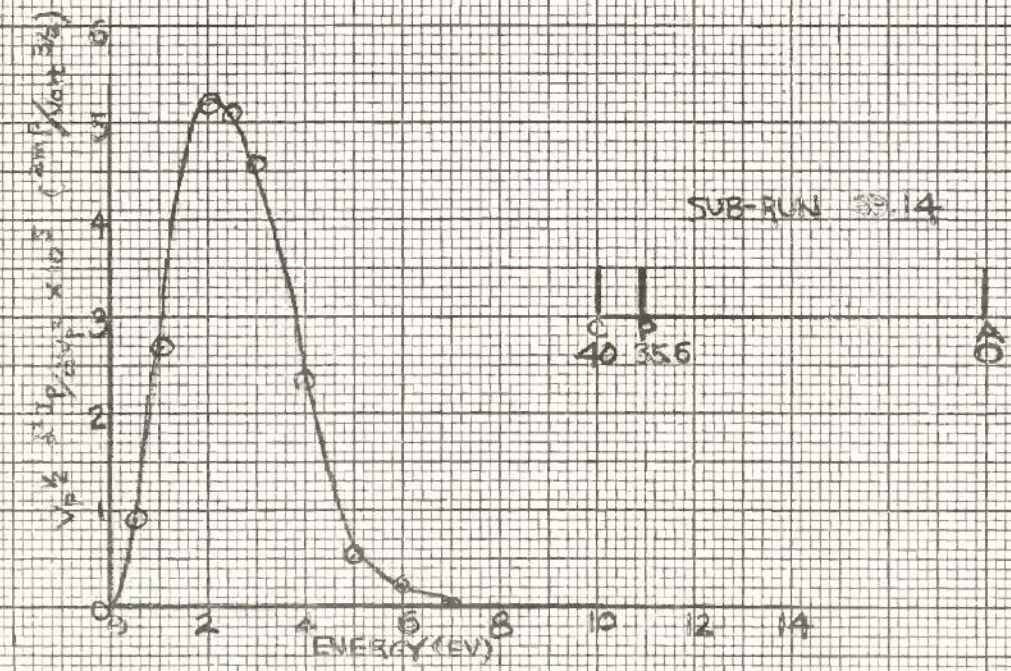

FIG. 63 ELECTRON ENERGY DISTRIBUTION, RUN 39 ARGON

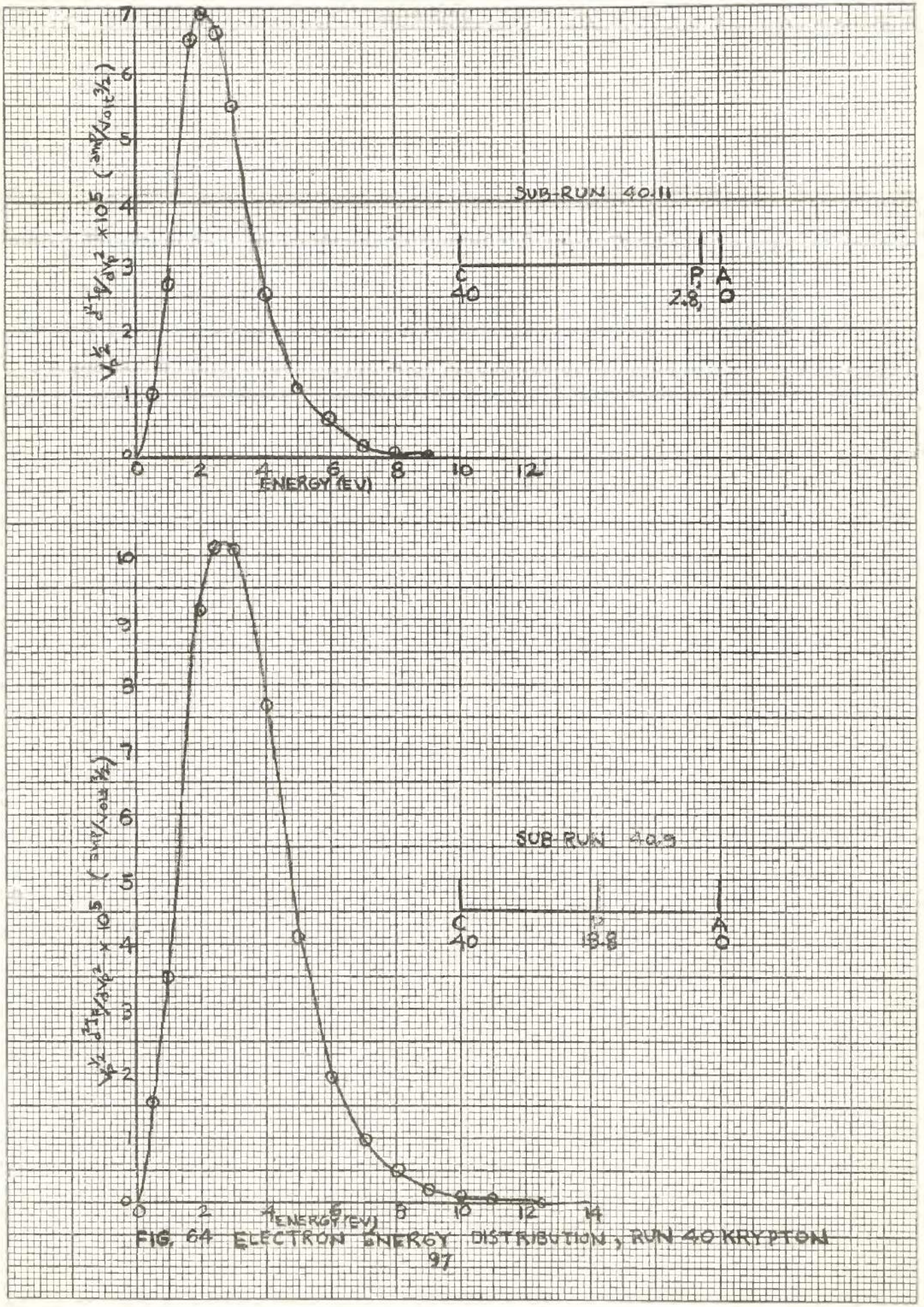

FIG. 64 ELECTRON ENERGY DISTRIBUTION, RUN 40 KRYPTON

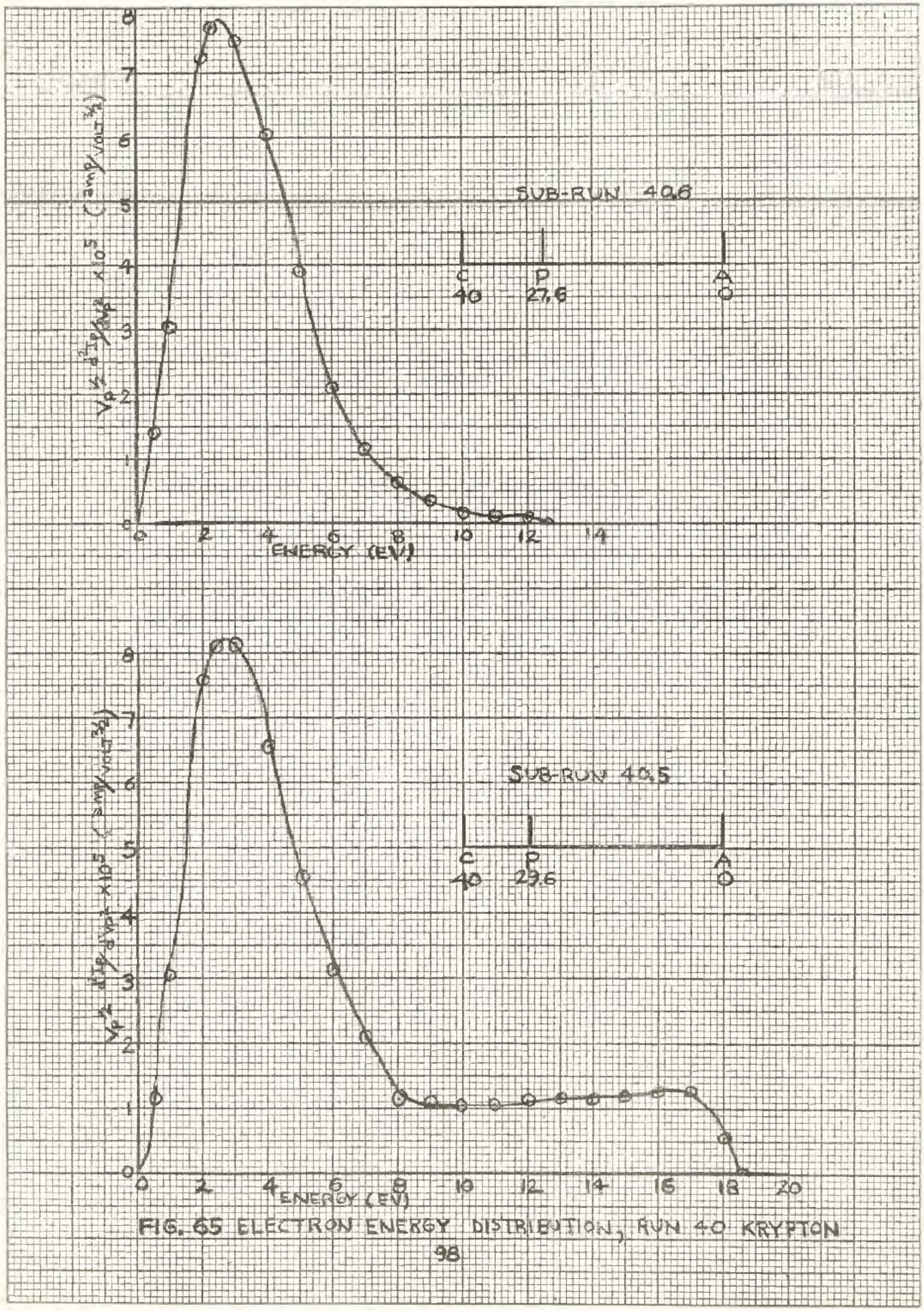

FIG. 65 ELECTRON ENERGY DISTRIBUTION, RUN 40 KRYPTON

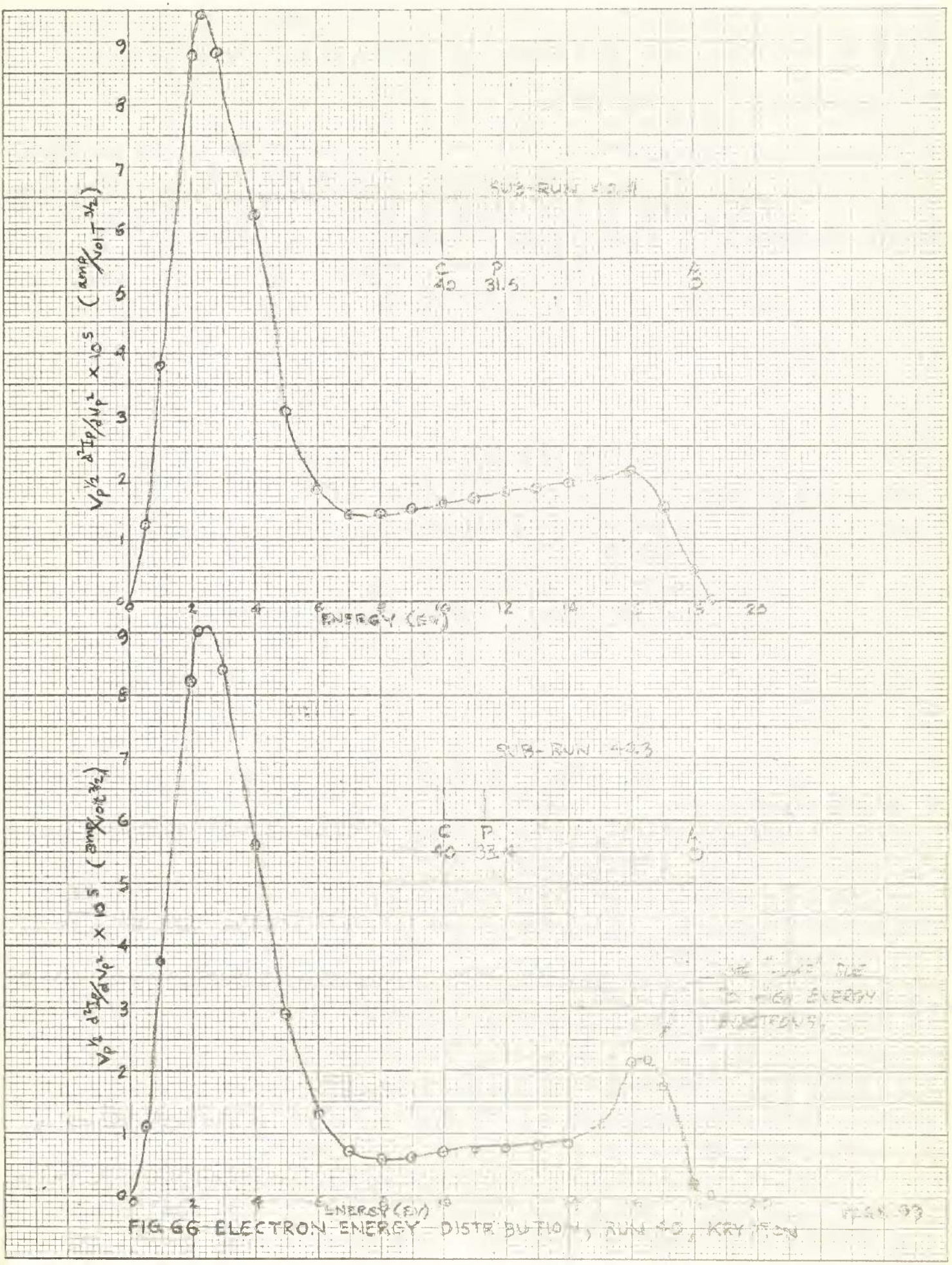

FIG 66 ELECTRON ENERGY DISTRIBUTION, RUN 40, KEY (EV)

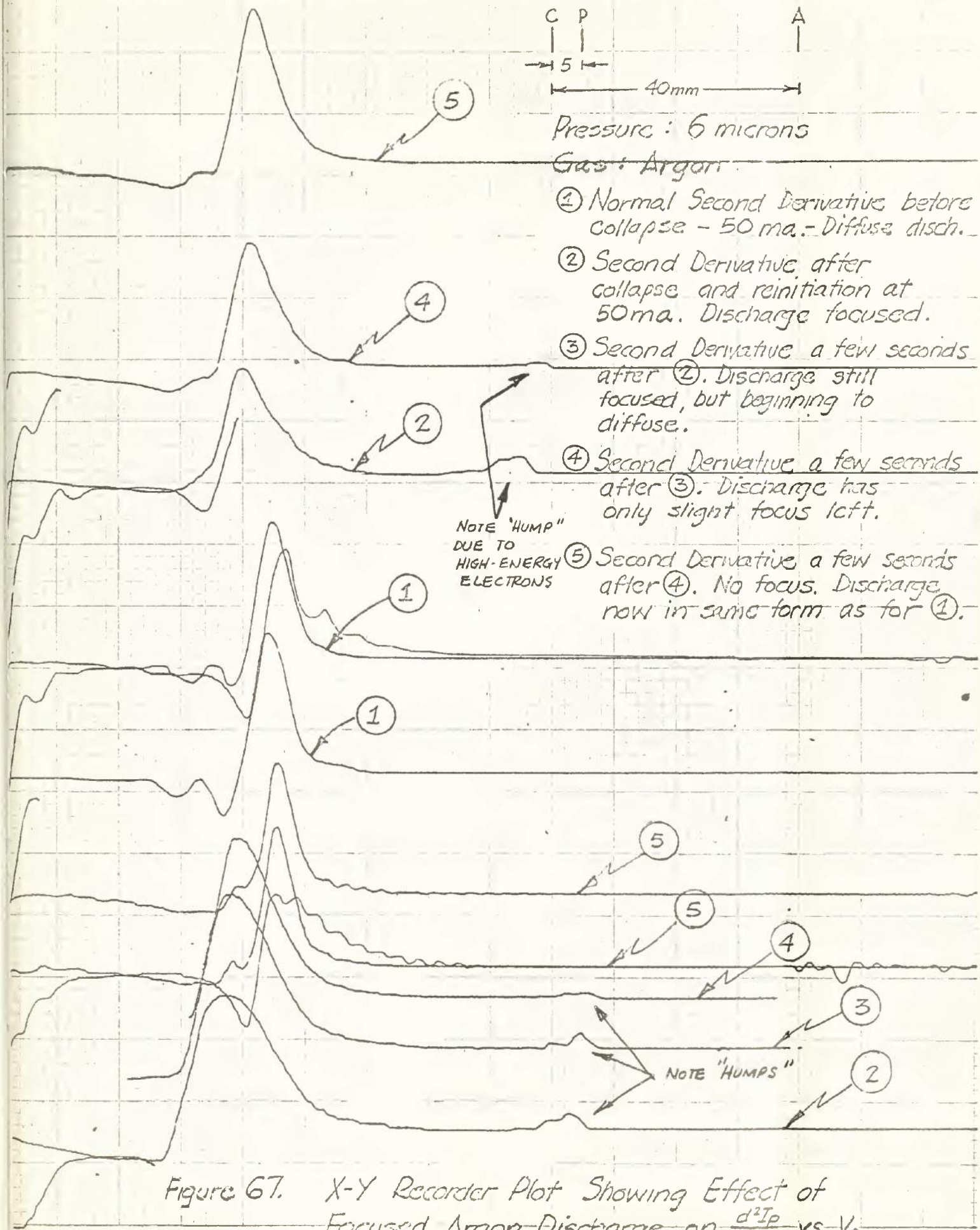

Figure 67. X-Y Recorder Plot Showing Effect of Focused Argon Discharge on $\frac{d^2I_p}{dV_p^2}$ vs. V_p

Run 19.5 Neon
Probe 14.5 mm from Anode

Run 19.6 Neon
Probe 19.7 mm from Anode

Run 19.7 Neon
Probe 24.6 mm from Anode

Figure 68. Sample Ion Oscillation Photographs

Run 21.5 Neon
Probe 16 mm from Anode

Run 21.6 Neon
Probe 22 mm from Anode

Run 21.7 Neon
Probe 29.8 mm from Anode

Figure 69. Sample Ion Oscillation Photographs

Run 39.1 Argon
Probe 2 mm from Anode

Run 39.2 Argon
Probe 4.8 mm from Anode

Run 39.3 Argon
Probe 7.5 mm from Anode

Run 39.13 Argon
Probe 32.5 mm from Anode

Run 39.14 Argon
Probe 35.6 mm from Anode

Figure 70. Sample Ion Oscillation Photographs

Run 40.1 Krypton
Probe 37.2 mm from Anode

Run 40.7 Krypton
Probe 24.9 mm from Anode

Run 40.2 Krypton
Probe 35.5 mm from Anode

Run 40.8 Krypton
Probe 22.6 mm from Anode

Run 40.3 Krypton
Probe 33.4 mm from Anode

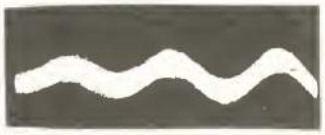

Run 40.9 Krypton
Probe 18.8 mm from Anode

Figure 71. Sample Ion Oscillation Photographs

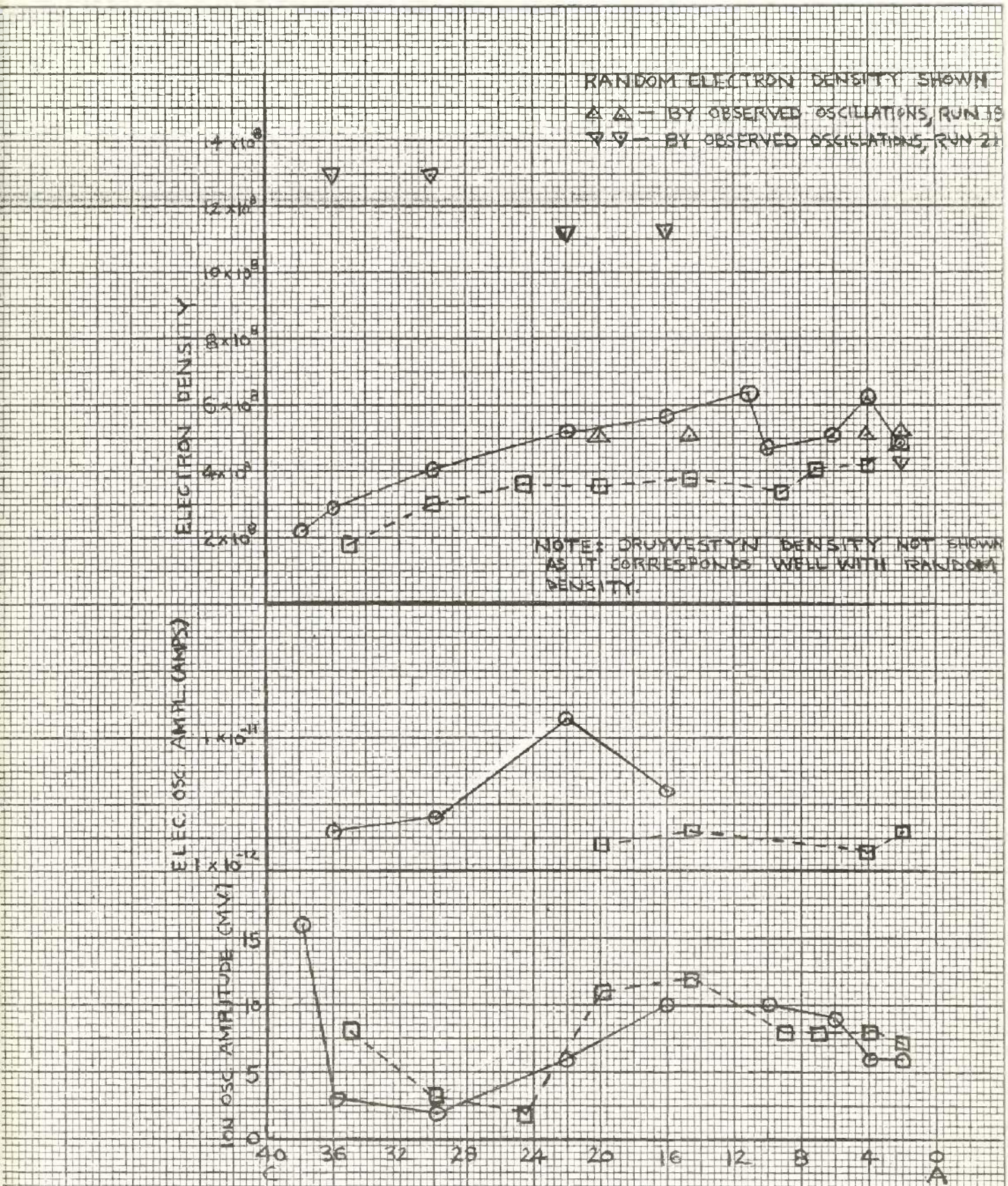

FIG. 72 ELECTRON OSCILLATION AMPLITUDE, ION OSCILLATION AMPLITUDE, ELECTRON DENSITY VS POSITION
□ □ □ — RUN 19, NEON
⊙ ⊙ ⊙ — RUN 21, NEON

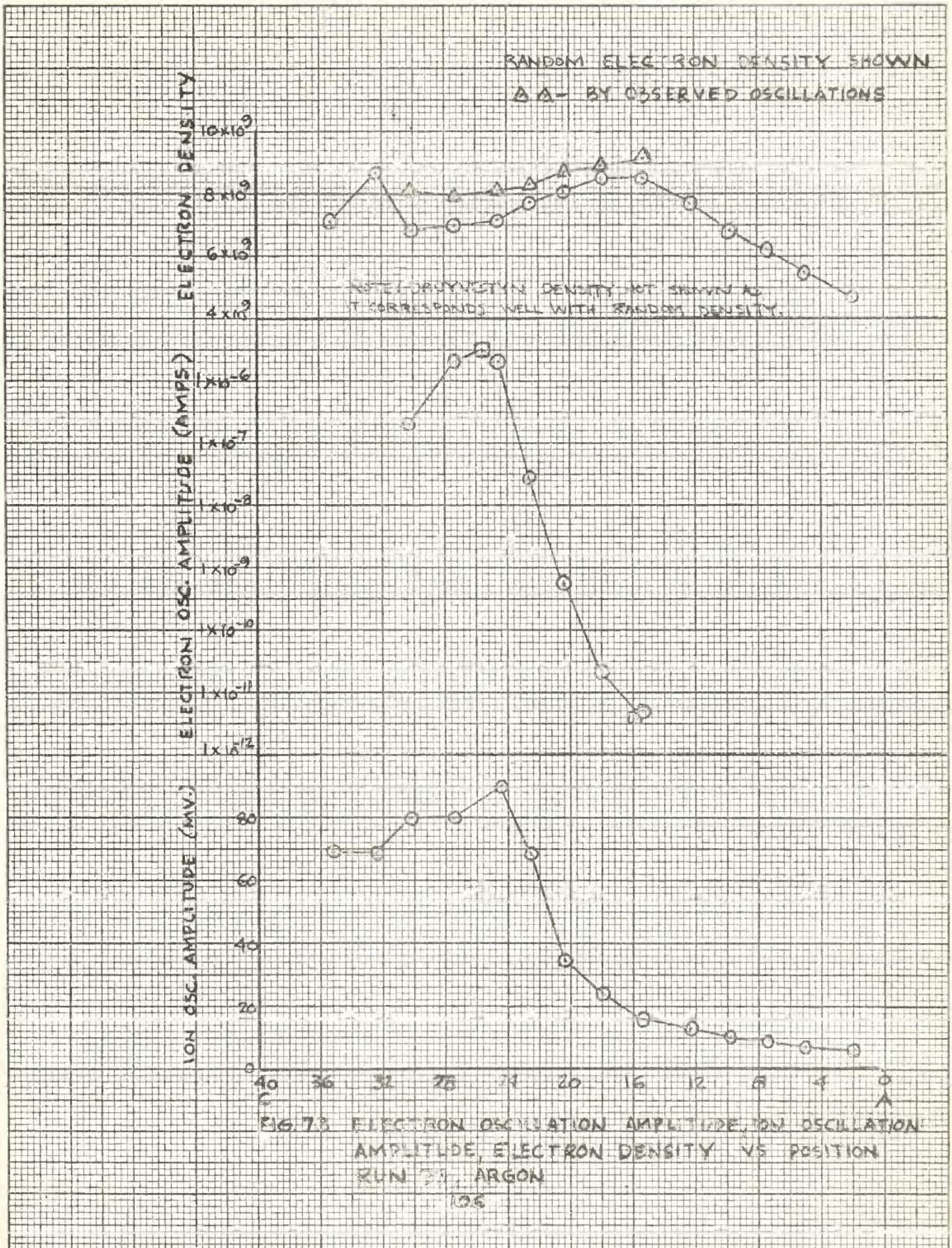

FIG. 7B ELECTRON OSCILLATION AMPLITUDE, ION OSCILLATION AMPLITUDE, ELECTRON DENSITY VS POSITION
RUN 30, ARGON

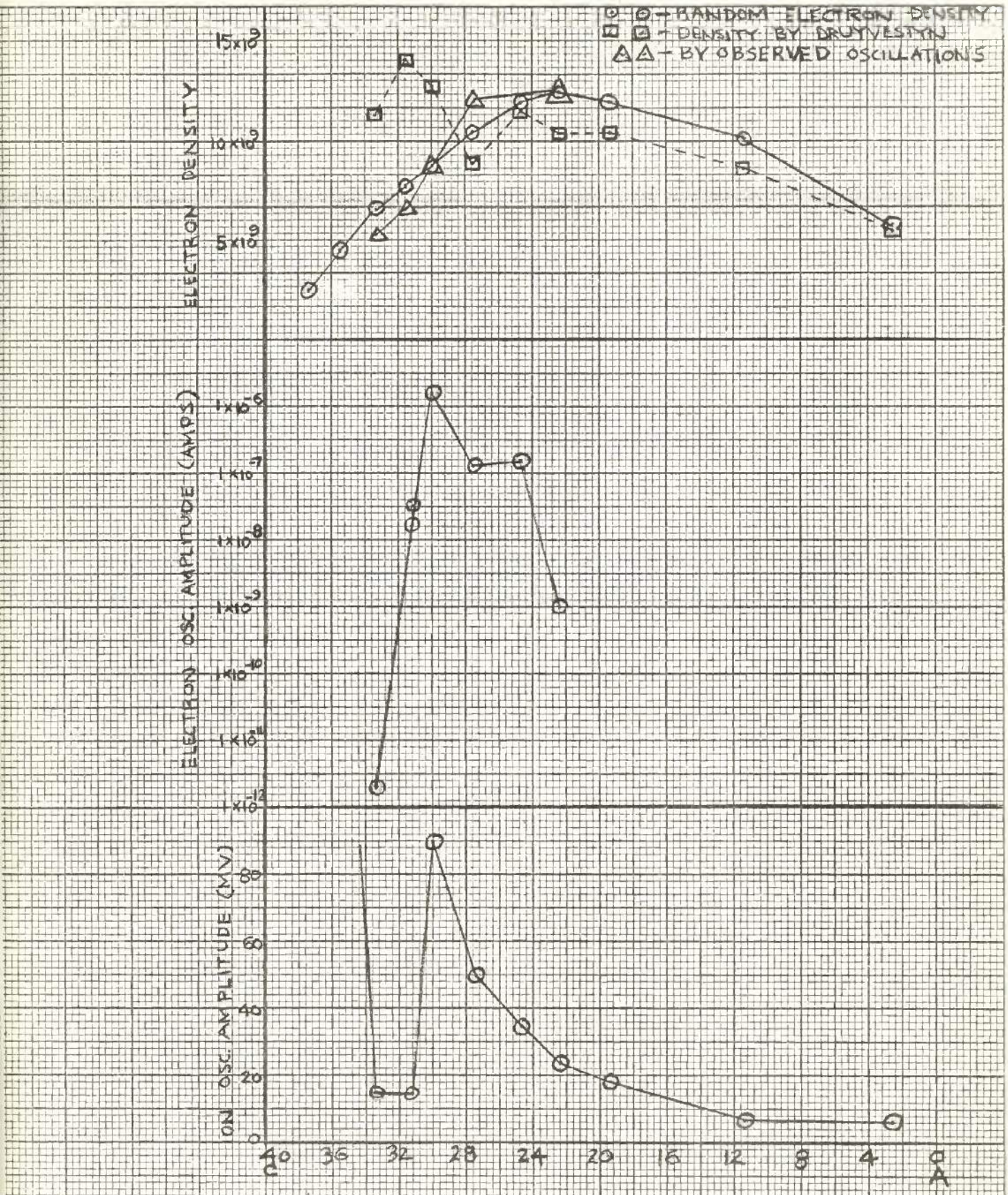

FIG 74 ELECTRON OSCILLATION AMPLITUDE, ION OSCILLATION AMPLITUDE, ELECTRON DENSITY VS POSITION RUN 40, KRYPTON

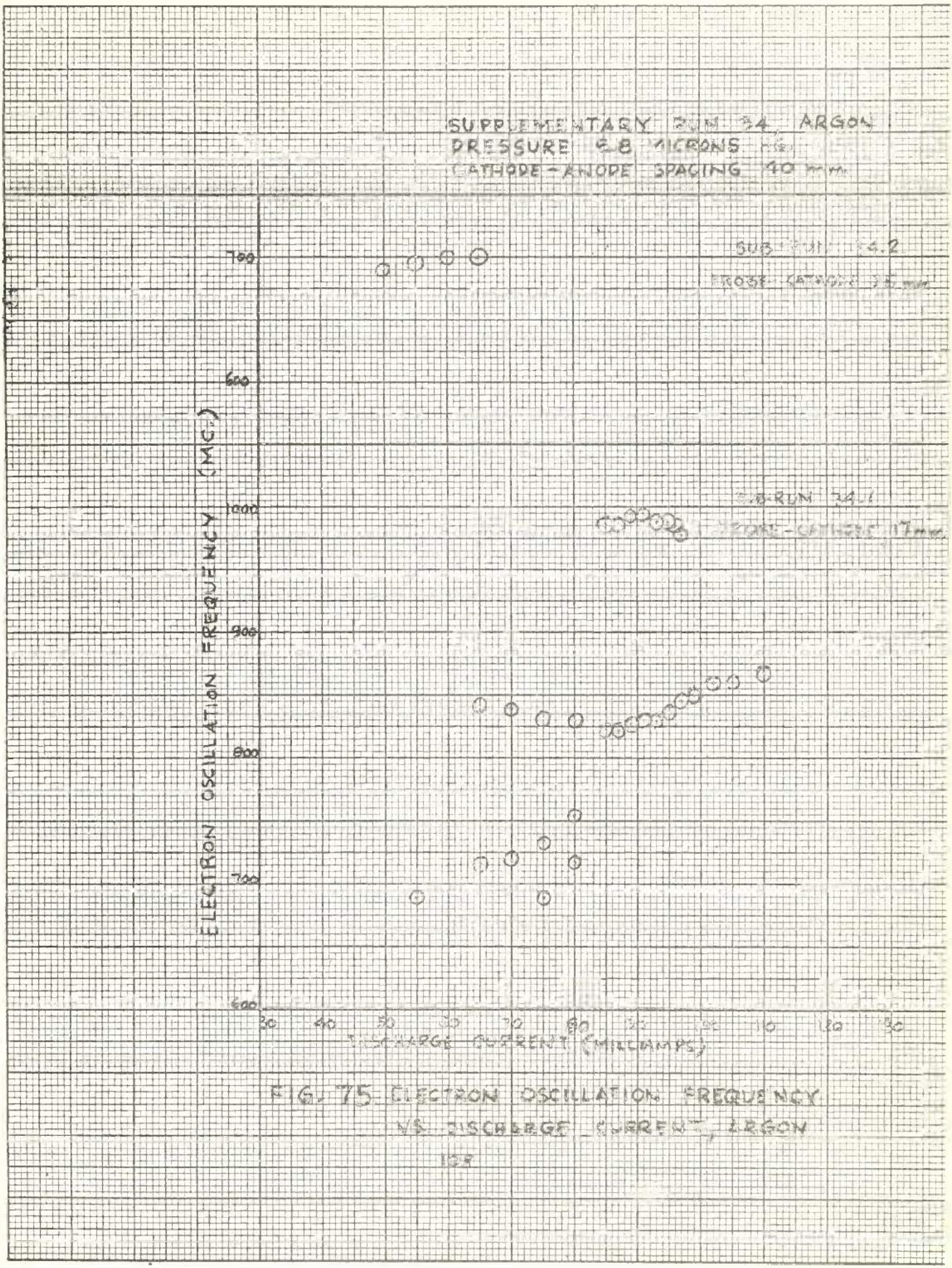

FIG. 75. ELECTRON OSCILLATION FREQUENCY VS. DISCHARGE CURRENT, ARGON

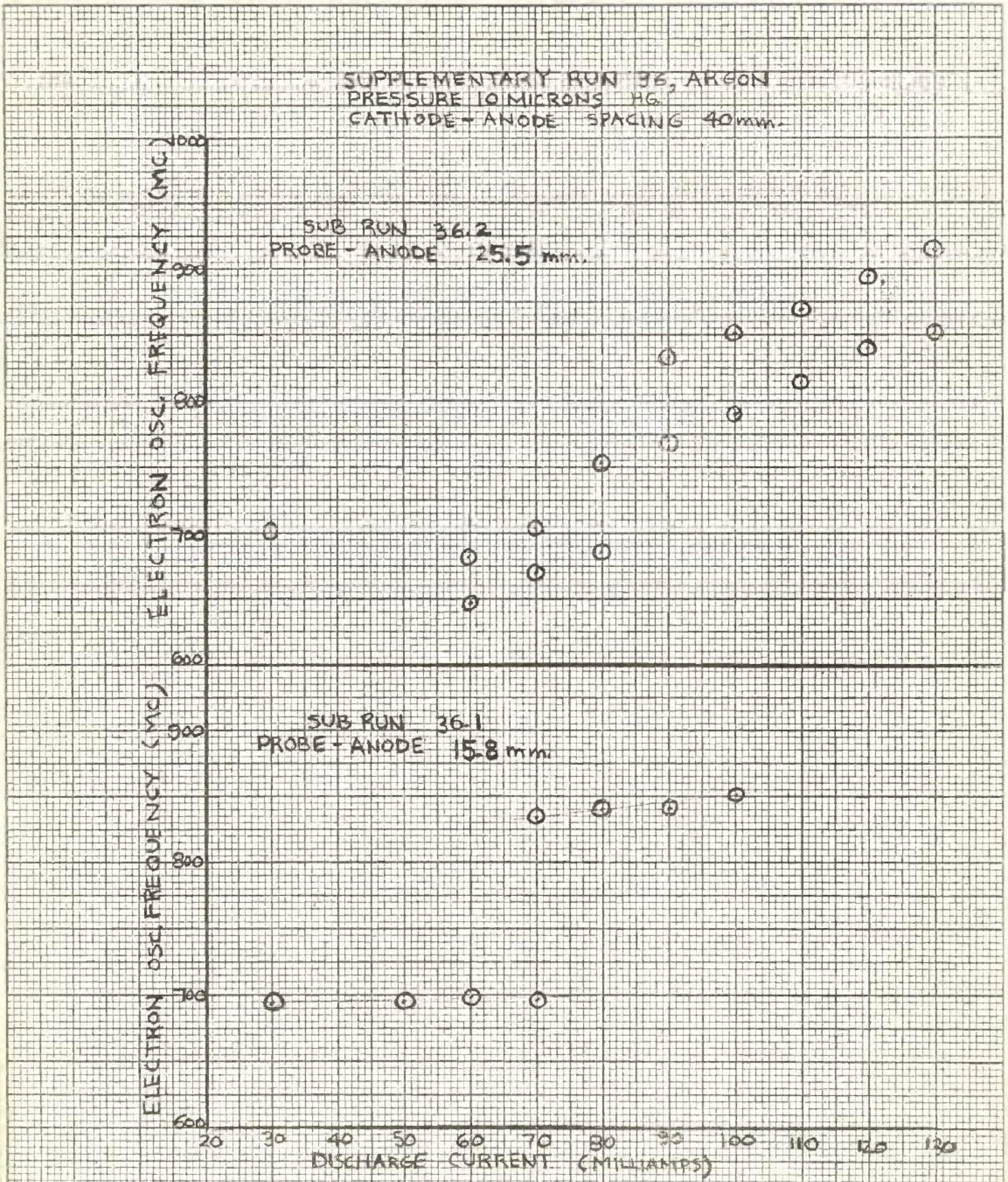

FIG. 76 ELECTRON OSCILLATION FREQUENCY VS. DISCHARGE CURRENT, ARGON

BIBLIOGRAPHY

1. J. G. Linhart, Plasma Physics, p. [illegible] ing Co., Amsterdam, 1960.

2. L. Tonks and I. Langmuir, Phys. Rev. 33 p. [illegible]

3. I. Langmuir and H. Mott-Smith [illegible] Phys. Rev. 44 [illegible]

4. I. Langmuir, Phys. Rev. 26 p. 585 [illegible]

5. A. F. Dittmer, Phys. Rev. 28 p. 507 [illegible]

6. Lewi Tonks and I. Langmuir Phys. Rev. 33 p. [illegible]

7. H. J. Merrill and H. W. Webb, Phys. Rev. [illegible] p. [illegible]

8. E. B. Armstrong, Nature 160 p. 713 [illegible]

9. K. G. Emeleus, et al, British Journal of Applied Physics Vol. 6 p. 320-322, September, 1955.

10. M. A. Easley, Journal of Applied Physics [illegible] p. [illegible]

11. N. L. Oleson and C. G. Found, Journal of Applied Physics 20, p. 416-417, 1949.

12. M. J. Druyvesteyn, Zeits. Phys. 29, 1958.

13. G. Medicus, Journal of Applied Physics [illegible] p. [illegible]

14. K. Takayama, H. Ikegama, and S. Miyazaki, Phys. Rev. [illegible] p. [illegible] 1960.

15. W. P. Allis, Electronic Waveguides, p. [illegible] Inst. Symposium Series, Vol. VI, [illegible]

16. D. W. Mahaffey, et al, Proceedings of the [illegible] Vol. 61, Sect. A, No. 9, 1961.

17. A. Carscadden, Experiments on Plasma Oscillations [illegible] Queen's Univ., Belfast, 1961.

18. K. G. Emeleus, Journal of Electronics and [illegible] p. 393, 1962.

19. T. K. Allen, Plasma Electron Oscillations [illegible] Univ., Belfast, 1954.

20. S. Kojima, K. Kato, and S. Nagakawa, [illegible] of Japan, Vol. 12, No. 11, p. 12[illegible]

21. S. Kojima, K. Kato, S. Hagiwara, and R. Matsuzaki, Journal of the Physical Society of Japan, Vol. 14, No. 6, p. 821-827, 1959.

22. I. Alexeff and R. V. Neidigh, Phys. Rev. 129, p. 516, 1963.

23. D. M. Alderson, Jr., and J. D. Leonard, Jr., Plasma Oscillations in a Low Pressure Neon Discharge (Master's Thesis), U. S. Naval Postgraduate School, June, 1962.

24. L. S. Hall, Probes and Magnetic Pumping in Plasma (Doctoral Thesis) University of California, Lawrence Radiation Laboratory; U. S. Department of Commerce, Washington, D. C., 1961.

25. G. R. Nicoll and J. Basu, Comparison of Microwave and Langmuir Probe Measurements on a Gaseous Plasma, Journal of Electronics and Control, January, 1962.

26. G. F. Haggquist, Plasma Resonance in Argon and Neon, (Master's Thesis) U. S. Naval Postgraduate School, June 1963.

APPENDIX

After compiling the data for this report, additional work was undertaken in Argon in an attempt to explain the non-appearance of high energy beam electrons near the cathode during our main runs in Argon.

Three separate investigations were made, each initially at 10 microns pressure, 100 ma discharge current, 40 mm anode-cathode spacing, and 1100°C cathode temperature. On one run these parameters were varied to observe the effect of the variation.

On the first run, after establishing the initial conditions and waiting approximately 30 minutes for equilibrium conditions to be established, a discharge was observed with definite visible structure:

The $\frac{dI}{dV_p}$ versus V_p plot revealed a "high-energy tail" or "high-energy hump" (see figure 67 for an example) indicating the presence of a group of high energy beam electrons when the probe was in region 1. When the probe was in region 2, no high-energy electrons were observed. In region 3, a "flame-shaped" dark space projecting from the cathode, the relative number of high energy electrons was greatly reduced (indicated by only a small

high-energy tail on the $\frac{d^2f}{dv^2}$ versus Vp plot). After some 30 minutes of investigation, and with no apparent change in any of the initial conditions, the visible structure disappeared; however, the high energy electron distribution remained essentially the same in the various regions. A check for detectable oscillations produced unusual results (compared to our previous results under like conditions). With the probe 6.5 mm from the cathode, in the region which had been the "flame-shaped" dark space, we at first detected no oscillations in the 200-2000 mc range. After 5 to 10 minutes, we began to pick up an oscillation whose frequency and amplitude appeared to be continuously changing. From the time it was first observed at 861 mc, the amplitude decreased from 1.0×10^{-7} amps to 3.0×10^{-9} amps at 796 mc and then disappeared. Since the oscillation frequency and amplitude were changing with the probe in a fixed position (center of the discharge), no radial probe movement was attempted.

On the second run after establishing identical initial conditions and waiting for at least 30 minutes, a discharge was observed with visible structure (but a structure entirely different from that observed on the previous run):

The [illegible] plot revealed high energy beam electrons in region 2, decreasing in relative number as the probe was retracted from the center of the discharge into region 1. Oscillations were observed of frequency and amplitude comparable to those detected in our "main runs" in Argon, for comparable probe positions in the center of the discharge.

On this second run, we varied cathode temperature, discharge current, and pressure to observe the sensitivity of discharge characteristics (particularly the appearance or non-appearance of high-energy beam electrons) with the variation of these parameters. Generally, the results were as follows:

(1) Decreasing the cathode temperature caused no visible change in structure; the relative number of high-energy electrons decreased.

(2) Increasing the cathode temperature caused no change in visible structure; the relative number of high energy electrons increased.

(3) Decreasing the cathode temperature, after having increased it, caused no visible change in structure; however, in this case the relative number of high energy electrons did not appear to decrease.

(4) Increasing the discharge current caused no change in the visible structure, but did brighten the discharge as a whole; the relative number of high energy electrons increased slightly. Decreasing the discharge current caused the opposite effect.

(5) Increasing the pressure caused a relative increase

in the number of high-energy electrons , and an increase in their energy.

(c) Changing cathode-anode spacing by as much as 10 mm produced no observable change.

On the third run, again with identical initial conditions, a diffuse discharge was obtained, similar in all respects to that obtained during our main runs in Argon, exhibiting no structure and no observable high energy beam electrons in any part of the discharge.

The runs were conducted on separate days, using identical procedures, but using separate charges of gas from the same source bottle. Prior to making the first run the cathode was carefully "activated" and the tube was flushed three times with Argon.

From this additional work, it appears that the non-appearance or disappearance, or the change in concentration, of the high energy beam in some way dependent upon the discharge structure or the probe position within the discharge; however, our particular apparatus was not sufficiently well adapted to making analyses of such a (e.g., our probe could not be moved in a radial direction without changing the distance between cathode and probe), to properly study all of the aspects involved.

It is recommended that further investigation of discharge structure be made using a discharge tube designed to allow for accurate radial movement of the probe over small distances.